Theoretical and Experimental Study of Piezoelectric Modulated AlN Thin Films for Shear Mode BAW Resonators

THÈSE N^{O} 5113 (2011)

PRÉSENTÉE LE 4 NOVEMBRE 2011
À LA FACULTÉ SCIENCES ET TECHNIQUES DE L'INGÉNIEUR
LABORATOIRE DE CÉRAMIQUE
PROGRAMME DOCTORAL EN SCIENCE ET GÉNIE DES MATÉRIAUX

ÉCOLE POLYTECHNIQUE FÉDÉRALE DE LAUSANNE

POUR L'OBTENTION DU GRADE DE DOCTEUR ÈS SCIENCES

PAR

Evgeny MILYUTIN

acceptée sur proposition du jury:

Prof. A. Mortensen, président du jury
Prof. P. Muralt, directeur de thèse
Dr D. Ekeom, rapporteur
Prof. N. Grandjean, rapporteur
Prof. I. Katardjiev, rapporteur

ÉCOLE POLYTECHNIQUE
FÉDÉRALE DE LAUSANNE

Suisse
2011

Abstract

The use of acoustic resonators for sensors application has opened a new branch in research and applications of piezoelectric materials and devices. The first generation of such sensors is constituted by the quartz crystal microbalance (QCM) based on AT-cut mono-crystalline quartz. High sensitivities of gravimetric sensing in both air and liquids were demonstrated. Since the 1980s, when the first QCM-based sensor was demonstrated for the detection of silver in a liquid solution, many other application in chemical, bio-medical and environmental sensing were realized using the same concept. QCM's exhibit a very good thermal stability. The AT-cut quartz plate leads to the excitation of shear waves when used in parallel capacitor geometry. This is important for achieving high quality factors in the immersed operation of the sensor. A second generation of gravimetric sensors is based on surface acoustic wave (SAW) structures, working for instance with Love waves in a SiO2 layer on top of a LiTaO3 single crystal. SAW devices are mainly used as RF filters in television and mobile phones. SAW sensors are a side product of the much larger telecommunication market. The evolution of thin film and MEMS technology has lead to a third generation of gravimetric sensors that is based on bulk acoustic wave (BAW) resonances in piezoelectric thin films. Again, such sensors are a side product from the large telecommunication market where such resonators are used for RF filters. With every generation, the oscillation frequency increased. While QCM's operate typically at 5 MHz, the SAW resonators work typically at a few 100 MHz, and the thin film BAW resonators (TFBAR) operate typically around 2 GHz. The increase of the frequency goes together with an increase in sensitivity, and a decrease of the thickness and mass range that can be measured.

The TFBARs are in some sense miniaturized analogs of QCM's operating at much higher frequencies. They are very promising as they reach higher sensitivities. This attracted the attention of researchers, and experimental evidence of the potential of TFBARs as sensors was delivered. In addition to the higher sensitivity, the miniaturization allows for using arrays of sensors with different immobilization layers as needed for drug screening. However, the application of the same TFBARs as used in telecommunications would not allow a good performance in immersed operation. It would only be good for operation in air. The principal characteristic of TFBARs used in mobile phones is the value of the electromechanical coupling and not the resonance mode at which this coupling is achieved. But for the in-liquid operated sensors, it's rather the opposite - the mode of the resonance should be such that the surface of the resonator, which tis in contact with liquid, should move parallel to the surface (in-plane motion, or transverse motion) to minimize emission of acoustic waves into the liquid. The coupling coefficient is of secondary importance in this case. Therefore, the development of shear mode TFBARs became an interesting task that was challenged by several research groups. One of the most successful solutions is the use of c-axis inclined AlN thin films. Inclination of c-axis in a parallel plate capacitor structure enables the coupling of the electric field to the shear strain, which enables the excitation of a shear mode. Such devices were successfully applied for selective sensing of organic species, such as DNA molecules, suspended in a liquid. Even if the process of deposition of c-axis inclined AlN films doesn't require hardware modification, the quality of the process is still far from the one for deposition of (0001)AlN films used in telecommunications. So the goal of this thesis was to find a solution for the shear mode TFBAR's based on (0001)AlN films.

In (0001)AlN films, the shear strain cannot be induced by the electric field produced in a parallel plate geometry as the coefficient e_{35} and e_{34} of the piezoelectric tensor are zero. But there are e_{15} and e_{24} coefficients that are not zero, meaning that in-plane electric field can be used to excite the shear waves. In the frame of this work, this concept was studied theoretically and experimentally. The in-plane electric field was generated via inter-digitated electrodes (IDE). A first device type was realized in solidly mounted resonator (SMR) design and based on uniform (0001)- oriented AlN thin films. The anti-phase of the electric field in adjacent half-periods of the IDE resulted in an anti-phase movement of the corresponding regions of the film. Finite element modeling and boundary element modeling (FEM-BEM) were carried out to clarify the kind of vibrations present in the device. A kind of shear/lingitudinal mode with elliptic motions was obtained. A device was fabricated and tested both in liquid and air. The resonance of the device was observed in the expected frequency range (1.86 GHz) and high quality factors under operations in air (Q=870) and silicon oil (Q=270) were obtained. The drop of the quality factor was explained by the up and down motion of the regions of the film located directly under the IDE electrodes. Such a motion is due to anti-phase motion of different regions of the film as mentioned above.

To prevent this effect, a second device type was studied. It is again based on the use of (0001)AlN thin films, but with modulated piezoelectric properties. Having different piezoelectric properties in the regions corresponding to adjacent half-periods of IDE, breaks the mirror symmetry of the device and allows for coupling the electric field to a pure shear mode. Analytical and numerical models explaining such a device were established and evaluated. The optimal situation is found when perfect Al-polar and N-polar regions of AlN are combined. This maximizes the coupling coefficient k that is derived as being proportional to the difference of e_{15} coefficients.

Finding a way to fabricate the AlN thin film with different piezoelectric properties was thus the next objective. Growth features to decrease the piezoelectric effect were first studied. Providing rougher regions on the otherwise smooth substrate allowed to modify locally the quality of AlN thin films. Device based on such films were fabricated and characterized. The resonance of a pure shear mode was found at the expected frequency (roughly 2GHz) when the piezoelectric effect was modulated. Devices without this modulation failed to show the resonance at the exact frequency, exactly as the theory predicted. We managed to reduce two times the

d_{33} coefficient of the film by inducing a increased roughness to the substrate - from 5.0 pm/V, corresponding to 1.5 degree rocking curve, down to 2.4pm/V, corresponding to 7 degree of rocking curve.

The final step of the thesis was the process development for the simultaneous growth of Al-polar and N-polar regions within sputter deposited (0001)AlN, in order to achieve the maximal possible "piezomodulation" effect. As the sputter deposition yielded only N-polar films, we included Al-polar films from another source as seed layers. High temperature epitaxial growth methods of GaN and AlN on Si(111) and Si(100) lead to Ga- and Al-polarities. On such films, the sputter deposited AlN copies polarity from the growth substrate. The selective polarity was then obtained by preventing the expitaxy locally through a patterned oxide layer. Wet etching tests together with PFM measurements were performed to prove the dual polarity in the sputter deposited film. Finally, the integration of this process into the process flow for device fabrication was investigated.

Keywords: AlN, sputtering, BAW, shear mode, sensors

Resume

L'utilisation de résonateurs acoustiques pour des capteurs gravimétriques a ouvert une nouvelle activité dans la recherche et les applications des matériaux et dispositifs piézo-électriques. La première génération de ces capteurs est constituée par la microbalance à cristal de quartz (QCM) sur la base de coupe AT d'un quartz mono-cristallin. Cette microbalance se distingue par la haute sensibilité de détection gravimétrique dans l'air ainsi que dans les liquides. Depuis les années 1980, lorsque le premier capteur à base de QCM a été réalisé pour la détection de l'argent dans une solution liquide, de nombreux capteurs pour les applications chimiques, bio-médicales, et environnementales ont été fabriqués en utilisant le même concept. Les QCMs présentent une très bonne stabilité thermique. Dans une plaque de quartz de coupe AT, des ondes de cisaillement sont excitées avec des électrodes dans la configuration de plaques parallèles. Le mode en cisaillement est important pour la réalisation de facteurs de qualité élevé dans le cas ou le capteur est plongé dans un liquide. Une seconde génération de capteurs gravimétriques est basée sur des ondes acoustiques de surface (SAW), par exemple avec ondes de Love dans une couche de SiO2 sur un monocristal de $LiTaO_3$. Les dispositifs SAW sont principalement utilisés comme filtres RF pour la télévision et les téléphones mobiles. Les capteurs SAW sont un produit secondaire par rapport au marché des télécommunications. L'évolution des technologies des couches minces et des microsystèmes a donné lieu à une troisième génération de capteurs gravimétriques, qui est basé sur des ondes acoustique en volume (BAW) piégées dans des films minces piézo-électriques. Encore une fois, ces capteurs sont un produit secondaire du grand marché des télécommunications, où les résonateurs sont utilisés pour des filtres RF. Avec chaque génération, la fréquence d'oscillation a augmenté. Les QCM fonctionnent généralement à 5 MHz, les résonateurs

SAW travail généralement à quelques 100 MHz, et les résonateurs BAW en films minces (TFBAR) fonctionnent généralement autour de 2 GHz. L'augmentation de la fréquence est accompagnée d'une augmentation de la sensibilité, et d'une diminution de l'épaisseur et de la gamme de masses qui peuvent être mesurés.

Les TFBARs sont d'une certaine manière des QCMs miniaturisés, qui travaillent à des fréquences beaucoup plus élevées. Ils sont très prometteurs car ils visent des sensibilités plus elevès. En plus, la miniaturisation permet d'utiliser des matrices de capteurs avec différentes couches d'immobilisation, ce qui faciliterait le dépistage de drogues. Toutefois, l'application du même type de TFBAR que celui utilisé dans les télécommunications ne permettrait pas une bonne performances en fonctionnement immergé. Il ne serait bon que pour des opérations dans l'air. La principale caractéristique de TFBARs utilisés dans des téléphones mobiles est la coefficient du couplage électromécanique et non le mode de résonance. Mais pour le fonctionnement immergé en liquide, le mode de résonance doit être tel que la surface du résonateur, en contact avec le liquide, doit vibrer parallèlement à la surface pour minimiser des émissions d'ondes acoustiques dans le liquide. Le coefficient de couplage est secondaire pour ce type d'applications. Par conséquent, le développement de TFBARs en mode de cisaillement est devenu un travail intéressant qui a été poursuivi par plusieurs groupes de recherche. L'une des solutions les plus efficaces est le l'utilisation de couches minces AlN ou ZnO qui possèdent une texture avec l'axe c incliné dans le même sens partout. Cette structure associée à des électrodes en forme de plaques parallèles permet de coupler le champ électrique à la contrainte de cisaillement, ce qui permet l'excitation d'un mode de cisaillement. De tels dispositifs ont été utilisés avec succès pour la détection sélective d'espèces organiques, telles que des molécules d'ADN, en suspension dans un liquide. Le processus de dépôt pour aboutir a l'axe c incliné n'est que difficilement réalisable à l'échelle industrielle. L'objectif de cette thèse était de proposer une solution pour réaliser des TFBAR's en mode de cisaillement qui sont basés sur des films AlN de texture (0001), donc identique à celle des filtres RF.

Dans des films de texture (0001) du AlN, les contraintes de cisaillement ne peuvent pas être induite par un champ électrique produit dans une géométrie à plaques parallèles, étant donné que les coefficients e_{35} et e_{34} du tenseur piézo-électriques sont nulls. Pour profiter des coefficients e_{15} et e_{24} qui ne sont pas nulls, il faut mettre le champ électrique dans le plan du film. Dans le cadre de ce travail, ce concept a été étudié théoriquement et expérimentalement. Un tel champ électrique a été généré par des électrodes inter-digités (IDE). Un premier dispositif de ce type a été réalisée sur un réflecteur acoustique (mirroir de Bragg). L'anti-phase du champ électrique dans des demi-périodes avoisinantes de l'IDE entraîne un mouvement d'anti-phase. Les modélisations par éléments finis et éléments de frontière (BEM-FEM) ont été menées pour identifier les types de vibrations présentes dans ces dispositifs. Une sorte de combinsation composé de mouvements en cisaillement et en longitudinal, forment ainsi un mouvement elliptique a été obtenu. Un dispositif de a été fabriqué et testé dans un liquide et à l'air. La résonance du dispositif a été observée dans la gamme de fréquence prévue (1,86 GHz). Les facteurs de qualité dans l'air ($Q = 870$) et dans un huile de silicone ($Q = 270$) étaient satisfaisants. La baisse du facteur de qualité dans le liquide s'explique par le mouvement ascendant et descendant des régions situées directement sous les électrodes IDE, qui est une conséquence du mouvement anti-phase des demi-périodes avoisinées.

Pour éviter cet effet, un second type de dispositif a été étudiée. Il est à nouveau basée sur l'utilisation de (0001) AlN films minces, mais contenant un film mince d'AlN avec des propriétés piézoélectriques modulées en phase avec la période des doigts d'électrodes. Cette modulation permet de coupler le champ électrique au mode de cisaillement pur. Les modèles analytique et numérique pour un tel dispositif ont été établis et comparés. La configuration optimale est obtenue lorsque les demi-périodes avoisinées possèdent les polarités parfaites de Al et de N en alternance. Cela maximise le coefficient de couplage k qui est calculée comme étant proportionnelle à la différence des coefficients e_{15}.

Par la suite, nous avons étudié des procédés pour réaliser un contrôle local de

la polarité du AlN. La premierè approche était de on l'effet piézo-électrique dans les régions définies par la lithographie, se basant sur le fait que les films du AlN sont différents selon la rugosité du substrat. Ainsi, nous avons introduit un film mince de silicium amorphe avec une rugosité augmentée, qui a été structuré pour contrôler la rugosité d'une manière locale. Les dispositifs réalisés suivant ce concept ont permis d'avoir le mode fondamental de cisaillement à la fréquence attendue (environ 2 GHz). Les dispositifs sans cette modulation, présents au voisinage, n'ont pas permis d'obtenir la résonance à la fréquence prévue. Nous avons réussi à réduire le coefficient piézoélectrique du film sur la surface rugueuse par un facteur 2 par rapport au valeur du film déposé sur la surface lisse.

La dernière étape de la thèse était dédié à la réalisation d'un dispositif contenant un film mince d'AlN(0001) avec les deux polarité en même temps, et prédéfinie selon l'endroit par une lithographie, pour obtenir l'effet maximal de la modulation de la piézoélectricité. Comme le dépôt par pulvérisation cathodique donne que des films N-polaires, nous avons inclus des films Al-polaire d'un procédé MOPVE pour faire germer cette polarité aussi dans les films pulvérisés. Une couche très fine de silice a été utilisé pour briser l'èpitaxie localement, et ainsi faire croître à ces endroits la polarité N. Le bon fonctionnement de cette méthode a été mis au jour par la gravure sélective dans une solution alcaline, et par la microscopie à force atomique mesurant le déplacement piézoélectrique.

Mots-clés: AIN, pulvérisation, BAW, mode de cisaillement, les capteurs

Contents

1

Introduction

Weighing the mass of an object is one of the earliest measurements that was made by mankind, and remained a crucial, technical prerequisite of economy and science through the centuries to nowadays. The classical balance principle, which is still employed at present, was already in use in Ancient Egypt (see fig. 1.1). Such a balance is a time-tested, and very much optimized tool that is used in everyday's life as well as in research in the fields of physics, chemistry and engineering.

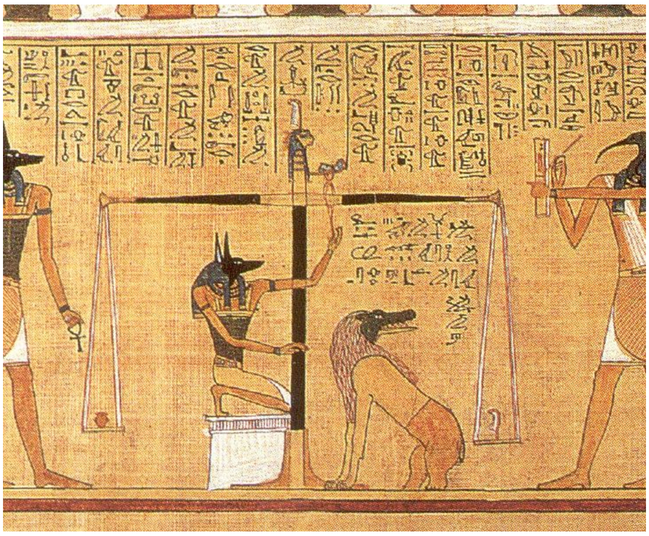

Figure 1.1: Anubis weighing the heart of Hunefer, 1285 BC

Being based on gravitation, such balances work fine in the static case with constant gravitation fields when carrying out a differential measurement with known reference masses. They do not work when gravitation is absent. This is the case in space. For such situations, there is another weighing principle available. Instead of using a static principle, one can use a dynamic principle to determine the inertial mass. For example, one of the methods studied in school is to determine the mass of a body by means of a spring pendulum as shown in fig. 1.2.

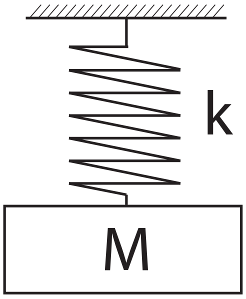

Figure 1.2: Spring pendulum - a way to measure the inertial mass

The oscillation frequency of such a pendulum is defined by the stiffness of the spring and attached mass through the well-known formula:

$$\omega_0 = (\frac{k}{M})^{1/2} \tag{1.1}$$

By measuring the oscillation frequency of the pendulum, and knowing the spring constant k, the unknown mass can be found. Moreover, by recording frequency changes $\Delta\omega$ caused by a changing mass ΔM, one actually can determine ΔM (case for small ΔM) through the equation:

$$\frac{\Delta\omega}{\omega_0} = -\frac{1}{2}\frac{\Delta M}{M} \tag{1.2}$$

In most cases of real life, it's easier to use balances that are based on Earth gravity to weigh the static mass of an object. However, the inertial principle as described on the example of the spring pendulum (fig. 1.2) found applications not only in space, but also in cases requiring dynamic measurements to detect mass changes, in cases where the measurement set-up cannot have a defined orientation with respect to gravitation force, and in cases where small mass changes need to be detected, i.e. for sensors. The spring-mass pendulum is of course not easily adapted for operation independently of gravitational forces, though quite some achievements were made for portable mechanical watches since the 18th century. A breakthrough for sensor applications was the quartz microbalance proposed by Sauerbrey (1). He substituted the spring-mass system by a quartz crystal plate vibrating at its eigenfrequency of the fundamental thickness mode resonance. As quartz is piezoelectric, two electrodes forming a plate capacitor (fig. 1.3) are used to excite the vibration. Sauerbrey proposed his apparatus for the measurement of thin film masses, specifically for the determination of thin film deposition rates in evaporation tools.

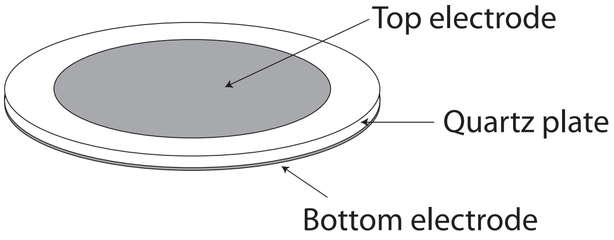

Figure 1.3: Quartz crystal microbalance - a quartz plate confined between two electrodes forming parallel plate capacitor

With such a device, the ratio of frequency change Δf per surface mass density change $\Delta\mu$ is obtained as:

$$\frac{\Delta f}{\Delta\mu} = Cf^2 \tag{1.3}$$

where C is a constant related to the mechanical properties and thickness of the quartz. The resonance frequency (eigenfrequency) f of the QCM is measured electrically by an RF circuit exciting continuously the shape resonance through the piezoelectric effect of quartz.

This tool is applied routinely in thin film technology to control the thickness of deposited films. Later it was also found that it can be applied as a sensor to measure the presence of the certain species in liquid media (2). The concept and further description will follow in the next sections.

1.1 Concept of gravimetric sensors

The principle of gravimetric sensing with a piezoelectric oscillator is depicted in fig. 1.4. The resonating body, usually a plane plate, is resonating at some frequency, defined by its geometry, and is immersed into the medium in which a species of unknown concentration must be sensed. The surface of the plate is covered with a specifically chosen material, called functionalisation layer, or sometimes also immobilization layer, which captures selectively the species to be sensed. Once the species are captured, the overall thickness, mass, and elastic properties are changed, leading to a change of the resonance frequency. The latter is the signal of the sensor, from which the amount of detected species is derived.

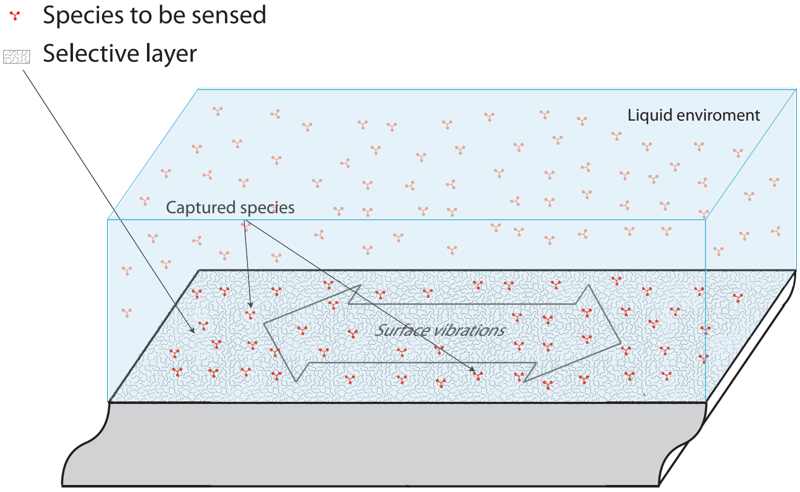

Figure 1.4: Principle of gravimetric sensing by acoustic device with functionalisation layer

The sensitivity of the sensor depends on the precision with which the resonance frequency is detected. An example of measured conductance of a thin film bulk acoustic wave resonator is shown in fig. 1.5 for illustration (3). The narrower the resonance peak, the more precise the resonance frequency can be derived. The resonance curve widens with energy losses of various origins, such as the viscous losses in the vibrating materials, electrical losses in the contacts, and acoustic emission into the environment. The fixation of the oscillator is critical, as well as the possibility to emit acoustic waves into the liquid in which the sensor is immersed. For this reason, the QCM sensors are based on shear mode vibrations, as shown in fig. 1.4. The surface of the plate vibrates then in the plane, and the mechanical coupling of the device to the liquid is dramatically reduced in comparison to the case of out-of-plane motion of the plate. Furthermore, shear waves are quickly damped in liquids and do not propagate. As a consequence, the acoustic coupling between resonator and liquid is much smaller as compared to the case of longitudinal modes and waves.

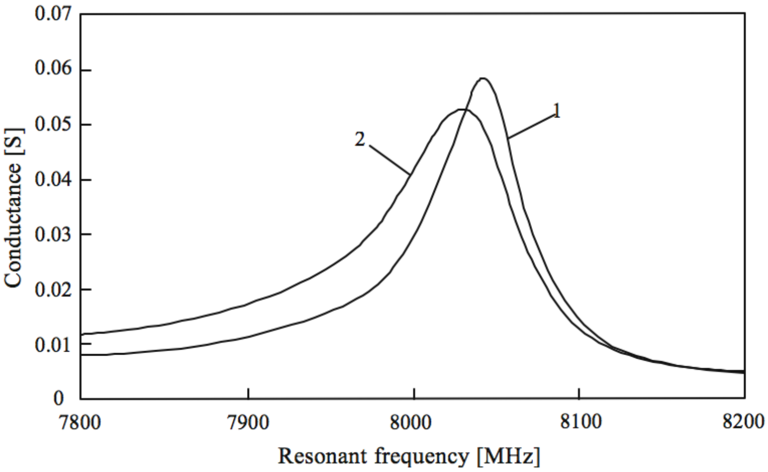

Figure 1.5: Resonance curves of a thin film bulk acoustic wave resonator. The shift from curve 1 to 2 is due to adding a self assembled monolayer to the top electrode, (3)

1.2 Functional layers for chemical and bio-medical sensors

The sensor as described above consists of two main parts: a piezoelectric transducer and a functional (immobilization) layer. The last one provides the selectivity of the sensor to certain species. These are captured by specific chemical reactions with the functional layer . This layer can be a simple polymer, as useful for temperature and PH measurements, or be the results of an elaborate chemistry to immobilize specific organic molecules. For bio-medical applications, also antigene-antibody reactions are employed. In the following, literature results with different functional layers are presented.

1.2.1 Sensing the presence of Vero cells in liquid media using QCM

D. M. Gryte et al. demostrated (4) an in situ technique based on QCM for continuous monitoring of attachment and detachment of anchorage-dependent mammalian cells on a metal surface. An example of such a process is shown in fig. 1.6. The authors conclude that QCM is a viable technique for monitoring anchorage-dependent cell attachment and detachment on surfaces.

1.2.2 Pd and Co-tetra-phenyl-porphyrin (Co-TPP) layers

M. Benetti et al., reported in their work (5), "Microbalance chemical sensor based on thin-film bulk acoustic wave resonators" the detection of H_2, CO and ethanol as

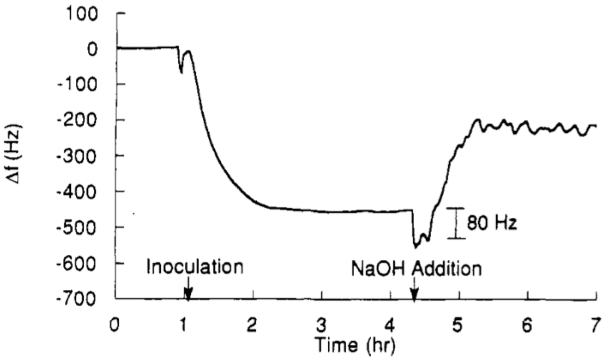

Figure 1.6: Resonant frequency change of a 5-MHz AT-cut quartz resonator as a response to the inoculation of Vero cells to the liquid media, (4)

low as about 2, 40 and 500 ppm concentrations in air, respectively, by using Pd and Co-tetra-phenyl-porphyrin (Co-TPP) layers (see fig. 1.7).

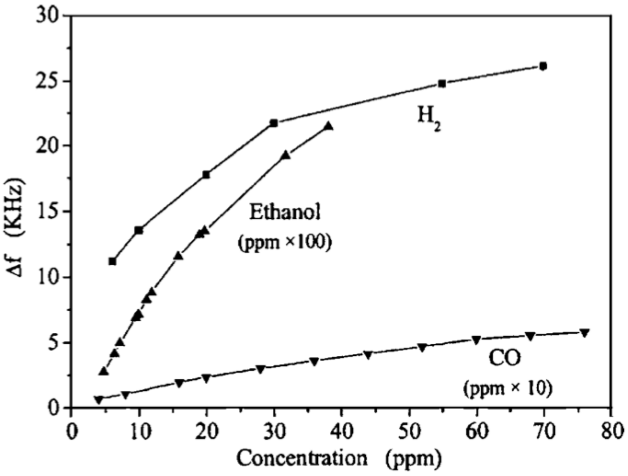

Figure 1.7: Calibration curves for the TFBAR sensors upon exposure to H_2 (Pd membrane), CO, and ethanol (Co-TPP membrane) (5)

1.2.3 Utilizazion of oligo layer for DNA and protein detection

In the work of R. Gabl et al (6), "First results on label-free detection of DNA and protein molecules using a novel integrated sensor technology based on gravimetric detection principles" utilization of 5′-thiolalkyl-ACC TCT TCT GGC TCA AAA AGA GAA T-3′-biotin oligo to detect Streptavidin and utilization of 5′-thiolalkyl-ACC TCT TCT

GGC TCA AAA AGA GAA T-3′ to detect its exact match to oligo (see fig. 1.8). The resonator structure was a shear mode BAW resonator based on tilted ZnO growth.

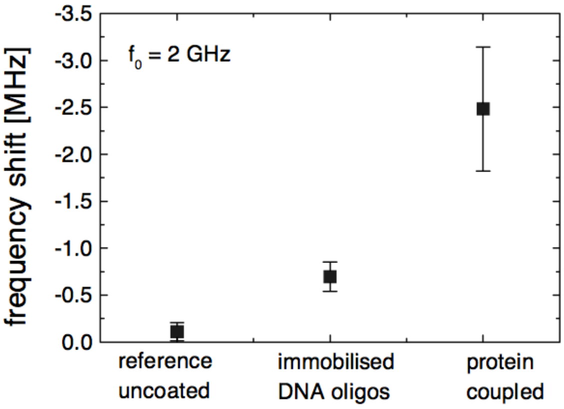

Figure 1.8: Resonance frequency shift due to the coating with the immobilization layer and the detection of the protein (6)

1.2.4 PMMA layer for detection of acetone vapors

In the work of S. Rey-Mermet et al (3), "AlN thin film resonators operating at 8 GHz used as sensors for organic films", a Polymethyl methacrylate (PMMA) layer was tested as acetone sensor in air. The presence of acetone in the vicinity to the device causes an increase of the mass density of the PMMA layer, which results in a frequency drop. Once the vapor source is removed, the absorbed acetone evaporates from the PMMA and the frequency is coming back to its original value (see fig. 1.9)

1.2.5 Detection of cocaine and heroine. Competitive binding

G. Wingqvist et al. reported in their work (7), "Immunosensor utilizing a shear mode thin film bulk acoustic sensor" the detection of drug molecules, such heroine and cocaine, presented in liquid media. The sensor was based on the detection by competitive binding. The surface of the device was first covered with antigens and then with antibodies that have specific affinity both to the antigens and to the target molecules. In addition, the affinity of the antibodies to the target molecule was higher than that to the antigen. That results in a release of antibodies once the target molecules are

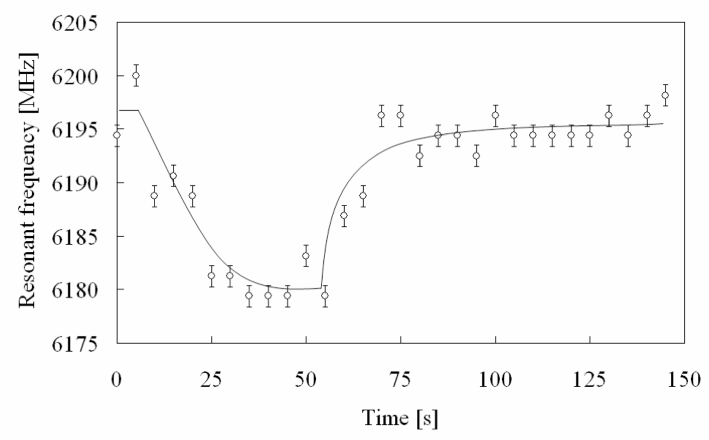

Figure 1.9: Resonant frequency change upon immersing the sensor in acetone saturated air, and upon removal from the acetone vapor (3)

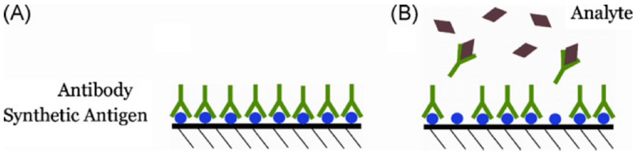

Figure 1.10: The antibodies bind to a synthetic antigen onto the surface of the resonator (A). The antibodies bind with higher affinity to the analyte and will therefore leave the surface (B), (7).

present in the liquid (see fig. 1.10). The response of the resonator during the process of functionalization and detection is shown in fig. 1.11.

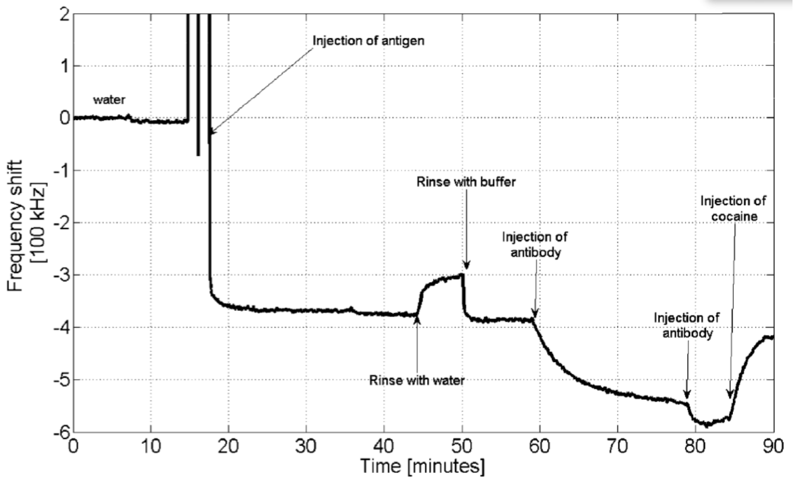

Figure 1.11: Frequency shift vs. time illustrating surface functionalization and detection of cocaine with competitive binding, (7).

1.2.6 Detection of avidin, BSA and anti-avidin in the liquid media

J. Weber et al investigated (8) the detection of avidin, bovine serum albumin (BSA) and anti-avidin by utilizing shear mode thin films BAW resonators. Dynamic measurements demonstrating the reaction of the device upon the in-turn injection of solutions containing the mentioned species are shown in fig. 1.12.

1.3 Piezoelectric transducers

There are different piezoelectric transducers that are employed in gravimetric sensors. In the early years, the piezoelectric oscillator was based on a resonating AT-cut quartz plate (2) whose frequency was defined by the thickness of the plate. In such a device – based on a bulk wave – the acoustic energy is mainly distributed inside the plate. Logically, the sensitivity with respect to surface effects will increase by thinning down the plate. This leads, however, to quite brittle structures. Further solutions were investigated, targeting at waves localized in a surface layer: surface acoustic waves (9), surface transverse waves (see in (10)), and Love waves (11), (12). Furthermore, membrane-type structures with Lamb wave plate modes (13) and, more recently, thin

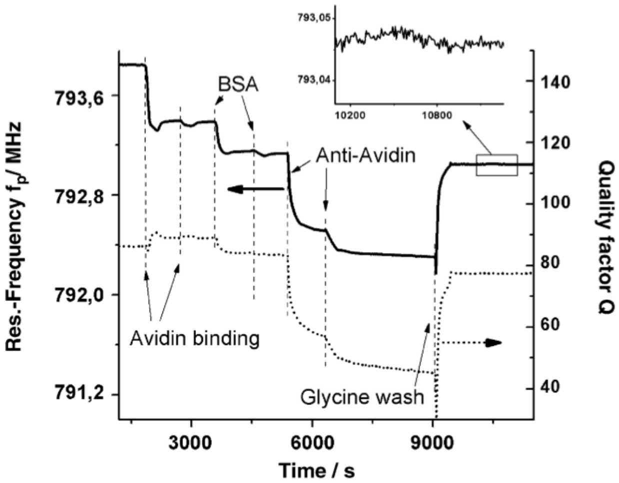

Figure 1.12: Frequency shifts vs. time caused by injections of avidin, BSA and anti-avidin (8)

film bulk acoustic resonators (TFBARs) (14) were investigated. The sensitivity S_μ defined as relative frequency shift per change of surface mass density (see 1.4) can be used as one of the figures of merit for transducers of different types.

$$S_\mu = \frac{1}{f_0} \lim_{\mu \to 0} \frac{|\Delta f|}{\mu} \tag{1.4}$$

where f_0 is the resonance frequency and Δf is the shift of the frequency per change of surface mass density μ.

An overview of sensitivity of mass density obtained with different devices is shown in fig. 1.13. The sensitivity as defined by equation 1.4 increases theoretically linearly with frequency (see (6)). Fig. 1.13 gives the experimental evidence for this behavior. In virtue of its high frequency, the BAW device has the highest sensitivity in comparison to others.

As already mentioned above, an important differentiation of the various acoustic excitation mechanisms is the ability to create exclusively shear displacements, meaning that at the surface, the displacement is tangential, as shown in fig. 1.4. This property is required for operations in liquids because shear modes do not emit waves into liquids and thus are able to maintain a high quality factor in immersed operation. Such shear mode sensors are required for the largest potential markets, which are medical

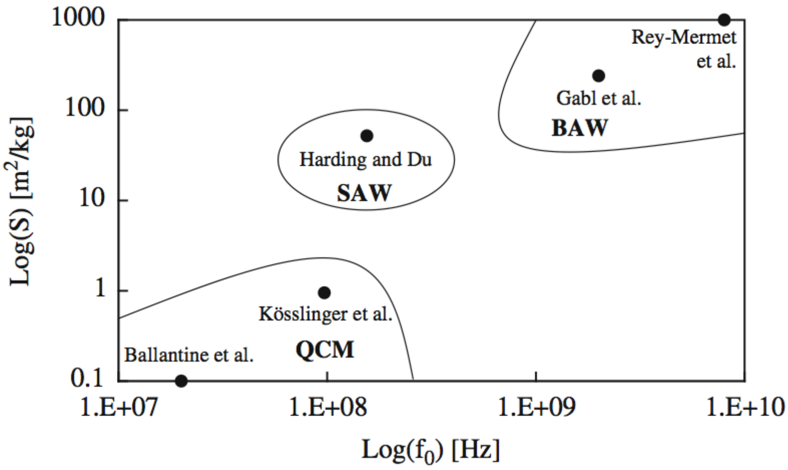

Figure 1.13: Overview of sensitivity of mass density obtained with quartz micro balances (QCM) (15), (16), SAW devices (17), and BAW devices (6), (3) following the sensitivity definition of 1.4 (fig. from (3))

diagnosis, drug screening, and, eventually, environmental sensors. The high sensitivity makes shear mode BAW resonators to be sensors with unique performance.

The following subsections will be mostly focused on topics related to shear mode BAW devices.

1.3.1 Transducer materials

The development of thin films technologies over the last decades enabled the fabrication of piezoelectric resonators and transducers that operate on the same principle as quartz resonators, but at higher frequencies. Aluminum nitride (AlN) and zinc oxide (ZnO) are the most used ones. These materials are about equivalent with respect to piezoelectric properties. However, AlN is a better electrical insulator, and better thermal conductor. Today, AlN is the standard material to fabricate FBAR's for RF-filters in mobile phones.

Detailed description of AlN and ZnO properties can be found elsewhere (18), (19). Considering a (0001)-textured, polycrystalline, columnar film slab as a free body, we would find a d_{33} coefficient that is equal to the δ_{33} of the single crystal column (3: crystal axes). The in-plane ordering is random, resulting in a cylindrical symmetry. This gives the same symmetry of the piezoelectric tensor as for hexagonal or tetragonal crystal symmetry. It follows that in the case of wurtzites, d_{31} is equal d_{32} and corresponds to the crystal $\delta 31$ value. In addition, the shear mode coefficients d_{15} and d_{24} coincide as well and again correspond to the single crystal value, see (1.5). Example of such a (0001)-textured AlN film is show in fig. 1.14.

$$d_{ni} = \begin{pmatrix} 0 & 0 & 0 & 0 & d_{15} & 0 \\ 0 & 0 & 0 & d_{15} & 0 & 0 \\ d_{13} & d_{13} & d_{33} & 0 & 0 & 0 \end{pmatrix} \tag{1.5}$$

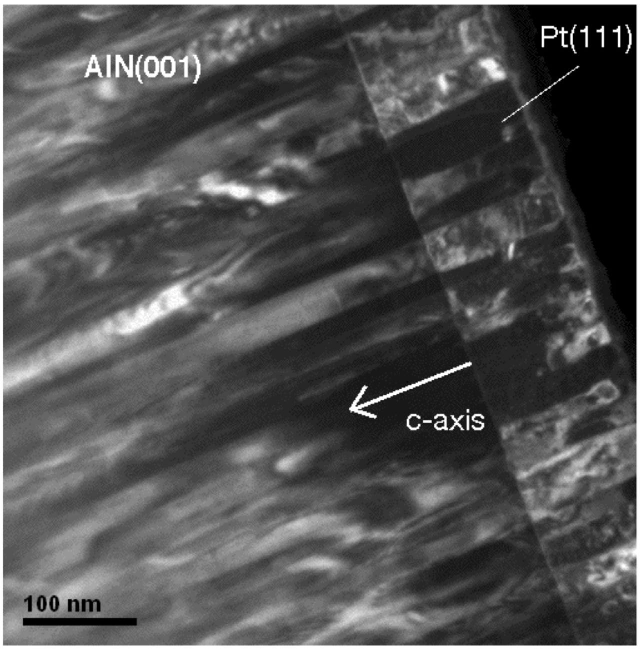

Figure 1.14: Example of (0001)-textured, polycrystalline AlN film with its typical fibrous or columnar grains, as seen by bright field transmission electron microscopy (20)

1.3.2 Fabrication techniques

AlN thin films for piezoelectric MEMS devices are almost exclusively deposited by means of reactive sputter techniques. This technique is the only one that provides highly-oriented, piezoelectric films at temperatures as low as 200 °C. The sputter source is a magnetron source, and the substrate chuck in face of the target preferentially allows for coupling in an RF bias. The tool is schematically shown in the fig. 1.15.

During the sputter process, ions from the plasma are accelerated in the cathode sheath and sputter off atoms from the target material. These atoms form a so-called

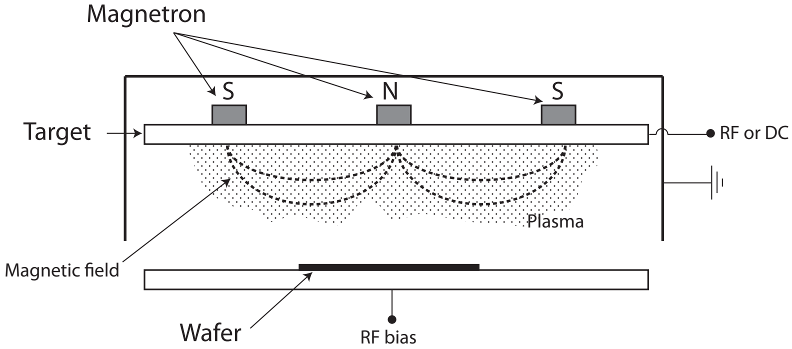

Figure 1.15: Constitution of the sputter deposition chamber

physical vapor and travel towards the substrate, on which they condense. The peculiarity of the method is that the energy of the atoms sputtered from the target bring a kinetic energy of a few eV. In addition, on an insulating substrate or film, the surface is negatively biased, attracting positive ions from the plasma. The substrate bias can be enhanced by the application of RF power to the substrate chuck. In this way, the bias voltage on the substrate becomes even more negative, thus attracting even more ions to bombard the growing film. Ion energies in the range of 20 to 40 eV are very suitable to enhance adatom diffusion on the surface. In this way, films can be grown with an apparent surface temperature that is higher than the real substrate temperature. A higher film quality is achieved as would be possible with a process at thermal equilibrium at the same substrate temperature. This phenomenon results in a peculiar growth mode, called zone T growth mode, which is due to the absence of bulk and grain boundary diffusion, but includes surface diffusion. In the Thornton structure zone diagram (Fig. 1.16) zone T is situated between the zones 1 (no diffusion at all) and zone 2, which is governed by thermally activated grain boundary and surface diffusion. The typical growth conditions for sputter deposited, columnar (0001) textured AlN thin films are indicated in the diagram with red color.

Non-reactive gases, such as argon, are usually used as sputtter gas to deposit films with the target composition. Nitrides and oxides can be obtained by using metallic targets, and adding N_2 and O_2 gas to the sputter gas. Nitride and oxide films are then obtained due to chemical reactions on the target and film surface. For example, thin films of AlN are obtained in the presence of N_2 gas while sputtering from a Al target. Such a process called reactive sputter deposition.

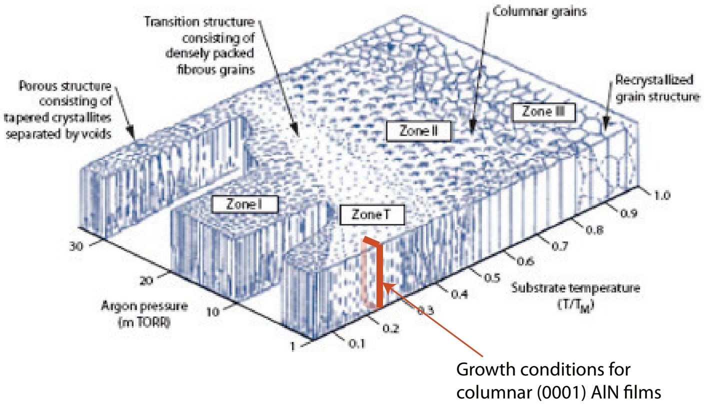

Figure 1.16: Growth conditions for the columnar (0001)-AlN films according to the Thornton structure zone diagram

1.3.3 Design of the shear mode resonator

Piezoelectricity is an anisotropic effect. The deformation depends on the direction along which the electric field is applied. The strain tensor is obtained from the multiplication of the piezoelectric tensor with the electric field vector (1.5). In case of single crystal transducers, the crystals are cut in specific directions to place the electrodes in an optimal way. For instance, the AT cut quartz is cut in such a way that the electric field perpendicular to the plate excites a pure shear deformation. This degree of freedom is not available in thin film transducers. Growth cannot be made along arbitrary crystalline directions.

The parallel plate capacitor design, as shown in fig. 1.17, is the most classical and simplest design. As the films investigated in this thesis grow naturally with a preferred (0001) texture, the exploitation of the d_{3*} is possible for such design. For (0002) oriented films of AlN and ZnO there are no coefficients among d_{3*} that couples to shear deformation. Thus no shear waves can be excited. Such device can applied as a sensor in gaseous environment and examples of such one already have been mentioned (6), (3).

In order to have coupling to shear mode while using plane plate capacitor design, one need to use a material that has d_{35} or d_{34} to be non zero. That can be achieved by using AlN or ZnO films with inclined (0002) axes (see fig. 1.18). Such a device was investigated by several groups (14), (8). The coupling coefficient of the device for longitudinal and shear mode depending on the angle of inclination from the vertical

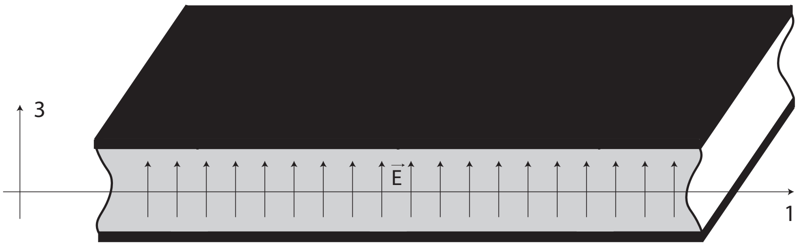

Figure 1.17: Plane plate capacitor with piezoelectric material

modeled is shown in fig. 1.19 (21). The difficulties related to growth of such inclined films were discussed in the previous subsection.

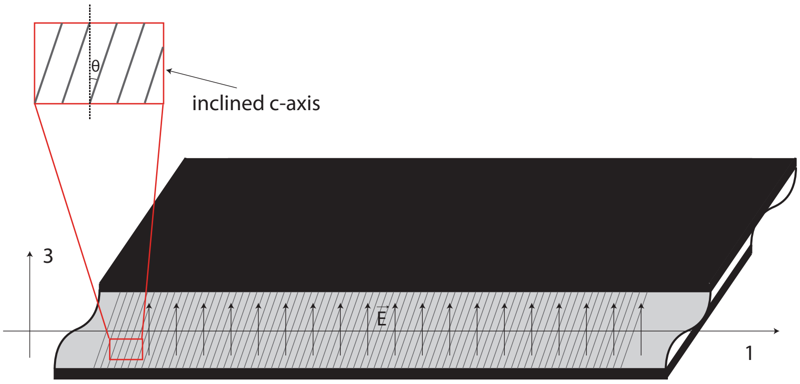

Figure 1.18: Utilization of AlN or ZnO with inclined c-axis to excite shear waves in the film by E_3 electric field

Considering devices based on (0002)-AlN or (0002)-ZnO, the only possibility of the direct excitation of the shear mode waves is through d_{15} (or d_{24}).

1.4 Sensitivity and cross-sensitivity

The mass change of material attached to the surface of the resonator is only one of the factors to which piezoelectric transducers are sensitive. There are also others factors that may cause a frequency shift. This may be practical and useful for some applications, but annoying for others. Such so-called cross-sensitivities should be taken into account to get correct results. First of all, there are external factors that may cause the change in the geometry and mechanical properties of the transducer itself. For example, temperature and pressure of the environment. In order to exclude that effect one can measure in parallel two devices - one that is sensitive to the environment and another

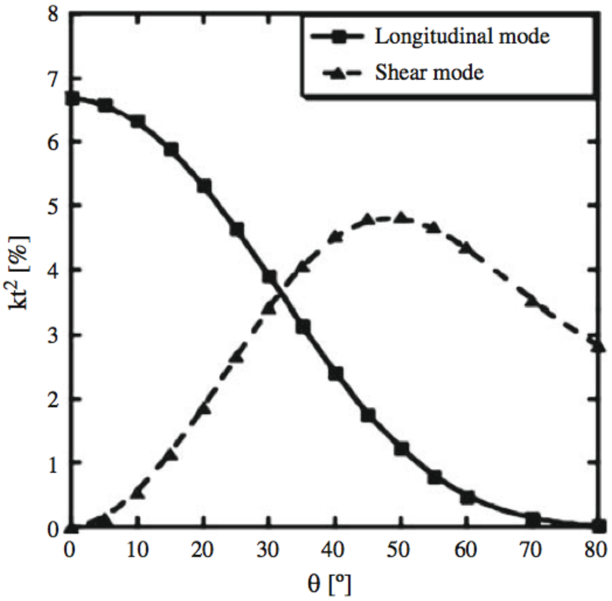

Figure 1.19: Coupling coefficient k^2 of plate thickness mode (shear and longitudinal) based on AlN film with inclined c-axis (21)

one that is sensitive to both environment and to the factor defined by functionalization layer.

The functional layer used to immobilize specific molecules, might do more than simply attach these molecules. Chemical reactions may happen that change elastic and viscous properties, as well as the thickness and density. For example, a change in stiffness and thickness may shift resonance frequency. In the work of N. Schuwer (22), the shift of the resonance frequency occurred due expansion or compression of the polymer brushes layer as a reaction on change of the pH of the liquid (fig. 1.20)

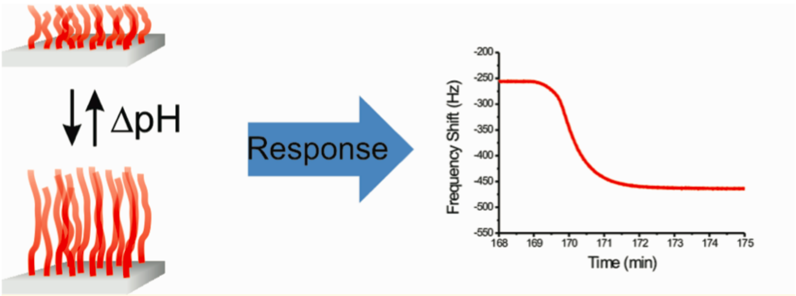

Figure 1.20: Sensing pH level in the liquid media using QCM with polymer brushes layer that is sensitive to pH, (22)

Last but not least, the change of viscosity of the liquid leads to a change of resonance frequency, too. The reason is that the viscosity defines the mass of the liquid involved in the vibration motion (see fig. 1.21). It's actually the way the QCM or other transducers can be a tool to measure the viscosity and it has been studied by several groups (23), (24).

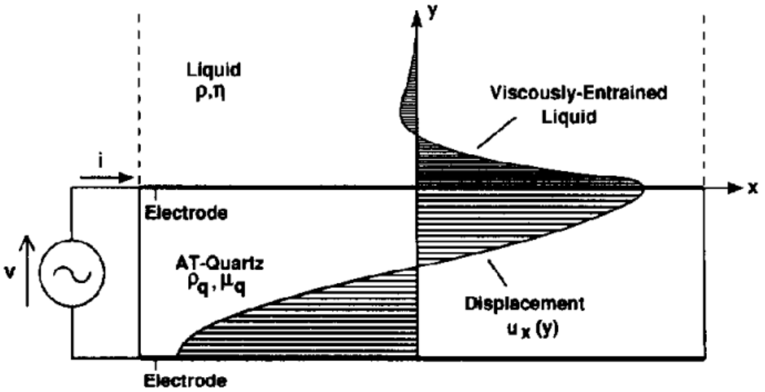

Figure 1.21: Cross-sectional view of a smooth TSM resonator with the upper surface contacted by a liquid. Shear motion of the smooth surface causes a thin layer of the contacting liquid to be viscously entrained, (23)

1.5 Goal of this thesis

As outlined in the previous sections, shear mode BAW resonator have a high potential for sensor applications. The growth of films with tilted c-planes appears to be rather difficult to up-scale for industrial production. It would be more interesting to use industrially available processes and thin films, such as (0002)AlN and (0002)ZnO.

The goal of this thesis is to study design and fabrication of shear mode BAW resonators that are feasible within existing industrial fabrication tools and materials, in particular (0002)AlN films.

2

Coupling the shear displacement in c-axis oriented AlN thin films

As mentioned in introduction, a shear strain in (0001) oriented AlN thin films is achieved through e_{15} by applying an electric field E_1 parallel to any direction in the film plane.

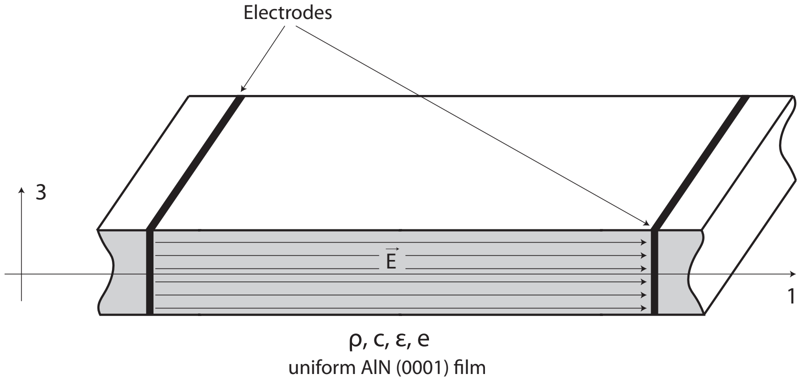

Figure 2.1: Thin film of AlN with in-plane electric field inside (ideal situation)

First, the ideal situation as given in fig. 2.1 was studied. The in-plane electric field causes a pure shear strain. In the following article, the exact, analytical one-dimensional (1D) model was treated, and admittance of an idealized capacitor was derived as follows:

$$Y = j\omega C_0(1 + k_{15}^2 \frac{tan(\varphi)}{\varphi}), \qquad \varphi = \frac{k_3 l}{2}, \tag{2.1}$$

where C_0 is the static capacitance between the electrodes, l is the thickness of the film and wave number $k_3 = \omega\sqrt{\frac{\rho}{c_{55}^E}}$ is defined through the mechanical properties of the film.

The coupling constant k_{15} is obtained as:

$$k_{15}{}^2 = \frac{e_{15}{}^2}{c_{55}^E \epsilon_{11}^S} \tag{2.2}$$

. The fundamental resonance occurs when the thickness of the film is equal to half the wavelength of the wave.

The theoretical value of the coupling coefficient as given by the formula (2.2) amounts to 2.5% for AlN. However, the idealized electrodes buried in AlN are very difficult to realize. Also it is not practical to obtain in-plane fields by very much distant electrodes, because the electrical impedance would be too large. A realistic device employs interdigitated electrodes as shown in fig. 2.2. In this way, the electrical impedance is kept at reasonable values. Between each pair of IDT fingers, an in-plane electric field will be induced and a shear strain is produced locally, which is expected to excite a shear mode excitation between the finger pairs (see fig. 2.2). However, the two adjacent pairs of IDT induce an electric field that is in anti-phase, so the motion of the film within these regions will be in anti-phase too. Overall, the regions between the fingers will be vibrating in a shear mode, with the exclusion of the regions below the electrodes.

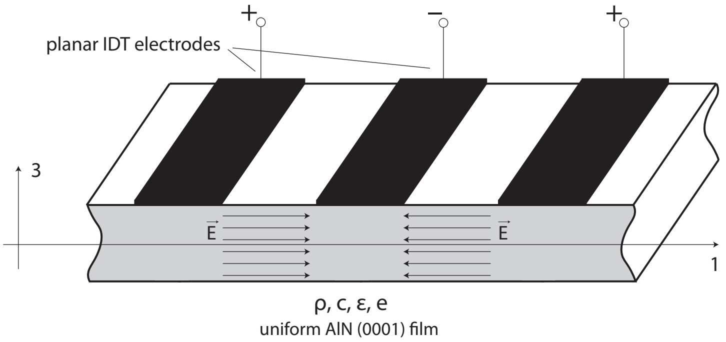

Figure 2.2: Using the IDT electrodes to create in-plane electric field locally in the film

A demonstration device was designed and fabricated. Acoustic decoupling from the substrate was obtained by the use of a Bragg reflector between substrate and active AlN layer. This reflector was optimized for the sought shear mode. Such decoupling is commonly called the solidly mounted resonator (SMR) design. It has the advantage of a more rugged structure than the membrane approach. In our case, it additionally helped to amplify the shear vibrations. The Bragg reflector consisted of 5 pairs of layers of AlN and SiO_2, a solution known from the past (25) and (26). A 3-dimensional view of the design is shown in fig. 2.3

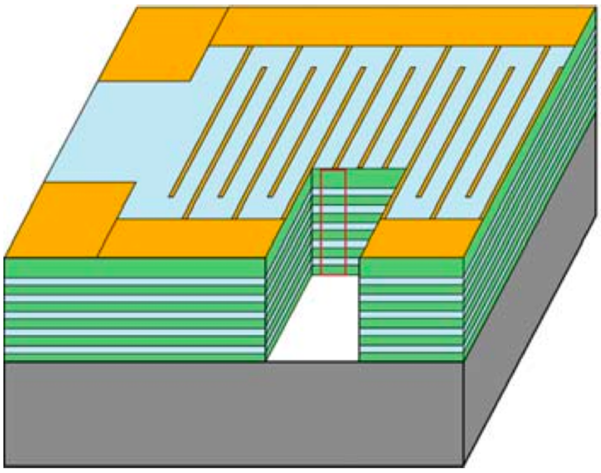

Figure 2.3: Schematic drawing of SMR shear mode BAW device with interdigitated electrodes

Combined finite element and periodic boundary element modeling (FEM-BEM) were employed to analyze the motion of the IDT device. The FEM-BEM confirms the in-plane motion of the regions located between electrodes (see fig. 2.4) as well as that e_{15} coefficient is essential for excitation of such wave. As mentioned, the film doesn't vibrate in shear mode as a whole, but locally between electrodes. It can be seen that Bragg mirror prevents the penetration of the wave to the substrate. Electrodes are moving up and down, that is a source of losses of acoustic energy from resonator into the liquid once it's immersed.

Following paper, "Shear mode bulk acoustic wave resonator based on c-axis oriented AlN thin film" is devoted to detailed theoretical investigation of the device shown in fig. 2.2 and to its fabrication and experimental characterization.

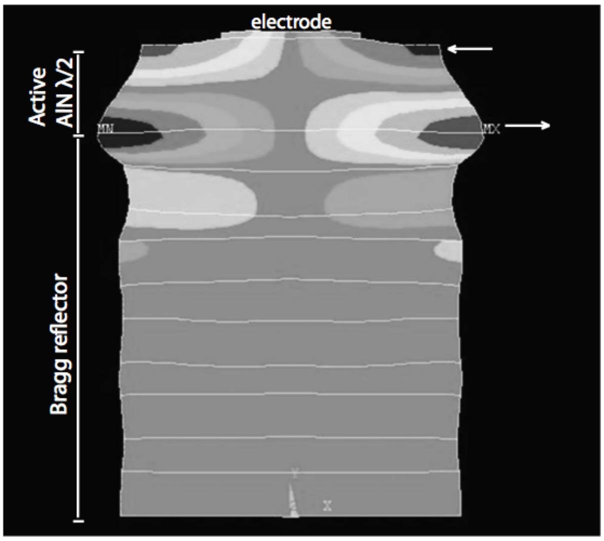

Figure 2.4: FEM-BEM simulation: motion of the device at resonance frequency

SHEAR MODE BULK ACOUSTIC WAVE RESONATOR BASED ON C-AXIS ORIENTED ALN THIN FILM

Evgeny Milyutin, Sandrine Gentil and Paul Muralt

Preprint for Journal of Applied Physics

I. IINTRODUCTION

In recent years, the rise of mobile communication has stimulated the development of thin film bulk acoustic wave resonators (TFBARs) to realize rf filters for the low gigahertz frequency range.[1,2] Such resonators are also potentially very interesting for gravimetric sensors,[3,4] which are traditionally based on AT-cut quartz plates.[5] The decrease in resonator thickness when passing from a single crystal to a thin film leads to a very marked increase in frequency. Theoretically, and also evidenced by experiments,[6] the relative frequency shift by mass loading increases linearly with frequency. The signal-to-noise ratio, however, does not increase as much. A recent comparative study showed a factor of 2 improvement of a TFBAR device as compared to a quartz microbalance device.[7] TFBARs of the type utilized in telecommunication devices are based on a longitudinal wave. The AlN or ZnO films are grown on metal electrodes and are *c*-axis oriented. The electric field is created by means of a parallel plate capacitor that points along the *c*-axis. This geometry leads to a piezoelectric stress excitation along the *c*-axis by means of the e_{33} piezoelectric coefficient. The border reflections lead to trapping of a wave running along the *c*-axis. This longitudinal mode is optimal for rf filters because the highest piezoelectric coupling is achieved in this way. The same geometry can be used for sensors operated in air.[3,4,6] However, sensors for immersed operation are more attractive because they are useful for biomedical and many environmental applications. In liquids, longitudinal waves are very much damped by acoustic emission into the liquid. For this reason it is better to use shear waves, which do not propagate in liquids.

Many efforts have recently been made to grow AlN and ZnO thin films whose *c*-axis is tilted with respect to the film normal.[8–11] In this way, the shear coupling through the e_{15} piezoelectric coefficient comes into play in parallel plate capacitors and a mixed, shear, and longitudinal excitation is achieved. The fact that the shear wave exhibits a much lower sound velocity than the longitudinal wave allows for trapping the shear mode selectively, thus suppressing the longitudinal mode to a large extent. The disadvantages of this method are associated with achieving a homogeneous *c*-axis tilt across the wafer. The design of the magnetron source for homogeneous tilting is not evident and certainly does not correspond to a standard tool as currently optimized by industry, which by now achieves impressive results in terms of uniformity of thickness and piezoelectric coupling of *c*-axis oriented AlN.

In this work, we investigate another solution. It is sought to use standard AlN thin films that are useful for rf filters, but instead we tilt the electric field into the plane of the film by using interdigitated electrodes (IDEs). We will first show that a BAW mode of shear symmetry can indeed be generated in this way. Important requirements for the realization of such a structure are: growth of good piezoelectric thin films on an insulator such as a SiO_2 layer and a design that avoids mixing of the desired shear bulk mode with Rayleigh, Love, or Lamb waves. We do not use a membrane structure but employ an acoustic reflector to suppress emission into the substrate. This eliminates the occurrence of Lamb waves. Attempts to create such resonators based on ZnO were very recently published by Corso *et al*.[12] A *Q*-factor of about 550 in air and the capability of operating in liquid were reported without, however, showing details for the latter. These authors employed a reflector based on W layers, which short circuit the electric field, leading to strong vertical components of the electric field below the electrodes, and only weak horizontal fields in between the two electrodes. According to their simulations, the active layer operates not in a shear mode but in some other mode type, probably due to transverse strain in the film plane (e_{31} coefficient). In our work we use a pure dielectric reflector stack AlN/SiO_2, which leads to an electric field that is mainly along the *x*-axis in the plane of the film. In addition, we extended the two electrodes to a larger IDE system.

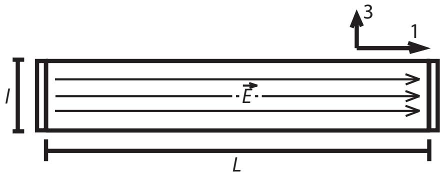

II. THEORETICAL BACKGROUND

A. Concept

The shear mode sought requires the exciting electric field to be perpendicular to the propagation direction. This is a major difference in the traditional longitudinal TFBAR. For this reason the major derivation steps are presented in this section to show that the existence of this mode also follows from simple analytical modeling (our approach differs to that of Corso *et al.*[12]). For an AlN plate with its *c*-axis oriented perpendicular to plane, Newton's wave equation is combined with Maxwell's equations including the electromechanical coupling,

$$\rho \ddot{u}_i = \frac{\partial T_{ij}}{\partial x_j}, \tag{1}$$

$$T_{ij} = c^E_{ijkl} S_{kl} - e_{nij} E_n, \tag{2}$$

$$D_n = \epsilon_{nj} E_j + e_{nkl} S_{kl}, \tag{3}$$

$$\text{rot } \vec{E} = 0, \quad \text{div } \vec{D} = 0, \tag{4}$$

where u_i, T_{ij}, S_{ij}, E_j, and D_n are mechanical displacement field, stress and strain tensors, electric field intensity, and electric displacement filed, respectively.

As usual, the upper index in c^E_{ijkl} denotes the condition at constant electric field. In the following, we will use reduced index notation, and understand c_{ij} to be for constant field. In the applied coordinate system, direction 3 points perpendicular to the film plane and is at the same time the sixfold polar axis of the AlN single crystal grain and the long growth direction of the grain. The overall symmetry of the polycrystalline textured film is cylindrical, and results in the same matrix symmetry as for single crystal AlN.

For an electric field pointing along the x_1 direction (Fig. 1), Eq. (2) becomes

$$T_i = c_{ij} S_j, \tag{5}$$

where $i,j = 1,2,3,4,6$ and

$$T_5 = c_{55} S_5 - e_{15} E_1. \tag{6}$$

We can see that only the S_5 strain of the film is coupled with the electric field E_1 and that this deformation is not coupled with any other deformation. Hence the excited wave contains only displacements corresponding to S_5.

For a clamped thin film, S_5 is equal to $\partial u_1 / \partial x_3$. Introducing the Maxwell equations, it follows that all variables depend on x_3 only. Then by solving Maxwell's equations and Newton's equation together with the equations of electromechanical coupling, we obtain

$$\frac{\partial E_1}{\partial x_3} = 0, \quad \frac{\partial E_1}{\partial x_1} = 0, \tag{7}$$

$$\rho \ddot{u}_1 = \frac{\partial T_5}{\partial x_3}, \tag{8}$$

$$\frac{\partial T_5}{\partial x_3} = c_{55} \frac{\partial S_5}{\partial x_3} = c_{55} \frac{\partial^2 u_1}{\partial x_3^2}. \tag{9}$$

So,

$$\rho \ddot{u}_1 = c_{55} \frac{\partial^2 u_1}{\partial x_3^2}. \tag{10}$$

The last equation describes shear waves that propagate in the x_3 direction [wave vector $(0, 0, k_3)$] and with displacement in the x_1 direction. The current and the voltage between electrodes can easily be derived and admittance $Y = I/U$ is finally equal to

$$Y = j\omega C_0 \left(1 + \frac{e_{15}^2}{c_{55}\epsilon_{11}} \frac{\tan(\varphi)}{\varphi} \right), \quad \varphi = \frac{k_3 l}{2}, \tag{11}$$

where C_0 is the static capacitance between the electrodes and wave number $k_3 = \omega\sqrt{\rho / c_{55}}$. Resonances are observed for infinite values of $\tan(\varphi)$. At the antiresonance frequency the admittance becomes zero. The difference between the resonance and antiresonance frequencies is proportional to the piezoelectric coupling constant $e_{15}^2 / c_{55}\epsilon_{11}$. Note that the value of e_{15} does not affect the resonance frequency but strongly affects the antiresonance frequency. This is the result of the fact that c_{55} at constant E-field is relevant for the wave propagation, as follows from Maxwell's Eq. (4). Our result contradicts the theory presented by Corso *et al.*[12] in which the wave number is derived as c^D dependent.

B. Field element modeling

As a first task infinite element method (FEM) simulation, we confirmed our theoretical results. An in-plane ac electric field is produced in a slab of AlN(001), as in Fig. 1, allowing motions in the field direction (index 1) only. The resulting displacements at resonance are exactly those expected of a pure shear mode (Fig. 2). The resonance frequency was found to obey exactly Eq. (11) of the analytical $1-d$ model. The coefficient e_{15} was varied from one to three times the literature value of $-0.48(C/m^2)$ for AlN. The dependence of resonance and antiresonance frequencies are depicted in Fig. 2, showing that the behavior of the analytical model is exactly reproduced.

In practice, it is difficult to create a pure in-plane electric field, because it would require very precise patterning of the active AlN film without avoiding completely stray fields. A more practical way of supplying in-plane electric fields is the use of IDEs. In this geometry, the electric field has opposite directions in neighboring IDE sections leading to an antiphase motion in adjacent regions. This will lead to some perturbation from the ideal case. For this reason, FEM modeling has been carried out to quantify the details of the resulting motion. The silicon substrate was included using the boundary element method (BEM). Apart from the regions of

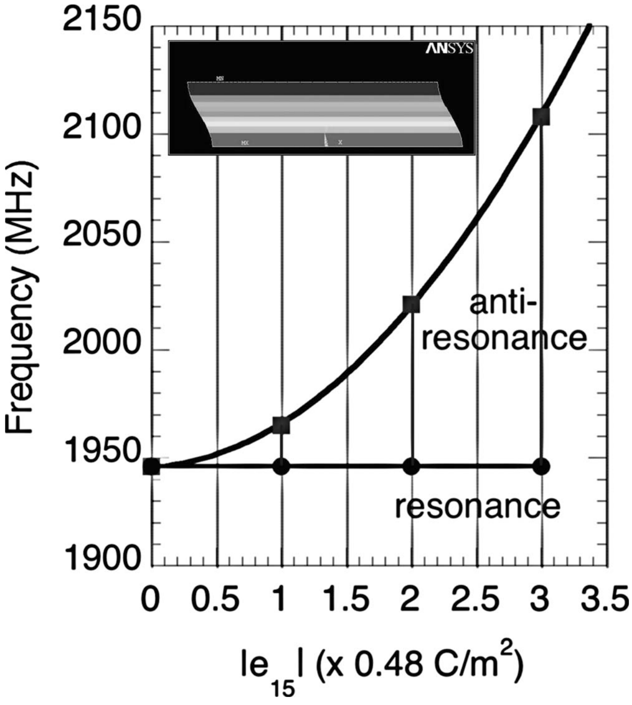

FIG. 2. Resonance and antiresonance frequencies as a function of the piezoelectric coefficient e_{15}, as obtained from FEM simulation. The insert shows the motion shape, i.e., the u_1 displacement intensity in a contour plot.

electrodes, FEM-BEM modeling shows that the electric fields of the IDEs lead to an excitation that is close to the ideal one, as used for the analytical calculation.

The properties of the solidly mounted resonator with a periodic planar electrode system were simulated with the help of ANSYS and the FEM-BEM coupling module from Microsonics. A half-period of the mechanical response at resonance frequency is shown in Fig. 3. The electrode is located in the center on the top of the structure, the bottom border is clamped to a semi-infinite substrate, and half-period conditions are established along the horizontal axis. The fact that we are dealing with shear waves can easily be ascertained from the type of resonant motion within the active AlN layer.

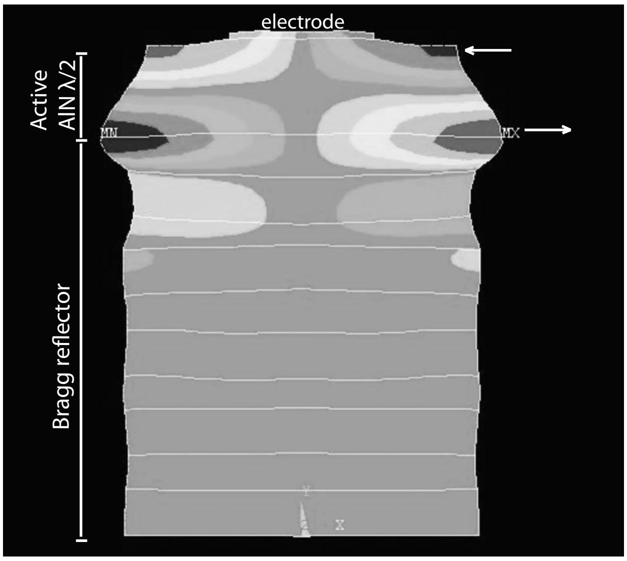

FIG. 3. FEM-BEM simulation: motion of the device at resonance frequency.

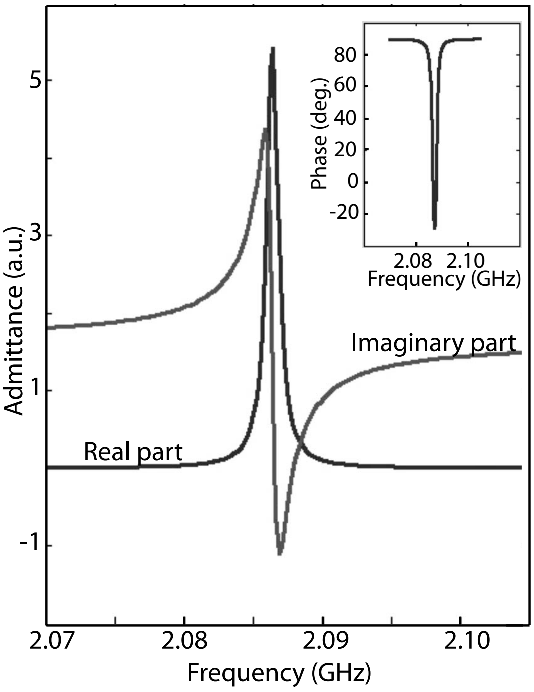

It is important to emphasize several peculiarities as follows. (1) A shear mode thickness resonance can be seen between the electrodes (at the left and right of the center of the structure). (2) The most intense motion is concentrated in the top layer of AlN and the amplitude decreases strongly within the Bragg reflector. (3) The displacement of the AlN surface between electrodes is mostly horizontal, which is very important for sensors in liquid applications. (4) There are small vertical displacements of the electrode, which are expected to contribute to losses in immersed operation. The simulated electrical admittance is shown in Fig. 4, from which a Q-factor of 2000 and coupling coefficient of 0.2% are derived.

The material constants used for AlN are given in Table I (from Ref. 13). The following material constants for SiO_2 were also used: density of 2200 kg/m^3, Poisson's ratio of 0.171, and Young's modulus of 70 GPa. Electrical resistivity of electrodes and mechanical losses of materials were not taken into account. The finite quality factor of the resonance results entirely from the acoustic emission into the substrate through the Bragg grating. The thickness of the electrode has only a minor effect on the resonance frequency. The latter was found to be 2086 and 2074 MHz for 100 and 150 nm thickness, respectively.

III. FABRICATION

A top view and a cross-sectional view of a typical device are shown in Figs. 5 and 6. The device consists of a reflector composed of five pairs of SiO_2 and AlN layers (similar as in Ref. 14). Such reflectors were originally proposed and fabricated by Lakin *et al.*[2] for rf filters based on the longitudinal

TABLE I. Properties of AlN used in FEM-BEM simulation.

Stiffness constants (GPa)				Piezoelectric coefficient (pm/V)			Density (kg/m^3)
c_{11}^E	c_{12}^E	c_{13}^E	c_{55}^E	d_{31}	d_{33}	d_{15}	ρ
345	125	120	118	−2.64	5.53	−4.07	3260

mode. They require more layers than the commonly used SiO_2/W type, but have the advantage of being electrically insulating. As explained earlier, this is extremely important for the IDE shear mode excitation. The critical issue in reflector stack deposition is the stress control to avoid accumulation of bending moments, as described in an earlier work of the EPFL group,[15,16] and later by the CSEM group.[17] We deposited the AlN thin films by pulsed dc reactive magnetron sputtering[18,19] and the SiO_2 films by rf sputtering at a temperature of 300 °C. The stress within AlN films can be adjusted more easily than that within SiO_2. For this reason, the AlN process was optimized to compensate the SiO_2 film stress of −200 MPa. The active $\lambda/2$ AlN layer is deposited on the top SiO_2 layer of the reflector. A very thin layer of SiO_2 on top of the active AlN layer was used to protect the AlN from being attacked by the developer solution during subsequent photolithography for aluminum electrode patterning. The 150 nm thick aluminum electrodes with chromium adhesion layers were evaporated at room temperature, and patterned by means of a lift-off process using a double layer resist (lift-off resist (LOR)+AZ1512 photo resist). This device thus needs only one photolithography step, and not two as the simplest possible TFBAR.

All devices were designed to have equal static capacitance, but at the same time the distance between the centers of neighboring electrode fingers was varied from 6 to 10 μm in order to test the resonance frequency dependence on the IDE dimensions. In case of a pure shear thickness mode excitation no such dependence must be observed.

IV. EXPERIMENTAL RESULTS AND DISCUSSION

The performance of the resonators was assessed using a Cascade Microtech probe and HP Network analyzer in air and in silicon oil [Poly(dimethylsiloxane), viscosity of 0.65 cS]. Typically, the resonance frequency of devices operated in air was between 1.8 and1.9 GHz, depending on the position on the wafer. This effect is due to a nonuniform AlN film thickness. The resonance frequency was found to change very weakly with increasing distance between adjacent finger electrodes. The change amounted to less than 2% when the distance between the fingers was almost doubled, from 6 to 10 μm (Fig. 7). The devices for this study were built near each other on the wafer, thus having equal thickness of all layers (active layer: 1.55 μm). The thickness mode nature of the resonance is thus confirmed, excluding any wave dependent on IDE periodicity. The small change in frequency with short electrode distance must be assigned to the stronger admixture of up and down motions below the center of the electrode, leading to a stiffening.

The sensitivity of the sensor depends crucially on the width of the resonance curve, because the shift of the resonance curve is more precisely measured when the resonance peak is narrower. This width is inversely proportional to the quality factor Q, which is evaluated as the ratio between full width at half maximum of the conductance peak, as a function of frequency to the resonance frequency. The maximum Q-factor was thus determined to be 870 in air (Fig. 8). This Q-factor is smaller than the simulated one, since the latter did not take into account material losses.

The coupling coefficient (k^2) amounted to 0.15% in this case, which is in agreement with simulations. As compared to FEM and analytical calculations, the experimental resonance frequencies turned out to be around 10% lower. It is possible that the shear stiffness of a columnar microstructure is smaller than that of an epitaxial film, as investigated by Tsubouchi *et al.*,[13] whose value of $c_{55}=118$ GPa was applied in FEM-BEM simulations.

The conductance curve of the device immersed in silicon oil is shown in Fig. 9. The peak amplitude is decreased as well as the Q-factor and a small shift of the resonance frequency (2 MHz) takes place. This shift may have two pos-

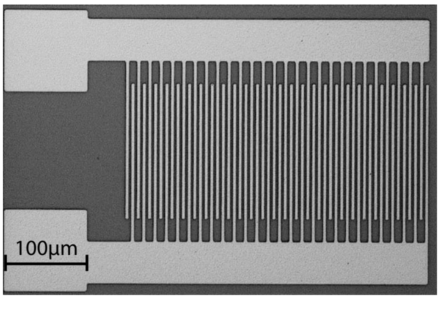

FIG. 5. Top view image of the typical resonator fabricated in this work.

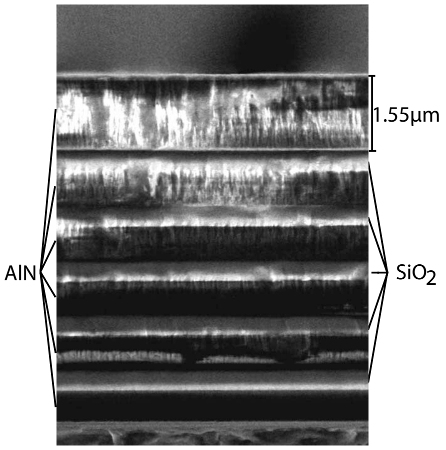

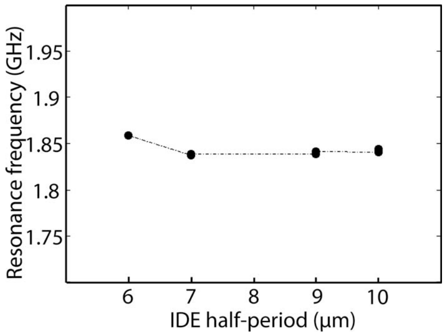

FIG. 7. Changes in resonance frequency vs IDE period.

sible origins. The first one can be a loading effect due to the local piston motion of the electrode regions, which contain the previously discussed longitudinal (i.e., vertical) wave component. As a second origin we can see surface roughness or asperities. As the liquid has some finite viscosity, it is dragged to a certain depth, and thus the shear wave is loaded as well. The *Q*-factor measured in immersed operation amounted to 260. According to our simulation calculations comparing the actual resonator with an ideal homogeneous shear resonator, the additional damping is mostly due to the piston movement in the electrode finger regions. However, the achieved *Q*-factor in the liquid is still high enough for sensor applications. In comparison, Wingqvist *et al.*[9] reported a *Q*-factor of 150 achieved by a shear mode thin film bulk acoustic resonator based on inclined *c*-axis AlN, operated at a lower frequency of 1.2 GHz.

In the future, the device will be completed as a sensor. It will be covered by a SiO_2 layer, on top of which an organic immobilization layer will be grafted. The resonant frequency is expected to shift when the surface mass density, or stiffness of this layer, changes upon adsorption of or reaction with organic molecules from the liquid (mostly water). The immobilization layer may contain, for instance, antigenes that attach the corresponding antibodies.

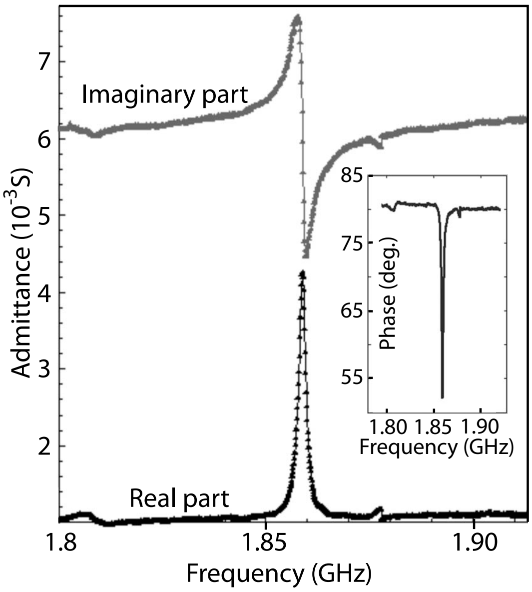

FIG. 8. Measured admittance curve (real and imaginary parts) for a device with an IDE period of 6 μm and a finger width of 3 μm.

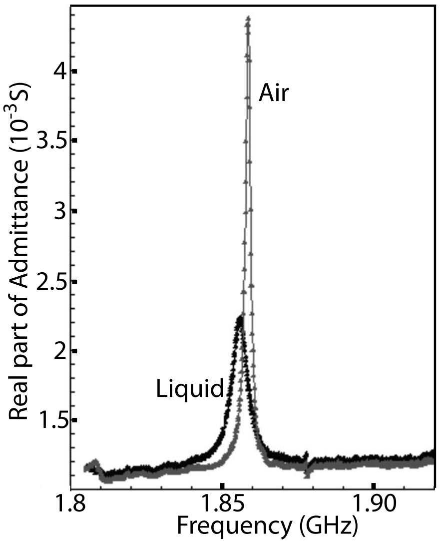

V. CONCLUSIONS

We have shown by a simple one-dimensional model that standing shear bulk acoustic waves can be excited in a piezoelectric slab with an in-plane electric ac field. In contrast to the well-known longitudinal bulk acoustic waves, their resonance frequency depends on the stiffness at constant *E*-field and not at constant *D*-field. The FEM simulation was extended to a full two-dimensional simulation model for a realizable device based on IDEs, including an acoustic reflector. A specific boundary element method was applied to deal with the boundary condition underneath the reflector. The model confirmed that IDEs excite mainly the desired shear mode, however, with a deviation from the ideal motion below the electrodes. We succeeded in the fabrication of test devices that show resonance frequencies close to the calculated ones, and that vary only slightly with the electrode spacing, as expected for such modes. Importantly for sensors, the immersion into a low-viscosity siloxane liquid still allowed for a high *Q*-factor of 260, and only slightly shifted the resonance frequency. The results achieved and the simplicity of the fabrication of such devices show their potential as gravimetric sensors for biomedical and environmental applications.

ACKNOWLEDGMENTS

The support of the Swiss National Science Foundation (Contract No. 20021-112204) and the Swiss Center of Competence on Materials is gratefully acknowledged. The device fabrication was carried out in the central micromachining facility of EPFL.

[1] R. C. Ruby, P. Bradley, Y. Oshmyansky, A. Chien, and J. D. Larson, Proceedings of the IEEE Ultrasonics Symposium (IEEE, Atlanta, 2001).

[2] K. M. Lakin, K. T. McCarron, and R. E. Rose, Proceedings of the IEEE Ultrasonics Symposium, Seattle, WA (IEEE, Washington, 1995).

[3] R. Gabl, H.-D. Feucht, H. Zeininger, G. Eckstein, M. Schreiter, R. Primig, D. Pitzer, and W. Wersing, Biosens. Bioelectron. **19**, 615 (2004).

[4] M. Benetti, D. Cannata, F. Di Pietrantionio, V. Foglietti, and E. Verana, Appl. Phys. Lett. **87**, 173504 (2005).

[5] E. Gizeli, in *Biomolecular Sensors*, edited by E. Gizeli and C. R. Lowe (Taylor & Francis, London, 2002).

[6] S. Rey-Mermet, R. Lanz, and P. Muralt, Sens. Actuators B **114**, 681 (2006).

[7] J. Weber, W. M. Albers, J. Tuppurainen, M. Link, R. Gabl, W. Wersing, and M. Schreiter, Sens. Actuators, A **A128**, 84 (2006).

[8] J. Bjurstrom, G. Wingqvist, and I. Katardjiev, IEEE Trans. Ultrason. Ferroelectr. Freq. Control **53**, 2095 (2006).

[9] G. Wingqvist, J. Bjurstrom, L. Liljeholm, V. Yantchev, and I. Katardjiev, Sens. Actuators B **123**, 466 (2007).

[10] T. Yanagitani, M. Kiuchi, M. Matsukawa, and Y. Watanabe, IEEE Trans. Ultrason. Ferroelectr. Freq. Control **54**, 1680 (2007).

[11] T. Yanagitani, M. Kiuchi, M. Matsukawa, and Y. Watanabe, J. Appl. Phys. **102**, 024110 (2007).

[12] C. D. Corso, A. Dickherber, and W. D. Hunt, J. Appl. Phys. **101**, 054514 (2007).

[13] K. Tsubouchi, K. Sugai, and N. Mikoshiba, in Proceedings of the 1981 Ultrasonics Symposium, edited by B. R. McAvoy (IEEE, New York, 1981). Vol. 1, p. 375.

[14] R. Lanz and P. Muralt, IEEE Trans. Ultrason. Ferroelectr. Freq. Control **52**, 936 (2005).

[15] M.-A. Dubois, P. Muralt, and V. Plessky, Proceedings of the IEEE Ultrasonics Symposium, Lake Tahoe, 1999, Vol. 2, pp. 907–910.

[16] M.-A. Dubois, P. Muralt, H. Matsumoto, and V. Plessky, Proceedings of the IEEE Ultrasonics Symposium, Sendai, Japan, 1998, pp. 909–912.

[17] M.-A. Dubois, Proceedings of the MEMSWAVE, Toulouse, 2003 (unpublished).

[18] M.-A. Dubois and P. Muralt, Appl. Phys. Lett. **74**, 3032 (1999).

[19] M.-A. Dubois and P. Muralt, J. Appl. Phys. **89**, 6389 (2001).

3

Modulation of piezoelectric properties to excite a pure shear mode

In Chapter 2 we treated interdigitated transducers made from homogeneous, c-axis oriented AlN thin films having everywhere the same polarity. We have seen that the excited shear strains are opposite to each other in neighboring sections. This resulted in antiphase vibrations of adjacent regions, and, as a consequence, in an up and down motion of the electrodes. Hence, shear mode could be excited only in the regions between electrodes and pure shear displacement of the whole film could not be achieved. The question was thus how to modify the device in order to obtain a pure shear mode, under the condition of keeping the c-axis orientation of the AlN thin film.

The idea came up to turn the polarity of the AlN film when going from one section to the next. In this way, the piezoelectric coefficient changes sign in phase with the in-plane electric field, and the shear strain would be the same in all sections. As a generalization of this concept, one can assume to have different piezoelectric properties of adjacent sections, as indicated in fig. 3.1 . That breaks the symmetry of the structure and removes constraints for the coupling in-plane plane shear waves to the electric field of the IDT electrode. The larger the difference between piezoelectric properties of two types of AlN, the higher the electromechanical coupling of the device. The idealized one-dimenensional model leads indeed to the simple result of:

$$k_t^2 \propto (e_{15}^{(1)} - e_{15}^{(2)})^2 \tag{3.1}$$

Theoretical description of such a device is given in the article "Electro-Mechanical Coupling in Shear-Mode FBAR With Piezoelectric Modulated Thin Film", reproduced on the following pages.

Such a concept can be realized in both, the membrane structures or solidly mounted resonators using Bragg reflectors (as described in Chapter 4). It can be argued, however, that the coupling coefficient is lower for SMR devices due to parasitic capacitances caused by the reflector layers (even if they are dielectric).

This design was also patented. The patent is described on the following pages.

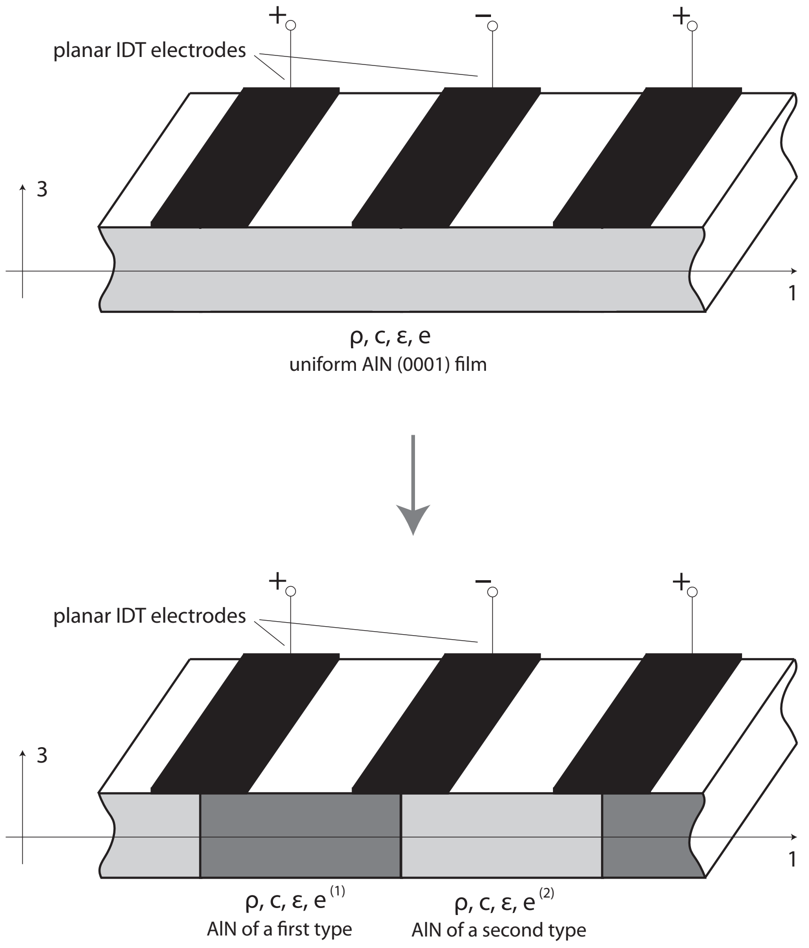

Figure 3.1: Modification of the design if using AlN of two different types

ELECTRO-MECHANICAL COUPLING IN SHEAR-MODE FBAR WITH PIEZOELECTRIC MODULATED THIN FILM

E. Milyutin and P. Muralt

Preprint for IEEE Transactions on Ultrasonics, Ferroelectrics and Frequency Control

I. Introduction

The use of quartz crystal microbalances (QCM) as gravimetric sensors for biomedical applications clearly shows the potential of this class of sensors, and has triggered the search for further types of shear acoustic wave resonators operating at higher frequencies, typically with SAW devices [1], or with thin film bulk acoustic wave devices [2]. Biomedical sensors must work in a liquid, and thus require the use of shear vibrations to avoid losses by acoustic radiation into the liquid. Because the relative sensitivity increases with working frequency, resonators operated at gigahertz frequencies are very promising for pushing down detection limits, sizes, and costs of the devices [2]. Shear mode thin film bulk acoustic resonators (TFBARs) based on AlN or ZnO thin films with tilted and parallel c-axis are studied by several groups as an alternative to QCM [3]–[5]. These works show promising results, however, deposition of tilted c-axis thin films is difficult to achieve with uniform properties, and constitutes a major deviation from standard (001) thin film deposition hardware as introduced in industry. Recently, we proposed the combination of standard c-axis oriented films with interdigitated electrodes (IDT electrodes) to excite a shear mode based on the piezoelectric coefficient e_{15} [6]. Attempts to create a similar device based on ZnO were also performed by Corso *et al.* [7]. The excited mode shows a substantial shear strain component. However, the alternation of electric field direction between the fingers leads to an alternate direction of the shear displacement, which results in a rather elliptical motion with a peaking

In this work, we present an improved device design that operates in a pure shear mode and is nevertheless based on a c-axis oriented AlN film. The idea is to alternate the sign of the piezoelectric coefficients in phase with the applied electric field. In the ideal case, the direction of the polar axes of AlN is switched by 180° exactly in the center line of each electrode finger, see Fig. 1(a). Similar ideas of alternation of piezoelectric coefficients to excite longitudinal and shear BAW were previously investigated [8]–[10] by using ferroelectric substrates and poling them locally to achieve ferroelectric domains with opposite polarities, eventually removing the poling electrodes and applying new ones. The presence of difference domains was confirmed by etching tests, and the approach was applied to demonstrate a transducer. However, no resonators were studied as is done in the current work. Moreover, no theoretical models were developed to describe the wave and the effect.

As a first step, we developed an analytical model describing the device shown in Fig. 1(a). It allows for the derivation of the coupling coefficient and the resonance frequency. For its verification, finite element modeling was performed as well. Both approaches were in good agreement. FEM particularly confirmed that such a device operates in a pure shear mode. A first realization of such a resonator based on a piezo-modulated structure was presented recently [11], [12].

II. 1-D Analytical Model

The case of a uniform (001)-oriented AlN thin film being excited to shear mode vibration by a homogenous in-plane electric field is described in our previous work by an analytical model [6]. The admittance Y was obtained as

$$Y = i\omega C_0\left(1 + \frac{e_{15}^2}{c_{55}^E \varepsilon_{11}^S}\frac{\tan\left(\frac{kh}{2}\right)}{\left(\frac{kh}{2}\right)}\right), \qquad (1)$$

where ω is the angular frequency, c_{55}^E is the shear stiffness at constant electric field E, h is the plate thickness, $k = \omega/v_s$ is the wave vector, and $v_s = (c_{55}^E/\rho)^{1/2}$ is the shear wave velocity. The resonance frequency is given by the shear wave velocity $v_s = (c_{55}^E/\rho)^{1/2}$ and the plate thickness only. This is in contrast to the longitudinal wave resonance frequency, which also depends on the piezoelectric coefficient. A homogeneous in-plane electric field is technically not realizable, which hampers the applicability of (1).

Now, let's consider the case of a thin film that is divided into periodically arranged sections that are identical in all respects, aside from their piezoelectric properties, as denoted by the different indexes $e^{(1)}$ and $e^{(2)}$ in Fig. 1(b). For the sake of simplicity, the electric field in the film is

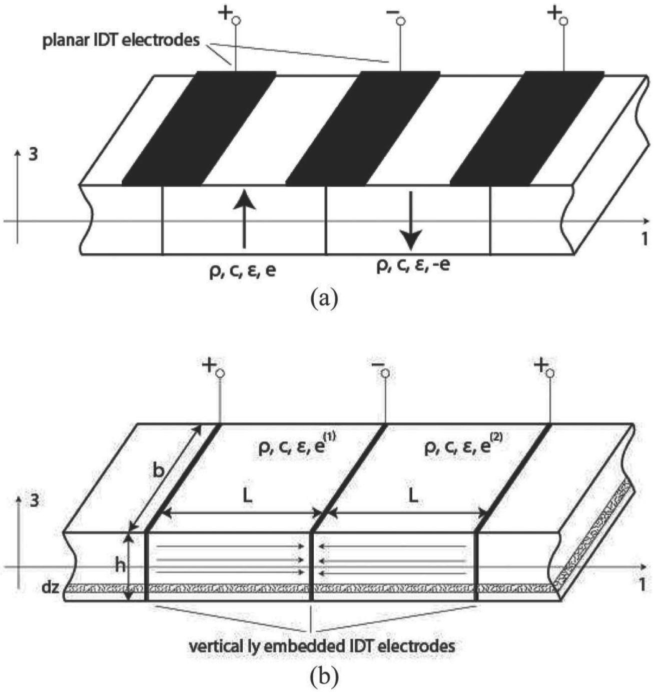

Fig. 1. (a) Design of an experimentally realizable device with planar IDT electrodes. The AlN polarity is switched by 180° (ideal case of polarity variation) in the center of each electrode. (b) Design of the model device with embedded IDT electrodes (arrows indicate the electric field), separated by the distance L.

induced by ideal interdigitated electrodes that are vertically embedded into the film.

The stress induced by the electric field in each piece can be described by the equations of state, considering that $E_1^{(2)} = -E_1^{(1)} = -E_1$:

$$\begin{aligned} T_5^{(1)} &= c_{55}^E S_5 - e_{15}^{(1)} E_1 \\ T_5^{(2)} &= c_{55}^E S_5 + e_{15}^{(2)} E_1. \end{aligned} \tag{2}$$

The equation of motion of the symmetric slabs swinging against each other in the film that are shaded in Fig. 1(b) can be written as follows:

$$\rho \ddot{u}_1 (2Lb\mathrm{d}x_3) = \frac{\partial T_5^{(1)}}{\partial x_3}(Lb\mathrm{d}x_3) + \frac{\partial T_5^{(2)}}{\partial x_3}(Lb\mathrm{d}x_3), \tag{3}$$

where the left side of the equation is the mass of the slab multiplied by its acceleration in the x_1 direction and the right side of the equation is the force applied to the slab, written in a way similar to that in [6], but as a sum of two terms: the first term is the force to the left half of the slab and the second term is the force to the right half of the slab. This sum is the total force acting on the complete period of length $2L$. From (2), we find

$$\rho \ddot{u}_1 \mathrm{d}x_3 = \frac{\partial}{\partial x_3}\left(\frac{T_5^{(1)} + T_5^{(2)}}{2}\right)\mathrm{d}x_3 = \frac{\partial T_5^{(\mathrm{av})}}{\partial x_3}\mathrm{d}x_3. \tag{4}$$

Here, $T_5^{(\mathrm{av})}$ represents the average stress in the film slab over one period $2L$. From (2), $T_5^{(\mathrm{av})}$ is equal to

$$T_5^{(\mathrm{av})} = c_{55}^E S_5 - \left(\frac{e_{15}^{(1)} - e_{15}^{(2)}}{2}\right)E_1. \tag{5}$$

This formula shows us that when the piezoelectric coefficients $e_{15}^{(1)}$ and $e_{15}^{(2)}$ are identical, there is no coupling between the interdigitated electrodes and no homogeneous shear deformation of the film over a distance $2L$.

Solving equation of motion (3), taking into account that $\partial E_1/\partial x_3 = 0$, as described in [6], and the fact that the displacement is asymmetrical in x_3, we come to the solution:

$$u_1 = A\sin(kx_3)\exp(i\omega t). \tag{6}$$

Constant A can be found from the boundary conditions, $T_5^{(\mathrm{av})}\big|_{x_3=\pm h/2} = 0$, and noting that

$$\begin{gathered} S_5 = \frac{\partial u_1}{\partial x_3} = Ak\cos(kx_3)\exp(i\omega t), \quad E_1 = \hat{E}_1 \exp(i\omega t): \\ A = \frac{1}{c_{55}^E k}\left(\frac{e_{15}^{(1)} - e_{15}^{(2)}}{2}\right)\frac{\hat{E}_1}{\cos\left(\frac{kh}{2}\right)}. \end{gathered} \tag{7}$$

The current flowing into the center electrode of Fig. 1(b) is composed of the current from the left side:

$$\begin{aligned} \hat{I}^{(1)} &= i\omega\Big(\int \varepsilon_{11}^S \hat{E}_1 \mathrm{d}x_2\mathrm{d}x_3 + e_{15}^{(1)}\int \hat{S}_5 \mathrm{d}x_2\mathrm{d}x_3\Big) \\ &= i\omega b\left(\varepsilon_{11}^S \hat{E}_1 h + e_{15}^{(1)}\int_{-h/2}^{h/2} \hat{S}_5 \mathrm{d}x_3\right) \\ &= i\omega b\Big(\varepsilon_{11}^S \hat{E}_1 h + e_{15}^{(1)}[\hat{u}_1(h/2) - \hat{u}_1(-h/2)]\Big) \\ &= i\omega\left(\varepsilon_{11}^S \hat{E}_1 bh + 2e_{15}^{(1)} bA\sin\left(\frac{kh}{2}\right)\right), \end{aligned} \tag{8}$$

and from the right side:

$$\hat{I}^{(2)} = i\omega\left(\varepsilon_{11}^S \hat{E}_1 bh - 2e_{15}^{(2)} bA\sin\left(\frac{kh}{2}\right)\right). \tag{9}$$

Therefore, the total current after substitution of A and $E_1 = V/L$ is given by

$$\begin{aligned} \hat{I}_{\mathrm{tot}} &= \hat{I}^{(1)} + \hat{I}^{(2)} \\ &= i\omega\frac{2\varepsilon_{11}^S bh}{L}V\left(1 + \frac{\left(e_{15}^{(1)} - e_{15}^{(2)}\right)^2}{4c_{55}^E \varepsilon_{11}^S}\frac{\tan\left(\frac{kh}{2}\right)}{\left(\frac{kh}{2}\right)}\right) \\ &= i\omega C_0 V\left(1 + \frac{\left(e_{15}^{(1)} - e_{15}^{(2)}\right)^2}{4c_{55}^E \varepsilon_{11}^S}\frac{\tan\left(\frac{kh}{2}\right)}{\left(\frac{kh}{2}\right)}\right), \end{aligned} \tag{10}$$

where $C_0 = (2\varepsilon_{11}^S bh)/L$ is the capacitance per period of the interdigitated electrodes.

This result shows that there is a resonance behavior at the frequency where the thickness of the film is one-half the wavelength of the shear acoustic wave in the film. The coupling of this mode depends on the difference of the

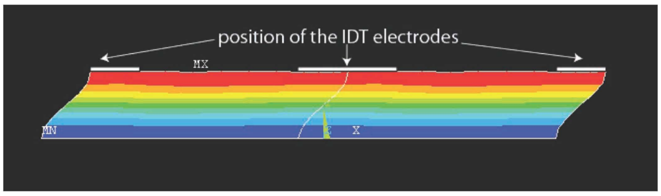

Fig. 2. Deformation (contour) and x-displacement (colored) of the membrane at the resonance frequency.

piezoelectric coefficients in the left and right parts of the film:

$$k^2 = \frac{\left(e_{15}^{(1)} - e_{15}^{(2)}\right)^2}{4c_{55}^{E}\varepsilon_{11}^{S}}. \tag{11}$$

The following FEM modeling will show the correctness of this formula.

III. 2-D FEM-BEM Model

A. Design With Embedded Electrodes

The analytical model from the previous section was verified using a 2-D FEM ANSYS model (ANSYS Inc., Canonsburg, PA). Electrical and mechanical periodic boundary conditions were applied along X-direction, matching the periodicity of IDT electrodes. The piezoelectric properties of the first type of AlN material were fixed, and of the second type were changed according to the principle $e_{nm}^{(2)} = \lambda e_{nm}^{(1)}$, where λ covers value interval $(-1{:}1)$. All other properties were fixed. It was found that the resonant frequency of the acoustic waves is defined by (10), independently of the value of λ.

The typical motion of the structure at resonance frequencies was shear type for these simulations, as shown in Fig. 2. The coupling coefficient for all FEM simulations in this work was calculated according to

$$k^2 = \frac{\pi^2}{4}\frac{f_{\mathrm{a}} - f_{\mathrm{r}}}{f_{\mathrm{r}}}, \tag{12}$$

where f_{r} and f_{a} are resonance and anti-resonance frequencies, respectively. As expected, the coupling coefficient is different for different values of λ, and is in agreement with (11) (see Fig. 3). It was also found that the resonance frequency is not dependent on the period of the IDT, which was varied from 10 to 16 µm in the simulation, meaning that we deal with a standing wave, and not with a horizontally traveling wave. The results depicted in Fig. 3 show that the 1-D analytical model and the 2-D FEM model are in exact agreement.

B. Design With Planar Electrodes

Producing a device with the design shown in Fig. 1 is complicated because of the difficulty of fabricating vertical electrodes. However, a design utilizing planar IDT electrodes is much easier to fabricate and can also be used to create a horizontal electric field in the film that should result in similar device behavior. To confirm this, 2-D FEM modeling was performed for IDT electrodes. A similar dependence on λ is observed (Fig. 3), but as expected, with reduced coupling caused by parasitic capacitances (because of E_3). The resonant frequency for the device with planar electrodes is only 0.3% different from the one modeled for the embedded IDT design, showing a good correlation with (10). The resonance frequency depends weakly on the IDT period for devices with planar electrodes. A change of 0.1% was calculated when increasing the period from 10 to 16 µm. The vibration mode of the device is a pure shear mode that is practically identical to an ideal shear mode as obtained in the model with vertically embedded electrodes (Fig. 2).

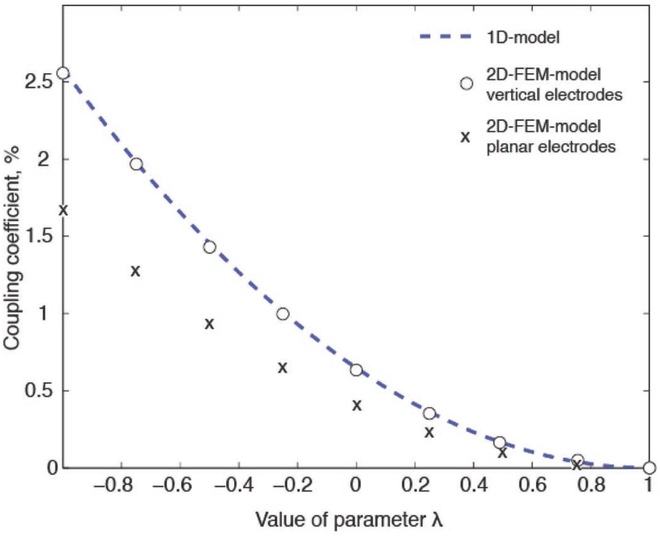

Fig. 3. Coupling coefficient of the resonator, depending on the piezoelectric properties of materials in its composition.

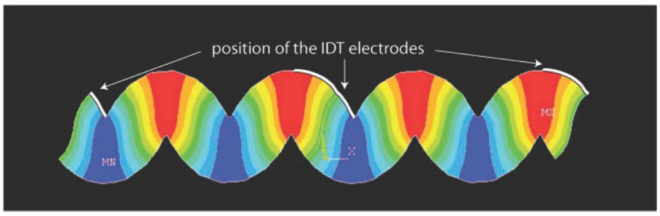

Fig. 4. Deformation (contour) and y-displacement (colored) of the standing Lamb wave ($n = 2$) in the AlN film.

C. Acoustic Parasitic Effects

Apart from the shear mode presented in Fig. 1, excitation of other types of waves may take place in such a design, for example Lamb waves. However, the modulation of piezoelectric properties leads to a weak coupling to traveling Lamb waves. Normally in Lamb wave resonators, the electrode is located in an antinode (maximum) of the displacement of the plate. In our case, however, the switching of the polarity in the center of the electrodes leads to a switching of charges in the center line of the electrode when the displacement is of the same sign below the electrodes. This means that the wave cannot be excited with the electrodes in the maxima. The excited wave thus moves the nodal lines to the center of the electrodes to compensate the switching of polarity with the switching of the displacement direction. Some coupling is achieved in this way. However, it is much smaller than with a homogeneous piezoelectric film. An example of such mode modeled with 2-D-FEM analysis is shown in Fig. 4. Such modes are excited when the condition $T = 2n\lambda$ is met (T is the period of the IDT, and $n = 1, 2, 3 \ldots$)

The resonance frequency of this (2nd order) mode at 1.6 GHz is far below the shear mode resonance at 2 GHz, and the coupling of 0.2% is 7 times smaller than with the shear mode BAW resonance. The next harmonic of this mode (3rd order) is even more loosely coupled (less than 0.03%) and appears far above the shear mode, at the frequency 2.7 GHz.

IV. Conclusions

An alternative structure for shear mode thin film BAW resonators is proposed and studied analytically and numerically. The structure is based on local polarity control of the piezoelectric film. A good agreement between analytical and numerical models is demonstrated. We showed that a pure shear mode is excited in the free-standing film. The resonance frequency is defined by its thickness, as required for BAW excitation. The value of the electromechanical coupling is derived for the ideal case, and simulated for the more practical case of interdigitated electrodes. Lamb waves are suppressed to a large extent and appear at frequencies other than the shear mode.

Acknowledgment

The research leading to these results has received funding from the European Community's Seventh Framework Programme (FP7/2007-2013) under grant agreement no. 223975.

References

[1] M.-I. Rocha-Gaso, C. March-Iborra, A. Montoya-Baides, and A. Arnau-Vives, "Surface generated acoustic wave biosensors for the detection of pathogens: A review," *Sensors*, vol. 9, no. 7, pp. 5740–5769, 2009.

[2] R. Gabl, H.-D. Feucht, H. Zeininger, G. Eckstein, M. Schreiter, R. Primig, D. Pitzer, and W. Wersing, "First results on label free detection of DNA and protein moecules using a novel integrated sensor technology based on gravimetric detection principles," *Biosens. Bioelectron.*, vol. 19, no. 6, pp. 615–620, 2004.

[3] G. Wingqvist, J. Bjurstrom, A.-C. Hellgren, and I. Katardjiev, "Immunosensor utilizing a shear mode thin film bulk acoustic sensor," *Sens. Actuators B*, vol. 127, no. 1, pp. 248–252, 2007.

[4] J. Weber, W. M. Albers, J. Tuppurainen, M. Link, R. Gabl, W. Wersing, and M. Schreiter, "Shear mode FBARs as highly sensitive liquid biosensors," *Sens. Actuators A*, vol. 128, no. 1, pp. 84–88, 2006.

[5] T. Yanagitani, M. Kiuchi, M. Matsukawa, and Y. Watanabe, "Characteristics of pure-shear mode BAW resonators consisting of (1120) textured ZnO films," *IEEE Trans. Ultrason. Ferroelectr. Freq. Control*, vol. 54, no. 8, pp. 1680–1686, 2007.

[6] E. Milyutin, S. Gentil, and P. Muralt, "Shear mode bulk acoustic wave resonator based on c-axis oriented AlN thin film," *J. Appl. Phys.*, vol. 104, no. 8, art. no. 084508, 2008.

[7] C. D. Corso, A. Dickherber, and W. D. Hunt, "Lateral field excitation of thickness shear mode waves in a thin film ZnO solidly mounted resonator," *J. Appl. Phys.*, vol. 101, no. 5, art. no. 054514, 2007.

[8] L. J. van der Pauw, "The planar transducer—A new type of transducer for exciting longitudinal acoustic waves," *Appl. Phys. Lett.*, vol. 9, no. 3, pp. 129–131, 1966.

[9] K. Nakamura and H. Shimizu, "Poling of ferroelectric crystals by using interdigital electrodes and its application to bulk-wave transducers," in *Proc. IEEE Ultrasonics Symp.*, Atlanta, GA, 1983, pp. 527–530.

[10] K. Nakamura, H. Shimizu, and N. Sato, "Basic characteristics of the planar ultrasonic transducers using piezoelectric ceramics poled with interdigital electrodes," *IEEE Trans. Sonics Ultrason.*, vol. SU-30, no. 6, pp. 345–349, 1983.

[11] E. Milyutin and P. Muralt, "PMBAR*—Shear mode TFBAR based on (001)AlN thin film," in *Proc. IEEE Ultrasonics Symp.*, Beijing, China, 2008, pp. 1215–1217.

[12] E. Milyutin, S. Harada, D. Martin, J. F. Carlin, N. Grandjean, V. Savu, O. Vaszquez-Mena, J. Brugger, and P. Muralt, "Sputtering of (001)AlN thin films: Control of polarity by a seed layer," *J. Vac. Sci. Technol. B*, vol. 28, no. 6, art. no. L61, 2010.

(12) INTERNATIONAL APPLICATION PUBLISHED UNDER THE PATENT COOPERATION TREATY (PCT)

(19) World Intellectual Property Organization
International Bureau

(43) International Publication Date
4 February 2010 (04.02.2010)

PCT

(10) International Publication Number
WO 2010/013197 A2

(51) International Patent Classification:
H03H 9/25 (2006.01) *H03H 9/64* (2006.01)

(21) International Application Number:
PCT/IB2009/053274

(22) International Filing Date:
28 July 2009 (28.07.2009)

(25) Filing Language: English

(26) Publication Language: English

(30) Priority Data:
61/085,479 1 August 2008 (01.08.2008) US

(71) Applicant *(for all designated States except US)*: **ECOLE POLYTECHNIQUE FÉDÉRALE DE LAUSANNE (EPFL)** [CH/CH]; EPFL-SRI Station 10, CH-1015 Lausanne (CH).

(72) Inventors; and
(75) Inventors/Applicants *(for US only)*: **MILYUTIN, Evgeny** [RU/CH]; Rue de Bassenges 33, CH-1024 Ecublens (CH). **MURALT, Paul** [CH/CH]; Ch. du Levant 31, CH-1315 La Sarraz (CH).

(74) Agent: **Cronin, Brian**; Cronin Intellectual Property, Chemin de Précossy 31, CH-1260 Nyon (CH).

(81) Designated States *(unless otherwise indicated, for every kind of national protection available)*: AE, AG, AL, AM, AO, AT, AU, AZ, BA, BB, BG, BH, BR, BW, BY, BZ, CA, CH, CL, CN, CO, CR, CU, CZ, DE, DK, DM, DO, DZ, EC, EE, EG, ES, FI, GB, GD, GE, GH, GM, GT, HN, HR, HU, ID, IL, IN, IS, JP, KE, KG, KM, KN, KP, KR, KZ, LA, LC, LK, LR, LS, LT, LU, LY, MA, MD, ME, MG, MK, MN, MW, MX, MY, MZ, NA, NG, NI, NO, NZ, OM, PE, PG, PH, PL, PT, RO, RS, RU, SC, SD, SE, SG, SK, SL, SM, ST, SV, SY, TJ, TM, TN, TR, TT, TZ, UA, UG, US, UZ, VC, VN, ZA, ZM, ZW.

(84) Designated States *(unless otherwise indicated, for every kind of regional protection available)*: ARIPO (BW, GH, GM, KE, LS, MW, MZ, NA, SD, SL, SZ, TZ, UG, ZM, ZW), Eurasian (AM, AZ, BY, KG, KZ, MD, RU, TJ, TM), European (AT, BE, BG, CH, CY, CZ, DE, DK, EE, ES, FI, FR, GB, GR, HR, HU, IE, IS, IT, LT, LU, LV, MC, MK, MT, NL, NO, PL, PT, RO, SE, SI, SK, SM, TR), OAPI (BF, BJ, CF, CG, CI, CM, GA, GN, GQ, GW, ML, MR, NE, SN, TD, TG).

Published:

— *without international search report and to be republished upon receipt of that report (Rule 48.2(g))*

(54) Title: PIEZOELECTRIC RESONATOR OPERATING IN THICKNESS SHEAR MODE

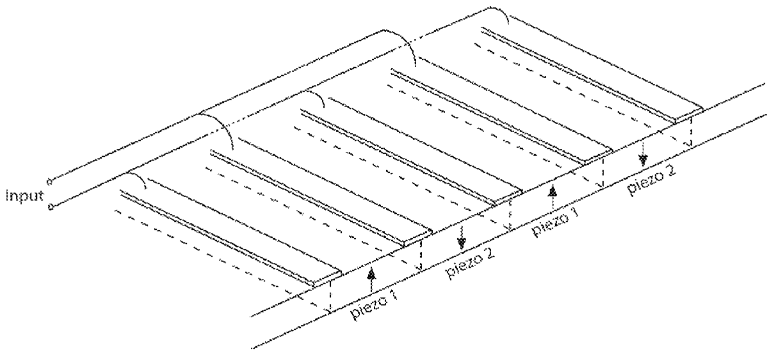

Figure 3

(57) Abstract: An acoustic wave resonator device comprising a resonant layer that comprises a series of side-by-side areas of first and second dielectric materials. In one embodiment the first dielectric material is a piezoelectric, in particular the first dielectric material can be a piezoelectric and the second dielectric material can be non-piezoelectric.In another embodiment,the first dielectric material is a piezoelectric of first polarity and the second dielectric material is a piezoelectric of opposite polarity or different polarity. Where needed, the resonant layer is supported on a reflector composed of series of layers of high acoustic impedance material(s) alternating with layers of low acoustic impedance material(s). For 10 example, the reflector comprises AlN,Al_2O_3, Ta2O5, HfO2or W as high impedance material and SiO2 as low impedance material.

WO 2010/013197 A2

PIEZOELECTRIC RESONATOR OPERATING IN THICKNESS SHEAR MODE

FIELD OF THE INVENTION

The present invention relates generally to piezoelectric micro-devices and, in particular, to thin film resonators operating in thickness-shear mode. Potential applications are in sensors, RF oscillators and transformers.

BACKGROUND OF THE INVENTION

A list of referenced documents is appended to the end of the Description.

Piezoelectric resonators are electro-mechanical resonators. The resonance is due to shape, density and elastic constants of the mechanically resonating body containing piezoelectric material. The piezoelectric effect permits to couple the mechanical resonance to an electric circuit. The use of piezoelectric thin films allows very large resonance frequencies in the 1-10 GHz range by trapping a bulk acoustic wave within the piezoelectric film slab. This is of great interest for wireless communication. Thin film piezoelectric resonators are indeed commercialized for applications in mobile phones. Main product is the RF filter at the carrier frequency in the receiver and emitter path. Such filters need a large pass band, meaning large piezoelectric coupling. For this reason, the largest piezoelectric coefficient is employed, i.e. the electric field is applied parallel to the polar c-axis (coefficient e_{33}). It happens that AlN and ZnO films can be very well grown in (001) texture, that is with the c-axis (index 3 in the crystal system) perpendicular to the film plane (this direction is designed with index z of the coordinate system). The electric field is then very conveniently applied between two parallel plate electrodes sandwiching the piezoelectric film. The piezoelectric effect is then written for instance as change of stress $T_z \text{`} -e_{33}E_z$. Using this mode, a longitudinal wave running along the 3-direction is trapped in the film slab, excited through the largest possible coupling based on e_{33}. Informations on this kind of devices are found for instance in the articles: Lakin [1], Ruby [2], Lanz [3].

Another promising application of the thin film bulk acoustic wave resonators (TFBAR's) has been identified in gravimetric sensing. High quality factor and high frequency make such device very sensitive to any particles or films that agglomerate at the surface of the device. However, such sensors are not able to operate in a liquid when using longitudinal waves as for mobile phones. The liquid is damping too much the resonance because longitudinal waves are emitted from the resonator into the liquid. Contrary to that, resonators that operate on shear acoustic waves will not be damped so much, because there is only a weak shear coupling into liquids. Shear waves do not propagate in liquids, and thus do not absorb energy from the resonator. A schematic view of a shear mode resonator combined with an immobilization layer to obtain gravimetric sensing is shown in Figure 1.

Excitation of shear waves in thin films was proposed in several ways. A first solution is tilted c-axis growth (Wingqvist, (Sensors, 2005 IEEE)[4]). The electrode geometry is the same as for mobile phone RF filters, however, the c-axis in the piezoelectric film is tilted away from the vertical (direction 3) by the angle alpha. In this geometry, quasi-shear waves running along the 3-direction are excited by an electric field pointing along the 3-axis, and are trapped in the film at resonance. The main disadvantage of this technique is the need for non-standard deposition tools and large difficulties to achieve uniform c-axis tilting. A second solution is to provide an in-plane electric field by means of interdigitated electrodes along with standard (001) AlN films. The advantage is thus that standard films with good uniformities can be used. The disadvantage is the creation of an S_3 component of strain below the electrode fingers, leading to a longitudinal wave component, and thus to emission into the liquid. The quality factor is thus not as optimal as it could be, even though better Q's were observed than with tilted c-axis growth (see article [6] of the inventors).

The publication Martin [5] discloses background information on growing thin AlN films, in particular with differently treated areas yielding different polarization.

SUMMARY OF THE INVENTION

The objective of this invention is to provide a way of pure shear acoustic wave excitation that can make use of standard AlN thin films (c-axis oriented). This is an improved version of the above-mentioned second solution.

According to a main aspect of the invention, there is provided an acoustic wave resonator device comprising a resonant layer that comprises a series of side-by-side areas of first and second dielectric materials. These materials can in particular be piezoelectric and non-piezoelectric materials, or piezoelectric materials with different polarities.

Thus, in one embodiment the first dielectric material is a piezoelectric and the second dielectric material can be non-piezoelectric, such as a disordered piezoelectric material with no or substantially no piezoelectric effect. In another embodiment, the first dielectric material is a piezoelectric of first polarity and the second dielectric material is a piezoelectric of opposite polarity or of different polarity (e.g. with vertical and horizontal orientations), in other words of different piezoelectric properties.

Where needed, the resonant layer is supported on a reflector composed of series of layers of high acoustic impedance material(s) alternating with layers of low acoustic impedance material(s). For example, the reflector comprises at least one of AlN, Al2O3 or W as high impedance material and SiO2 as low impedance material. Also these materials can be mixed or used in combination. For example, one layer of high impedance material can be W, and another layer of high impedance material can be AlN or Al2O3 in the same reflector.

In another embodiment, the resonant layer is a membrane with mechanically free surfaces.

The piezoelectric material is typically AlN, ZnO or GaN.

The inventive acoustic wave resonator device can comprise an electrode system allowing excitation of shear thickness resonance of acoustic waves, or an electrode system allowing in-phase electric filed production in piezoelectric parts of the resonant layer.

The inventive acoustic wave resonator device can comprise interdigitated electrodes.

In order to compensate for non-uniform loading of the inventive acoustic wave resonator device, it can also comprise a patterned electrodes system consisting of patterned electrodes made of an electrically-conductive first material separated by an electrically non-conductive second material with similar mechanical properties to the first material. For example the first material of the electrodes is based on Al and the second material is SiO2.

The inventive acoustic wave resonator device can be incorporated in a media sensing apparatus, in particular a media sensing apparatus for liquid immersion. The invention also concerns an integrated circuit device, in particular a transformer, comprising an acoustic wave resonator device as set out above.

The invention also provides a piezoelectric transformer comprising: an input part (which is assimilated to the primary winding of the transformer); a matching part; and an output part (which is assimilated to the secondary winding of the transformer), wherein the input part or primary winding comprises the inventive acoustic wave resonator device, the output part or secondary winding comprises a piezoelectric material and the matching part is arranged to acoustically couple the input and output parts constituting the primary and secondary windings. This output part can be made of AlN or ZnO and the matching part made of SiO_2.

BRIEF DESCRIPTION OF THE DRAWINGS

The invention will further be described by way of example with reference to the accompanying drawings, in which:

FIG. 1 shows principle of a resonator as a sensor.

FIG. 2 is a schematic cross-section through a part of one embodiment of a resonator according to the invention composed of alternatively piezo and non-piezoelectric segments, complying with the electrode system for optimal excitation, and showing the principle of the design.

FIG. 3 is a schematic perspective view of a modification of this resonator using alternative polarities of the piezoelectric material.

FIG. 4 is a cross-section showing the solidly mounted resonator based on piezo-patterned AlN thin film wherein an acoustic reflector is applied to concentrate the resonance within the AlN layer.

FIG. 5 shows the simulated motion of a free film at resonance frequency with a structure like that shown in Fig. 2; the electrodes are defined as infinitely thin.

FIG. 6 is a graph of electrical admittance against frequency for a resonator according to the invention (as in Fig. 2).

FIG. 7 is a graph showing the electrical admittance against frequency for a resonator according to the invention (as in Fig. 4) under operations in air, showing real and imaginary parts vs frequency, assuming HZ=AlN, and LZ=SiO_2.

FIG. 8 is a graph showing the electrical admittance against frequency for a resonator according to the invention (same as Fig. 7) under operations in water, showing real and imaginary parts vs frequency.

FIG. 9 is a graph showing a simulation of the phase of the electrical admittance for a resonator according to the invention under operations in air (solid line) and water (dashed line) (from simulation data as Figs 7 and 8).

FIG. 10 is a schematic perspective view of a sample design of a transformer based for example on a piezo-patterned film of AlN.

FIG. 11 shows the motion of the transformer in resonance.

FIG. 12 is a graph showing the electrical conductance vs frequency for a device modulated according to the invention and a comparative non-modulated device.

DETAILED DESCRIPTION OF THE PREFERRED EMBODIMENT

In Fig. 2, one period of a (002) AlN film patterned alternately with piezo and non-piezo regions is shown. Excitation of shear acoustic wave is possible in this case by applying an electric field in such a way that in every piezo-active region the electric field is in phase with the wave. Then, non-piezo regions do not react on the electric field, they just follow the motion of piezoelectric regions adjacent to them resulting in a perfect shear motion of the film.

Fig. 3 shows a perspective view of multiple periods of the resonator in the case of a modification where the alternating regions are piezoelectric regions of different polarities, in this case with opposite polarities.

Fig. 3 also shows the electrical connection of the alternating electrodes to opposite poles of the electric supply. The given configuration of the electrodes on the upper face of the resonator adjacent the boundaries of the piezo and non-piezo regions or the piezoelectric regions of different polarities (see Figs. 2, 3 and 4) enables the electric field to be produced in phase with the waves corresponding to the piezoelectric material or the piezoelectric regions of different polarities. However, the same effect can be achieved even if the electrodes are shifted slightly but still remain close to the boundaries between the different regions.

As illustrated in Figs 2, 3 and 4, the adjacent areas of piezo and non-piezo material, or piezo materials of different polarities, are of unequal length. However, the adjacent areas could be of the same length and equally spaced, if desired, as in case of oppositely polar regions.

In particular for AlN substrates, alternating piezo and non-piezo regions can be obtained by modulating the surface roughness of the SiO_2 substrate on which the AlN is grown. In smooth areas piezoelectric regions will grow. In areas roughened for example by depositing polycrystalline silicon on the SiO_2, the AlN still grows but is non-piezoelectric.

Piezoelectric areas of different polarities can be obtained as described in reference [5].

In Figs 5 and 6, results of device simulations are shown, treating the ideal case of a free, segmented layer as defined in Fig. 2. The piezoelectric segment is c-axis oriented AlN with standard properties, and the non-piezoelectric AlN has the same mechanical properties. The motion at resonance frequency is represented in Fig. 5. Thickness shear displacement of the structure can be clearly identified. The displacements are according to a pure shear mode, as desired, and required for gravimetric sensing.

This modeling was done under condition that both surfaces of the film are exposed to air. In order to emphasize ability of excited mode to operate in water without much damping, modeling with a condition that top surface of the film is exposed to water was implemented. Comparison of the properties of the resonance in case of water and air are shown on Fig. 6. Damping by the water is small. The Q factor amounts still to over 50000 (from Fig. 6), which is largely acceptable. Other losses (acoustic losses in materials, resistive losses in the electrodes, excitation of Lamb waves, etc.) of a real device are larger.

The shown example represents the principle of excitation of shear acoustic waves in an c-axis oriented AlN or ZnO film. In a real device, an acoustic isolation is needed. Both known principles, the membrane resonator (material below the resonator is locally etched away to form bridge or membrane structures) and the solidly mounted resonator (SMR) based on an acoustic reflector can be proposed. The SMR type (as shown in Fig. 4) seems to be more promising than the membrane one. The reflector in SMR should be acoustically matched with the resonator. For designs of Bragg reflector, high (HZ) and low (LZ) acoustic impedance materials should be used, preferentially electrical insulators, for example, HL = SiO_2 and HZ $= AlN$, Al_2O_3, Ta_2O_5, HfO_2, or W (though with limitations). . All theses films can be deposited by sputtering techniques. Sputtering of c-axis AlN films is well known in the art and high uniformity of deposited films is achieved in industry nowadays. The process of deposition of SiO_2 films is also well-known. Thicknesses of layers should be in range of 0.5-1.5 microns in order to obtain resonance around 2.4 GHz. An electrodes system can be defined by photolithography or by evaporative shadow mask.

When operating at GHz frequencies, loading of the electrodes becomes significant, possibly affecting the performance. This problem can be cured by a using matching layer of some dielectric material that has similar acoustic properties to the electrodes and is located between the electrodes, as shown in Fig. 4. For example, aluminum and silicon dioxide (SiO_2) may be used as materials for electrodes and matching dielectric respectively.

Different processes to create non-piezoelectric AlN are now under study. As described above, one possibility is to apply a surface modification on the areas where piezoelectricity has to vanish. For instance, surface roughness is introduced to reduce surface diffusion of the atoms of sputtered film and provoke random nucleation of grain orientation.

The results of a realistic SMR design are presented in Fig. 4. AlN and SiO_2 can be used as materials for the reflector, but as mentioned above, other materials with high and low acoustic impedance also could be used. In Fig. 7 and 8, simulated electrical properties of a realistic resonator under operation in air and water are shown. The phase images of the resonance in liquid and water are shown in Fig.9. The derived Q-factors amount to 9000 and 6000, respectively.

Demonstrated results mean that also in SMR design radiation losses into the liquid are not the dominant loss mechanisms. Shear type of the motion of the device can be seen from Fig. 10, where behavior of the SMR at resonance frequency is shown.

Fig. 12 shows the electrical conductivity vs frequency for a device modulated according to the invention and a comparative non-modulated device. The device according to the invention had side-by-side areas of different piezoelectric properties wherein an AlN piezoelectric film has areas with ordered AlN for the first type of dielectric and disordered AlN with reduced piezoelectric properties for the second type of dielectric. The comparative non-modulated device was fabricated on the same wafer but with a uniform AlN piezoelectric film. The devices were otherwise identical and close to each other to exclude any variation of film properties. As can be seen in Fig. 12, a resonance frequency is formed at around 2.0GHz in the inventive modulated device, but not in the non-modulated comparative device.

EXAMPLES

The following examples are presented to describe some practical applications of the invention.

Example 1: High performances in-liquid sensing

A principle of in-liquid sensor based on shear mode resonator is shown in Fig. 1. The top surface of the device is functionalized to attract certain types of impurities from liquid. Once the impurities are attached to the surface, acoustic properties of the resonator have been changed and that results in a shift of resonance frequency. By the size of shift, the quantity of attracted substances can be determined and conclusions drawn about the concentration of the impurities in the liquid. By using different chemical tools for functionalization of the surface it is possible to fabricate sensors for different kinds of impurities. Generally speaking, everything that can affect acoustic properties of the resonator may be detected.

In fact, such sensor is the analog of the well-known quartz crystal microbalance (QCM) device that provides sensing in a similar way. QCM is based on a special cut of mono-crystal of quartz and then is polished to be a thin plate. The polishing process puts restrictions on the limit thickness of the plate, and so induces a limit of several MHz for the resonance frequency of QCM. That is very important, because the relative sensitivity of such device is proportional to the operating frequency. So, a sensor operated at GHz frequencies is hundreds of times more sensitive in comparison with a standard QCM.

Example 2: Piezoelectric transformer

Another potential application is a piezoelectric transformer (PT). A potential device, shown in Fig. 10, consists of a primary winding (top layer), matching layer, and secondary windings (bottom layer). The primary winding is a patterned AlN thin film, and the secondary one is a non-patterned, standard piezoelectric AlN film. A floating electrode can be added to the secondary winding. An input AC voltage is applied to primary winding and an output AC voltage is taken from the secondary one. In operation, the primary and secondary windings are acoustically coupled by thickness-shear mode of vibration through matching layers, as shown in Fig 11. Excitation of shear wave is produced in the primary winding in the same way as in the resonator.

Nominal value for output/input transformation is equal to the number of periods in a patterned film. For the simulation shown in Fig. 11, it is equal to 2. However, it should be recognized that the transformation ratio also depends on loading of the PT.

A matching layer in the structure performs the role of acoustic connector and electrical isolator between windings.

LIST OF REFERENCES CITED

[1] Lakin, K.M., K.T. McCarron, and R.E. Rose. Solidly mounted resonators and filters. in IEEE Ultrasonics Symposium. 1995. Seattle (Washington, USA): IEEE, p 905-908.

[2] Ruby, R.C., P. Bradley, Y. Oshmyansky, A. Chien, and J.D. Larson. Thin film bulk acoustic wave resonators for wireless applications. in IEEE Ultrasonics Symposium. 2001. Atlanta: IEEE, p. 813-821.

[3] Lanz, R. and P. Muralt, Bandpass filters for 8 GHz using solidly mounted bulk acoustic wave resonators. IEEE Trans. UFFC, 2005. 52: p. 936-946.

[4] Wingqvist, G. Bjurstrom, J. Liljeholm, L. Katardjiev, I. Spetz, A.L., Shear mode AlN thin film electroacoustic resonator for biosensor applications. Sensors, 2005 IEEE, 2005, 4 p. 492-495.

[5] Martin, F. Muralt, P, Cantoni, M. and Dubois M.-A. Re-growth of c-axis oriented AlN thin films. In IEEE Ultrasonics Symposium 2004, p 169-172.

[6] E. Milyutin, S. Gentil, P. Muralt, Shear mode bulk acoustic wave resonator based on C-axis oriented AIN thin film, J. Appl. Phys. Vol. 104, no 084508 (2008).

CLAIMS

1. Acoustic wave resonator device comprising a resonant layer that comprises a series of side-by-side areas of first and second dielectric materials, of which one or both materials are piezoelectric, wherein either:
(a) the first dielectric material is a piezoelectric and the second dielectric material is a non-piezoelectric; or
(b) the first and second dielectric materials are piezoelectrics of different piezoelectric properties.

2. Acoustic wave resonator device of claim 1 (a) wherein the second dielectric material is a disordered piezoelectric material with substantially no net piezoelectric effect.

3. Acoustic wave resonator device of claim 1 (b) wherein the first dielectric material is a piezoelectric of first polarity and the second dielectric material is a piezoelectric of opposite polarity or of different polarity.

4. Acoustic wave resonator device of any preceding claim wherein the resonant layer is supported on a reflector composed of series of layers of high acoustic impedance material(s) alternating with layers of low acoustic impedance material(s).

5. Acoustic wave resonator device of claim 4 wherein the reflector comprises at least one of AlN, Al2O3, Ta2O5, HfO2 or W as high impedance material and SiO2 as low impedance material.

6. Acoustic wave resonator device of any one of claims 1 to 3 wherein the resonant layer is a membrane with mechanically free surfaces.

7. Acoustic wave resonator device of any preceding claim wherein the piezoelectric material is AlN, ZnO or GaN.

8. Acoustic wave resonator device of any preceding claim comprising an electrode system configured for excitation of shear thickness resonance of acoustic waves.

9. Acoustic wave resonator device of any preceding claim comprising an electrode system configured for in-phase electric field production in the plane of piezoelectric parts of the resonant layer.

10. Acoustic wave resonator device of any preceding claim comprising interdigitated electrodes.

11. Acoustic wave resonator device of any preceding claim comprising a patterned electrodes system consisting of patterned electrodes made of an electrically-conductive first material separated by an electrically non-conductive second material with similar mechanical properties to the first material.

12. Acoustic wave resonator device of claim 11 when the first material of the electrodes is based on Al and the second material is SiO2.

13. A media sensing apparatus comprising an acoustic wave resonator device of any preceding claim.

14. A media sensing apparatus for liquid immersion comprising an acoustic wave resonator device of any of claims 1 to 12.

15. A piezoelectric transformer comprising:

an input part;

a matching part; and

an output part,

wherein the input part comprises an acoustic wave resonator device of any of claims 1 to 12, the output part comprises a piezoelectric material and the matching part is arranged to acoustically couple the input and output parts.

16. The piezoelectric transformer of claim 16 wherein the output part is made of AlN or ZnO.

17. The piezoelectric transformer of claim 15 or 16 wherein the matching part is made of SiO2.

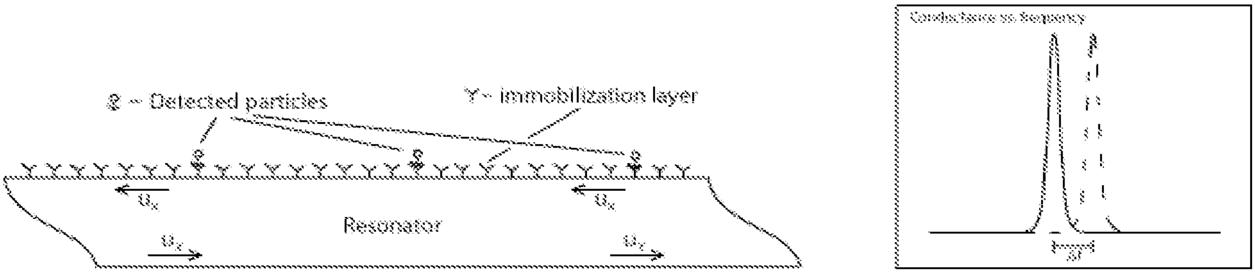

Figure 1

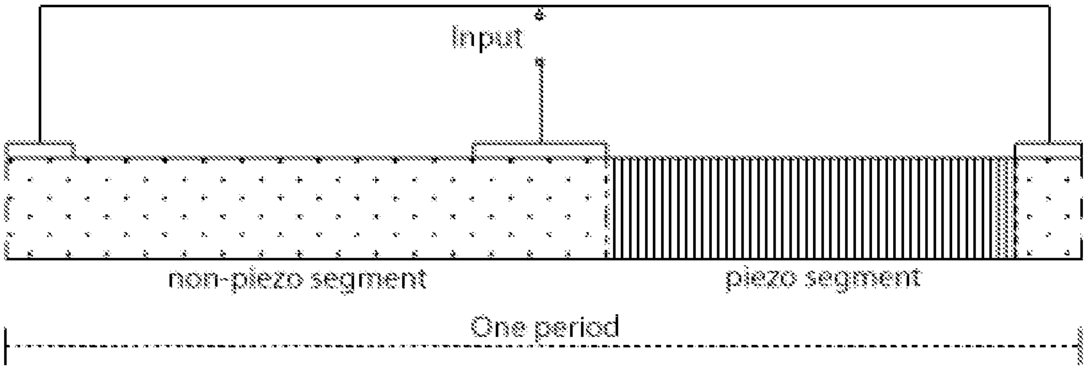

Figure 2

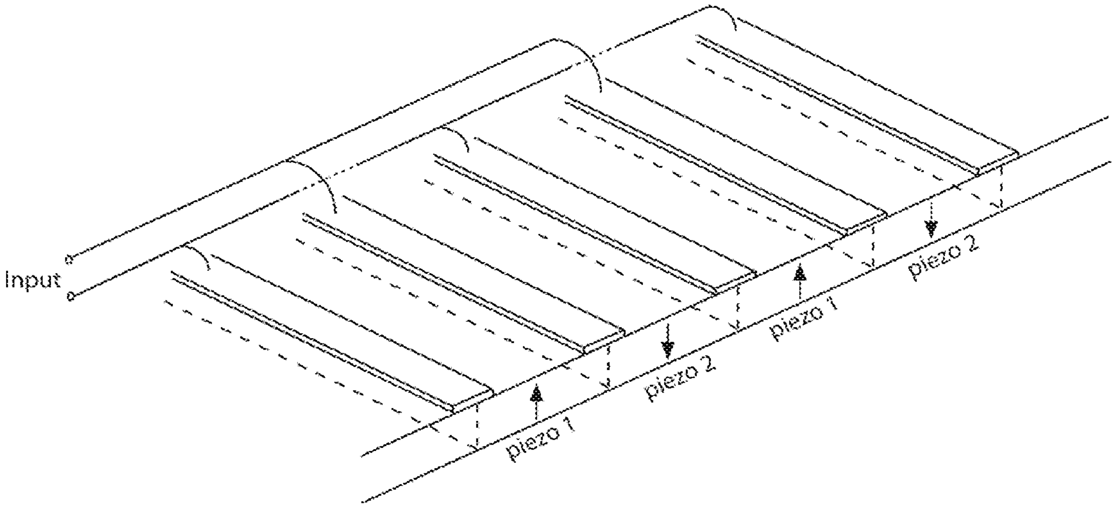

Figure 3

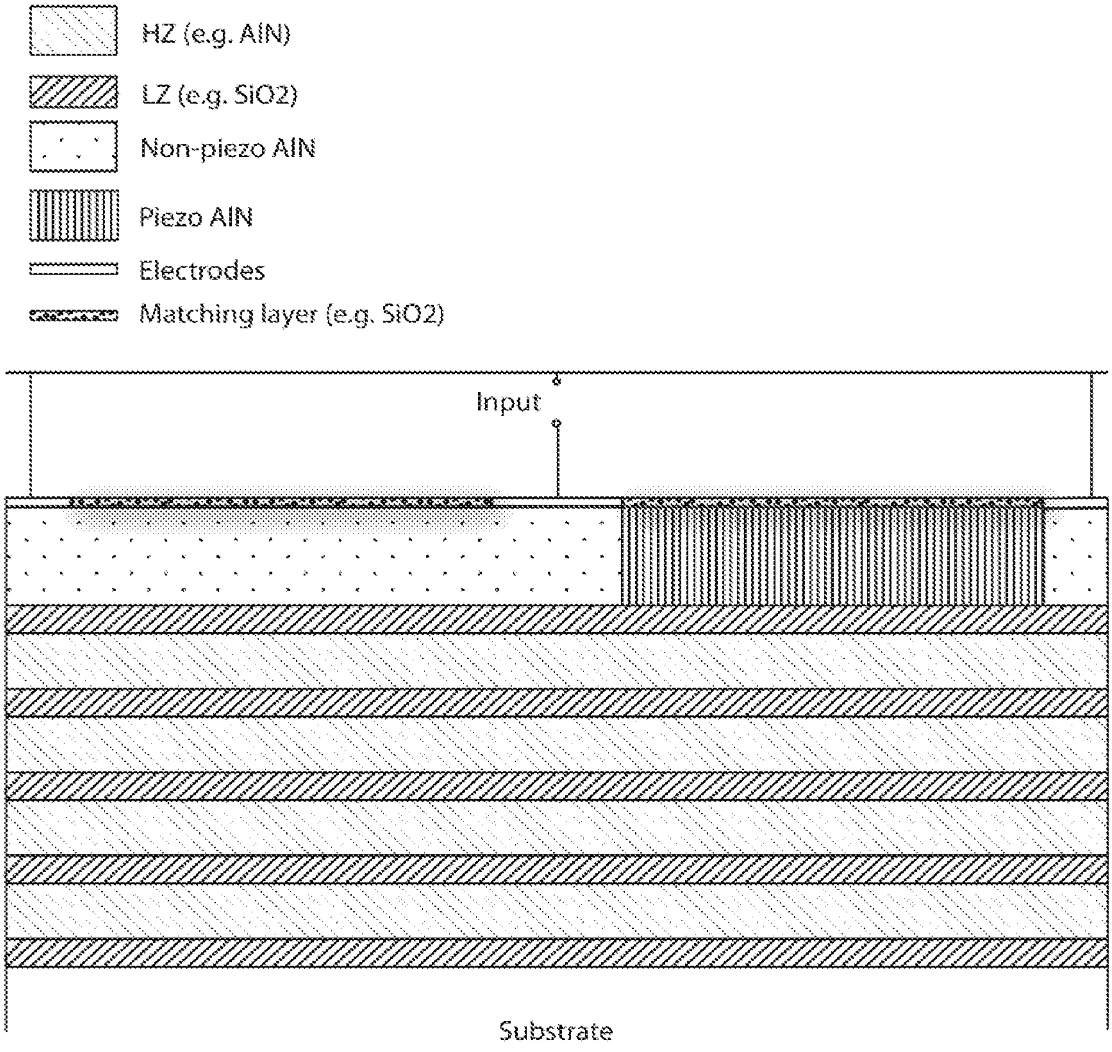

Figure 4

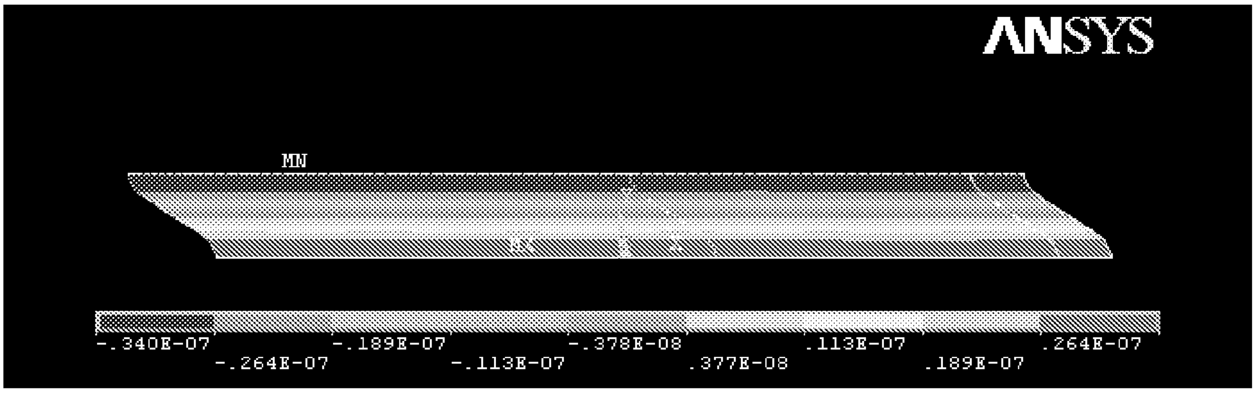

Figure 5

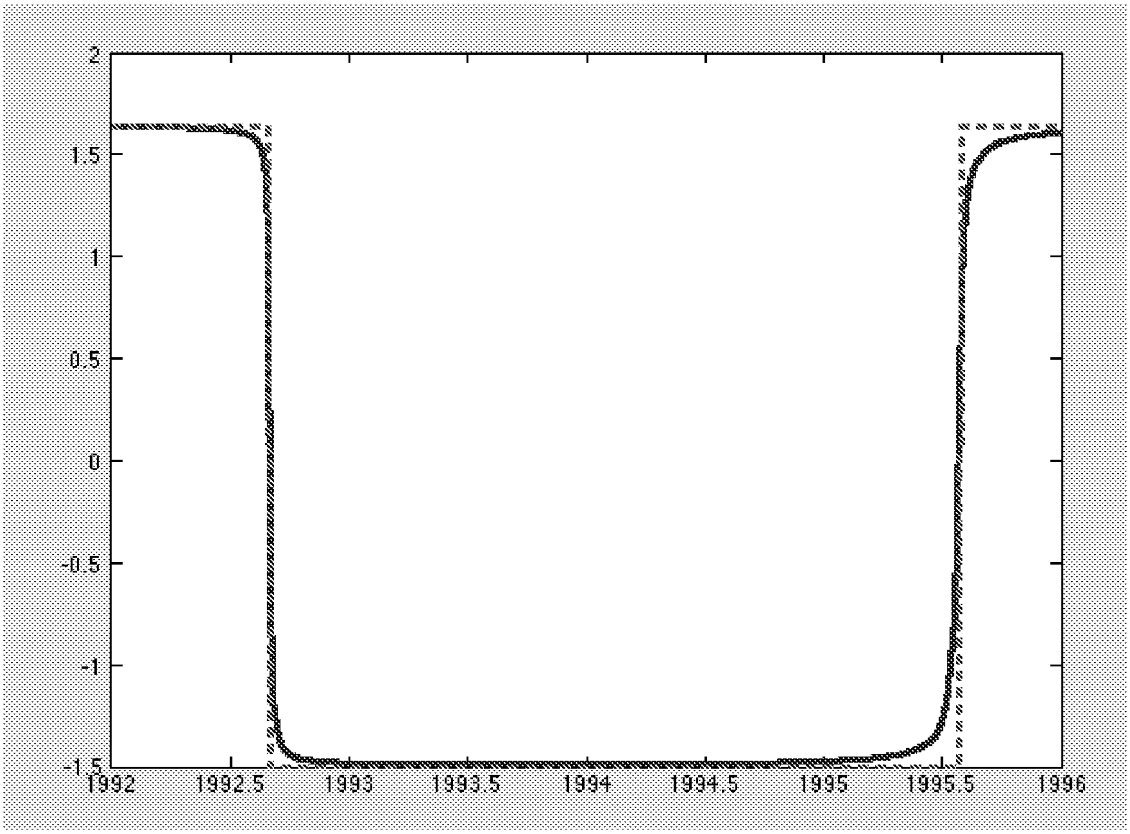

Figure 6

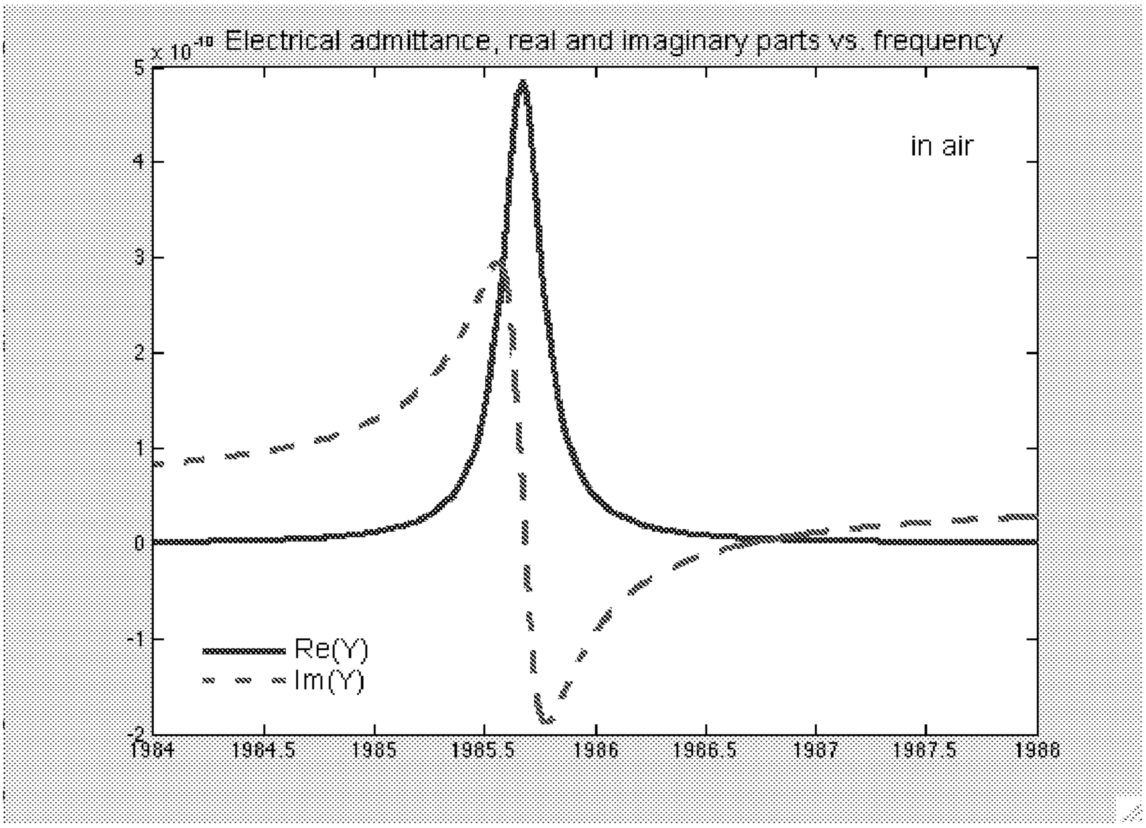

Figure 7

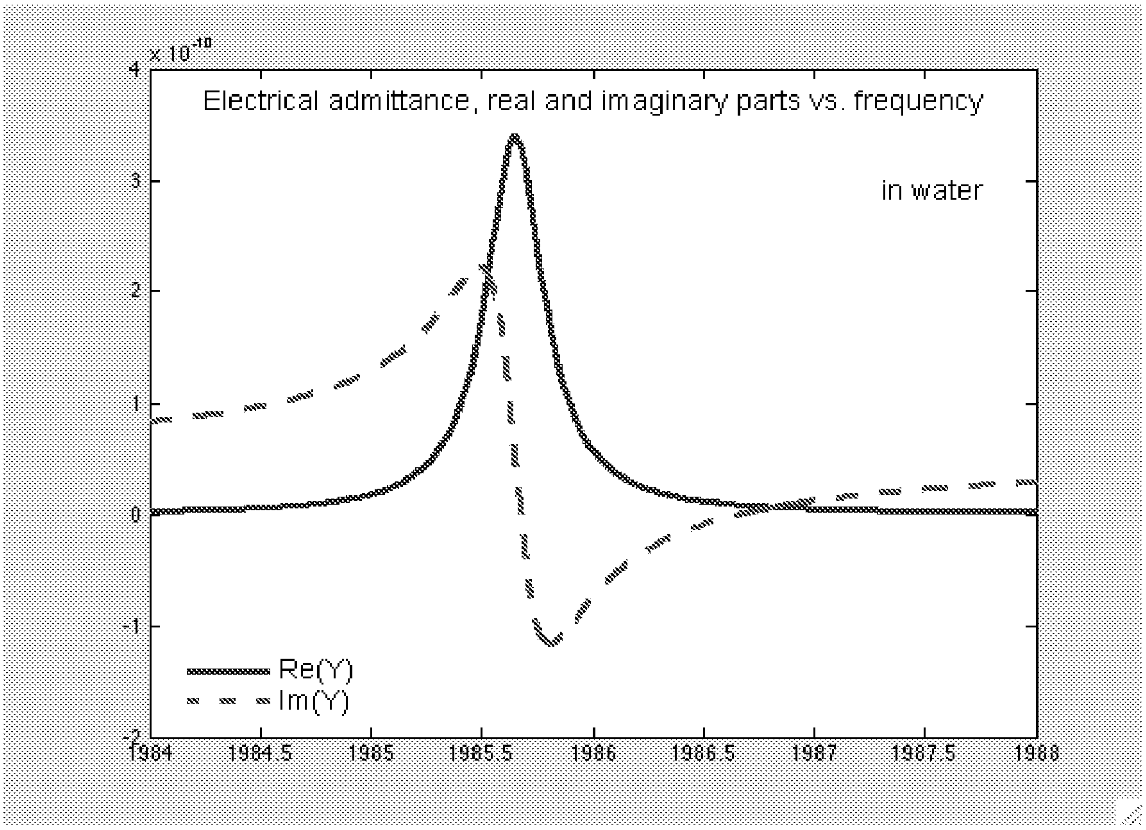

Figure 8

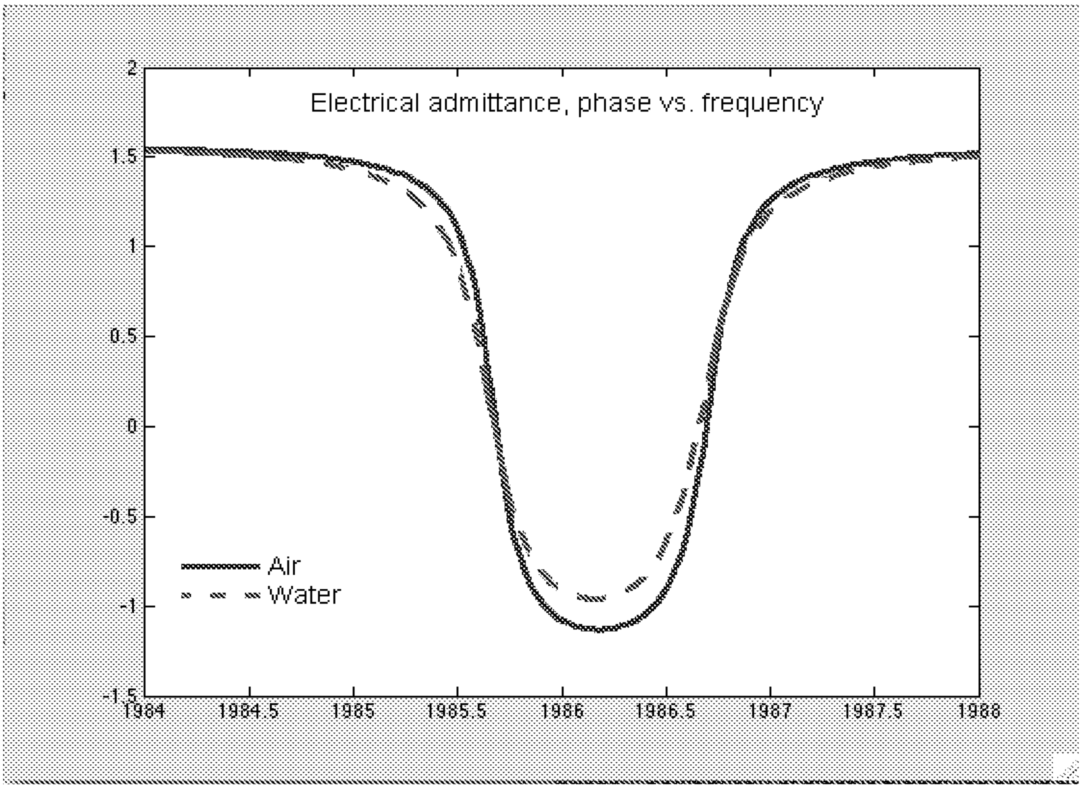

Figure 9

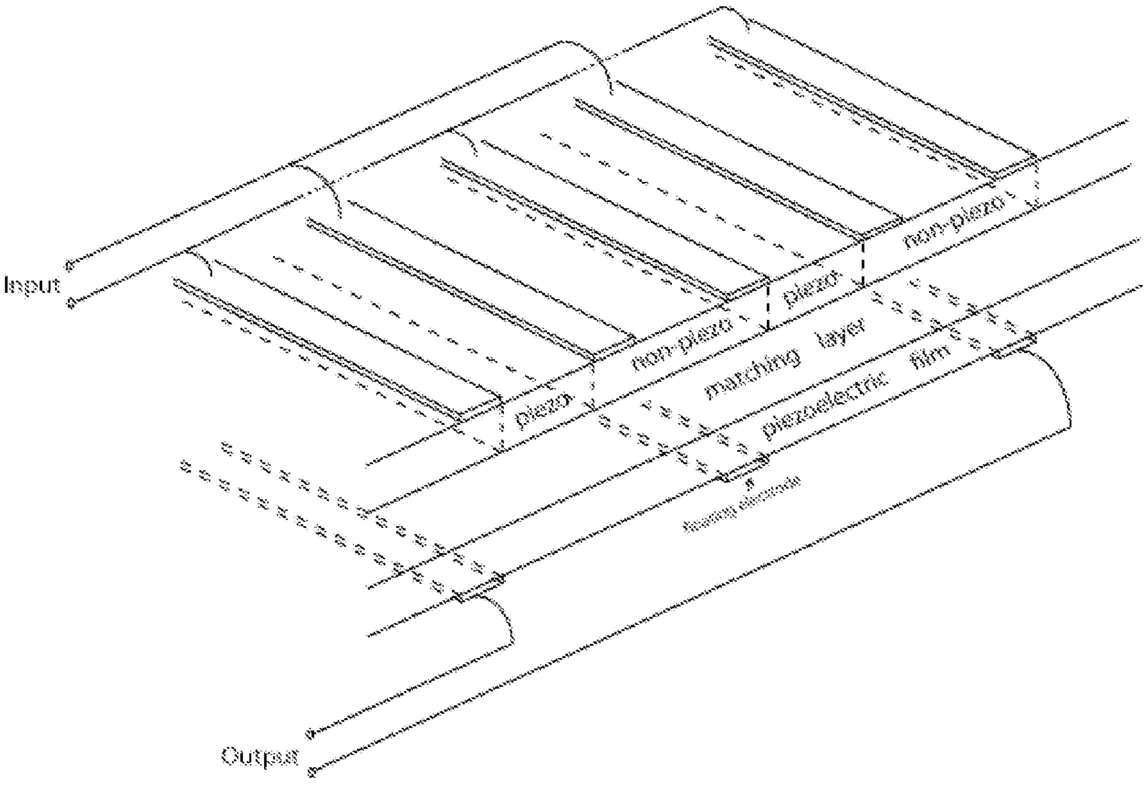

Figure 10

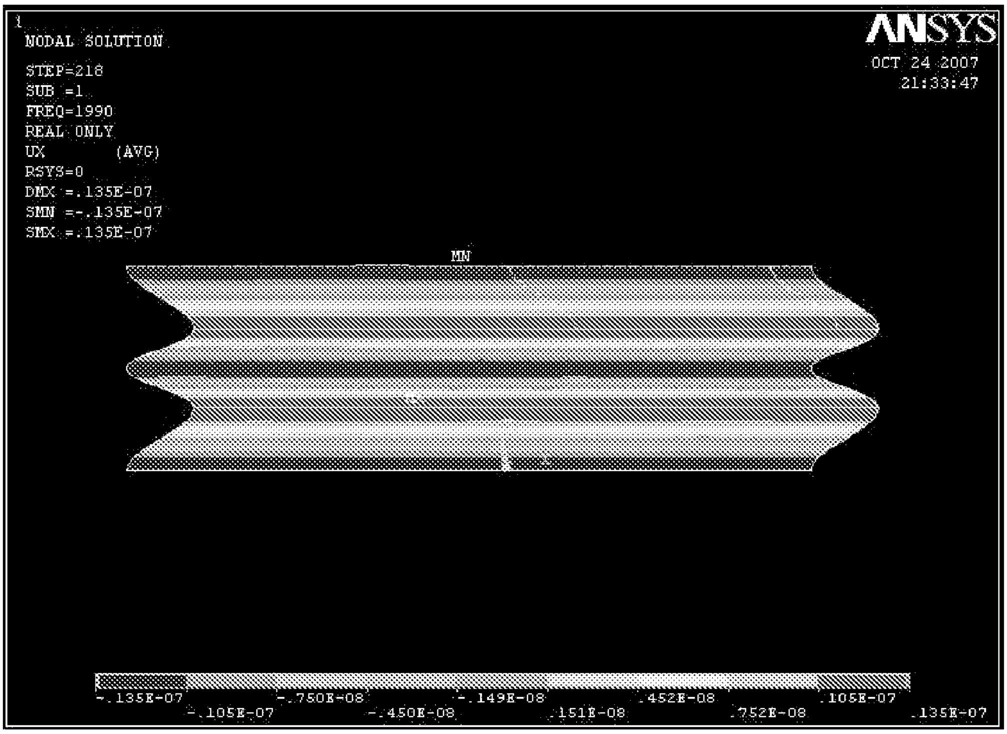

Figure 11

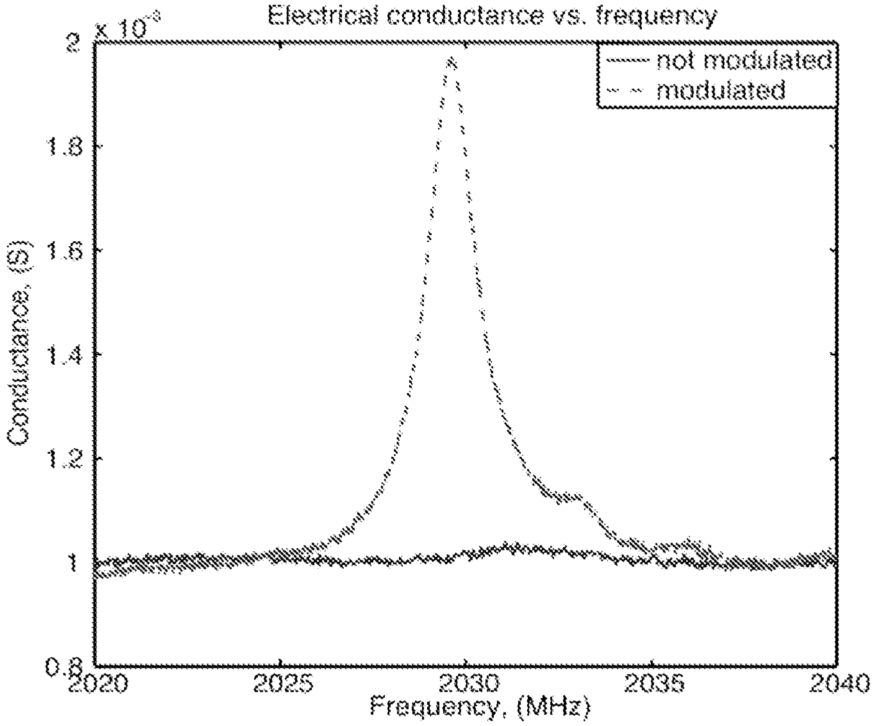

Figure 12

4

Experimental device with piezo-modulated AlN in SMR design

In this chapter we report on the first realization of a piezoelectric modulated IDT transducer. The goal was to decrease piezoelectric coefficients in every other section, and to demonstrate the existence of a pure shear mode.

4.1 Seeking a method to locally reduce the piezoelectric effect in AlN sputtered thin films

Process-microstructure-property relations of AlN thin films are the topic of many many research targeting to optimize the piezoelectric coefficient $d_{33,f}$, or the coupling coefficient k_t^2. A major microstructural parameter is the rocking curve width of X-ray diffraction peaks. This width depends firstly on the tilting of the corresponding planes (i.e. the deviation from parallelism with respect the film plane), and secondly on the coherence length within these planes. The first effect is related to the roughness of the substrate, the second to the density of grain boundaries and dislocations. From these works one can draw a simply conclusion: the better the crystalline quality of AlN, the better the piezoelectric properties and vice versa. This was evidenced in the early work of Dubois and Muralt (19), where two (001)-textured AlN films with rocking curves of 2.41 and 7.24 degree show an almost factor 2 difference in the $d_{33,f}$ coefficient (see fig. 4.1). The difference in film quality was achieved through different deposition conditions. Such an approach would not work to obtain local variations.

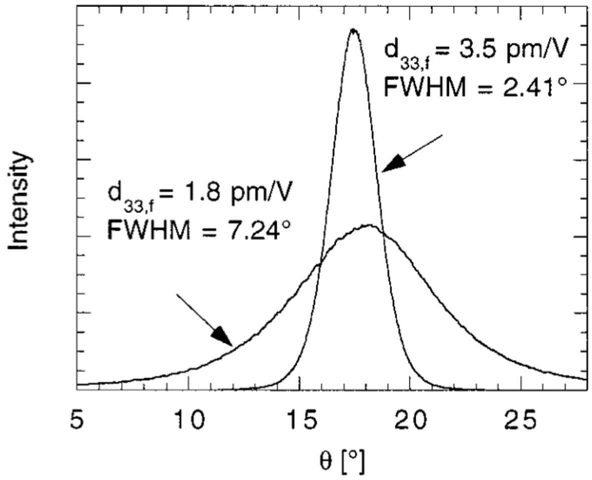

Figure 4.1: X-ray rocking curves and $d_{33,f}$ coefficients of AlN films deposited on Pt with under diffirent conditions (with different values of bias: of either -42V or -27 V) (19)

Of course it is essential that the film is completely (001) textured to achieve good piezoelectric coefficients. Iborra et al (27) show that a considerable reduction in coupling factors was obtained when other orientations were present. However, also complete (001) texture is no guarantee for a good piezoelectricity. In this work, thin films of AlN were sputter deposited under different conditions and their piezoelectric responses were derived from the frequency response of SAW devices 4.2. Tonisch et al. (28) reported the dependence of $d_{33,f}$ from the (002) rocking curve width of full (001) textured AlN films prepared by sputtering and MOCVD (see. fig. 4.3)

In the works mentioned above, the difference of AlN quality was achieved by changing deposition conditions and methods. S. Mishin et al. (30) also investigated the relationship between quality of sputtered films and substrate surface roughness. They showed that the rocking curve width (FWHM) tends to increase as a function of substrate surface roughness (fig. 4.4).

This work was followed by the research of A. Artieda et al (31), who investigated the dependence of the rocking curve width and of stress of AlN thin films sputtered on amorphous Si films with varied roughness. Similar results as by Mishin are reported: the rougher the substrate the broader the rocking curve (fig. 4.5)

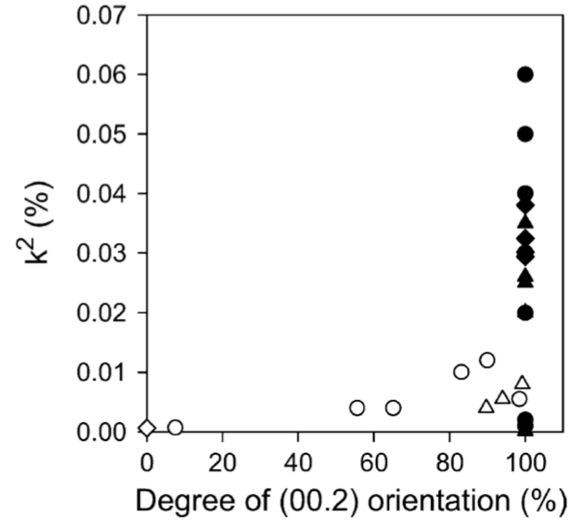

Figure 4.2: Electromechanical coupling factor k^2 as a function of the degree of (002) orientation, defined as the ratio of the peak intensity of the (002) XRD reflection over the sum of the peak intensities of all the reflections in the XRD pattern, for AlN films deposited at different pressures (27)

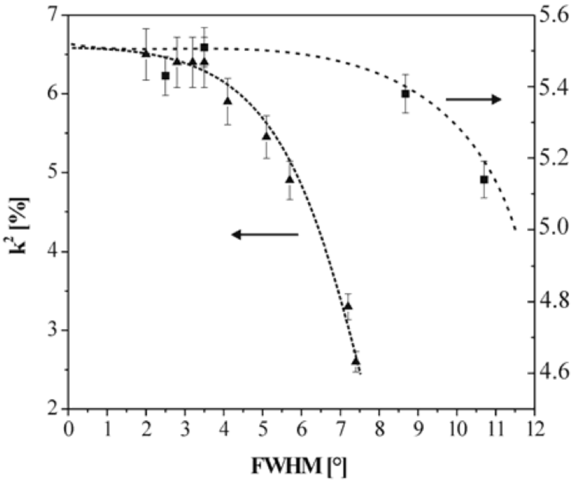

Figure 4.3: Dependence coupling factor k^2 (29) and $d_{33,f}$ (28) on the FWHM of the (002) rocking curve width (FWHM) of AlN films

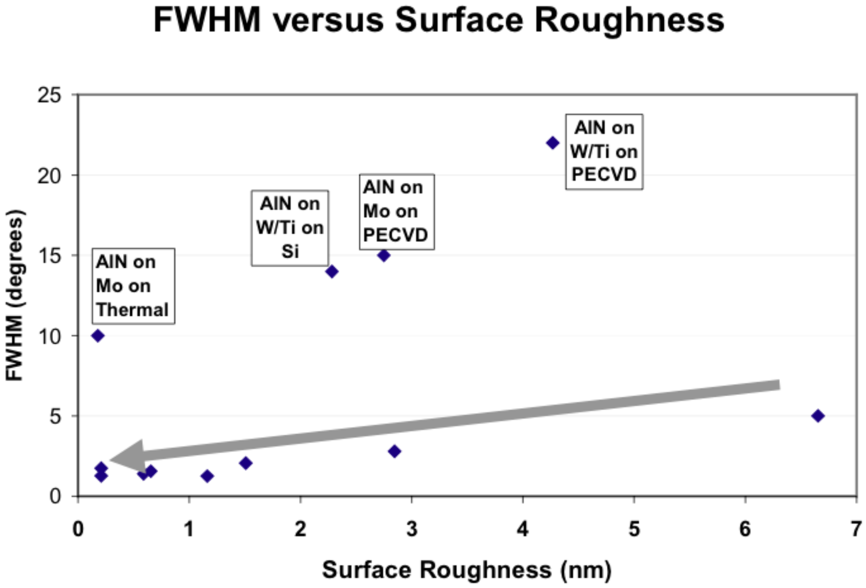

Figure 4.4: Correlation between FWHM of AlN films and substrate surface roughness (30)

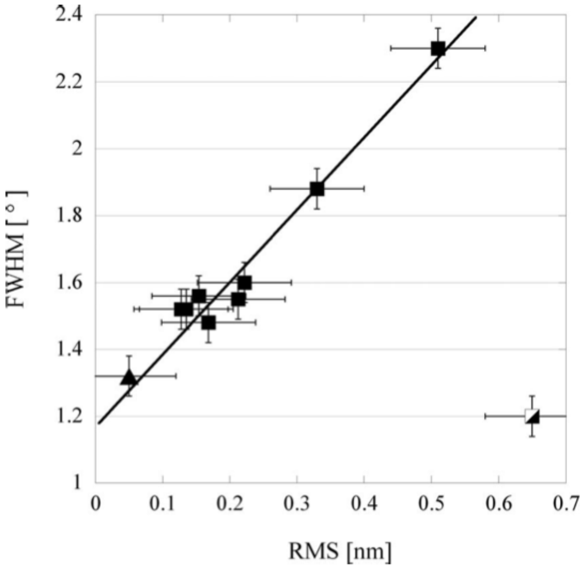

Figure 4.5: Rocking curve FWHM of AlN (002) peak as a function of rms of substrate. Black squares: substrate with Si sputtered layer; white-black square: substrate with (111) Pt layer; and black triangle: substrate of thermal oxide SiO_2. (31)

Seeking a process for the fabrication of AlN thin film with locally different piezoelectric properties, the most promising technique to deteriorate piezoelectric properties appears to be the local control of substrate roughness. The roughness must be tuned to the process that is used to achieve good AlN on smooth surfaces.

4.2 Methods to make rough surfaces

In this section, we studied processes to reduce the piezoelectric coefficients by locally roughening the growth substrate. In the design of the device described in chapter 3, layers under the AlN thin film should be electrically isolating. For engineering the roughness, we need an additional layer that allows the tuning of the roughness. We must be able to introduce the roughness locally, meaning that we need a patterning step. For electrical and acoustic reasons, the AlN film is grown on a SiO_2 layer. This applies for both designs, the SMR design with the reflector, and the membrane design.

We investigated two ways to create roughness. In a first method we add a rough layer locally: the added layer method. In a second method we replicate the roughness of a rough layer that is removed afterwards: the replica method. In both cases photolithography is used to define the places where roughness is introduced. Within the added layer method, an amorphous layer of amorphous silicon (a-Si) is sputtered deposited and lifted off afterwards, remaining only in desired places (see. fig 4.6).

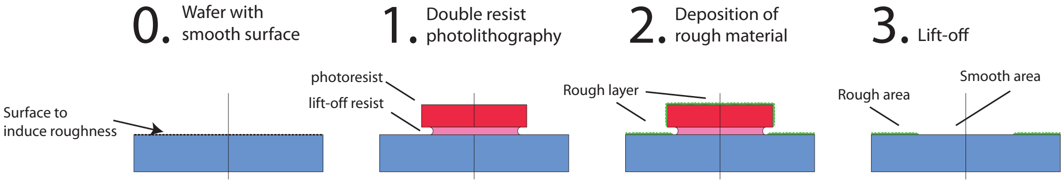

Figure 4.6: Process of inducing roughness by depositing a layer of rough material

Within a replica method, an a-Si layer is sputtered deposited onto the oxide layer through a lift-off mask, i.e. a patterned resist layer. The sputtered material is chosen to have a lower etching rate than the underlying SiO_2 layer during a dry etching process, in our case with C_4F_8, He, CH_4. In this way, during partial or complete removal of the the amorphous layer by dry etching, the roughness of the the amorphous layer is replicated into the SiO_2 surface with a magnification. After etching the eventual rest of the amorphous layer and the resist are removed (see fig. 4.7).

Both processes have their advantages and disadvantages. For device functionality, the roughened surface should in average have the same height as the smooth surface in order to avoid steps between the two surfaces. If we would like to achieve a higher roughness with an added layer, we need to deposit a thicker layer, thus creating steps. In addition, it might lead to problems to lift-off the layer at the border of the resist.

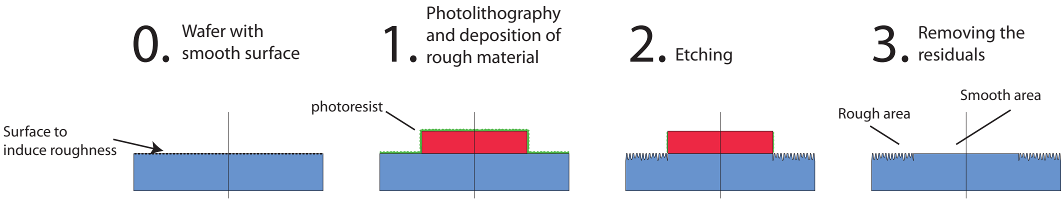

Figure 4.7: Process of inducing roughness by etching

In order to have clean lift-off processes, a double layer resist (LOR) was used with high under-etching of the first layer as shown in fig. 4.6. Sputtered amorphous Si with thickness of 30-50 nm was used as a rough layer on the top of the Bragg reflector that had roughness of around rms=0.15-0.2nm after CMP process. That allows to make a roughness of rms=0.5-0.7nm according to (31). After patterning the layer, the AlN film was deposited. Fig. 4.8 shows the cross-section of the film sputtered onto the surface with patterned roughness. The quality of lift-off process is reflected in the quality of the AlN film. In order to avoid residues from the lift-off process, underetching of 1.5-2 microns of of the lift-off resist was required. The example of defects that appear on the device in case if some residues left during lift-off are shown in fig. 4.9

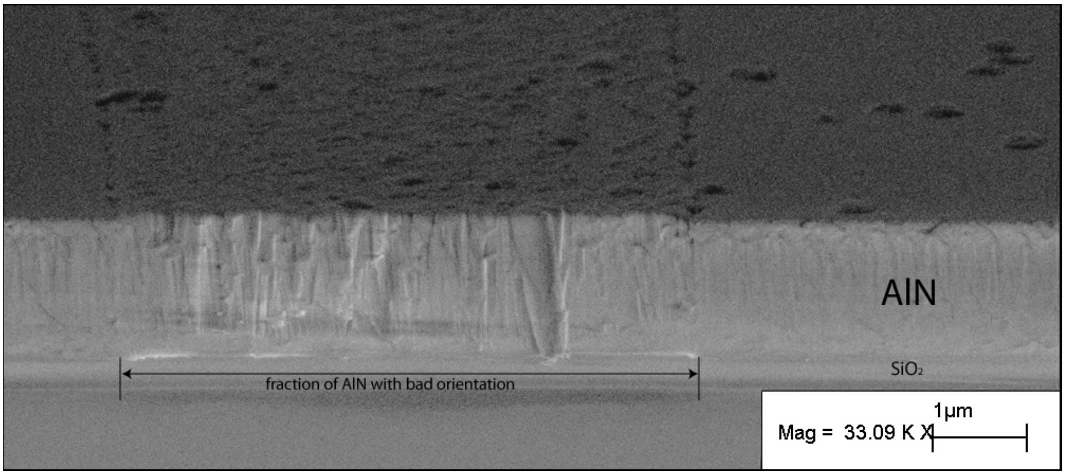

Figure 4.8: AlN thin film sputtered onto SiO_2 with different roughness achieved by added layer method

The second method has the disadvantage that one needs to stop the dry etching process at the right time, thus avoiding to etch too much of SiO_2. The thickness uniformity of the roughness layer can especially be different from the etching uniformity.

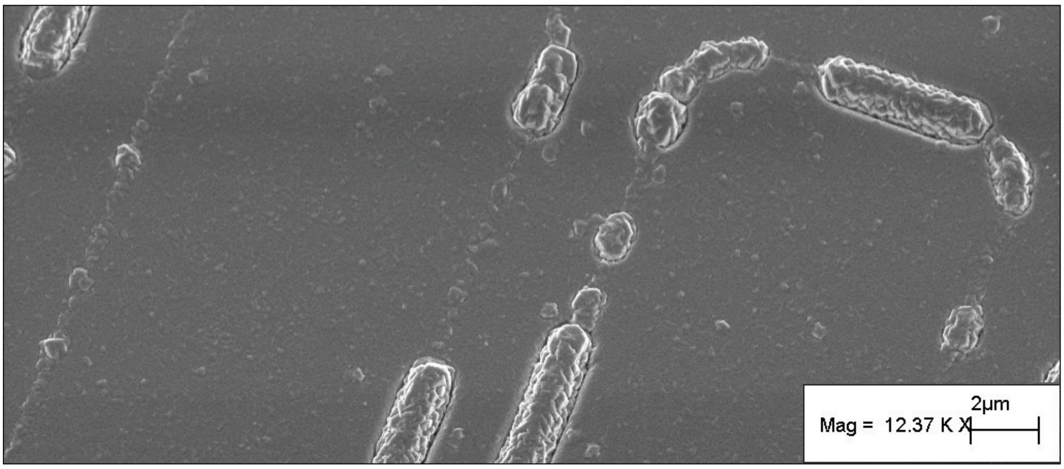

Figure 4.9: Defects on AlN due to residues from lift-off process using the method of added roughness layer

As a result, an optimal result is achieved on a part of the wafer only. We used again an a-Si film as an amorphous layer and then the dry etching process for SiO_2 to achieve the roughness replication. The process use gasses C_4F_8, He, CH_4 at 17 sccm, 150 sccm and 13 sccm respectively. The selectivity with respect to Si is high, i.e. around 20. The a-Si was striped with wet-etching in the HNO_3:H_2O:HF - 50:20:3 solution and the resist was removed. Without inducing much of topography variations, the roughness was considerably increased to 1.5-2nm. The roughness measured with AFM is represented on fig. 4.10 for rough and smooth areas.

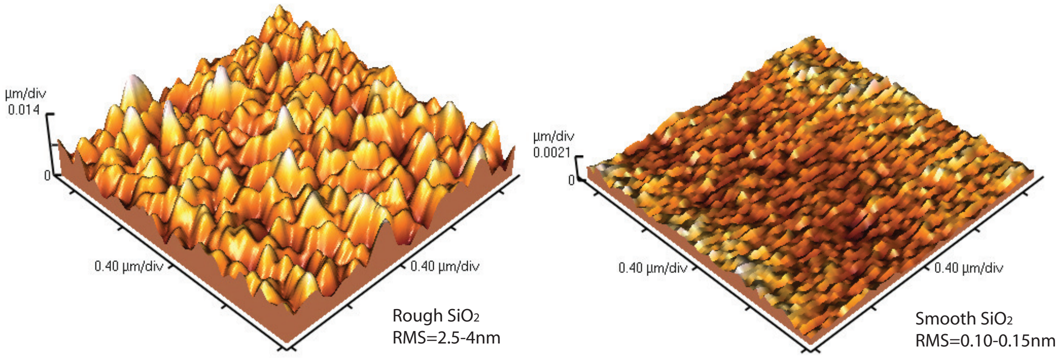

Figure 4.10: AFM measurements of surface roughness of rough and smooth areas after the replication process

4.3 Decrease of piezoelectric properties of AlN

The AlN thin film obtained on a rough amorphous surface by the replica method was characterized by XRD diffraction, comparison of the XRD scans for these films is shown in fig. 4.11. A rocking curve width of 7.2 degrees was observed. As there is no bottom electrode below AlN, it was not possible to measure $d_{33,f}$. For this reason, we prepared a sample with identical AlN process that included a bottom electrode below the oxide film. We obtained the rocking curve width less than 7.2 degree - of 5.6 degrees. This structure could be characterized by double side interferometry for deriving the clamped $d_{33,f}$ ($=e_{33}/c_{33}$) as 2.4 pm/V. We think that the AlN on the insulating reflector stack will have the same $d_{33,f}$ or less, on the parts with the added rough layer.

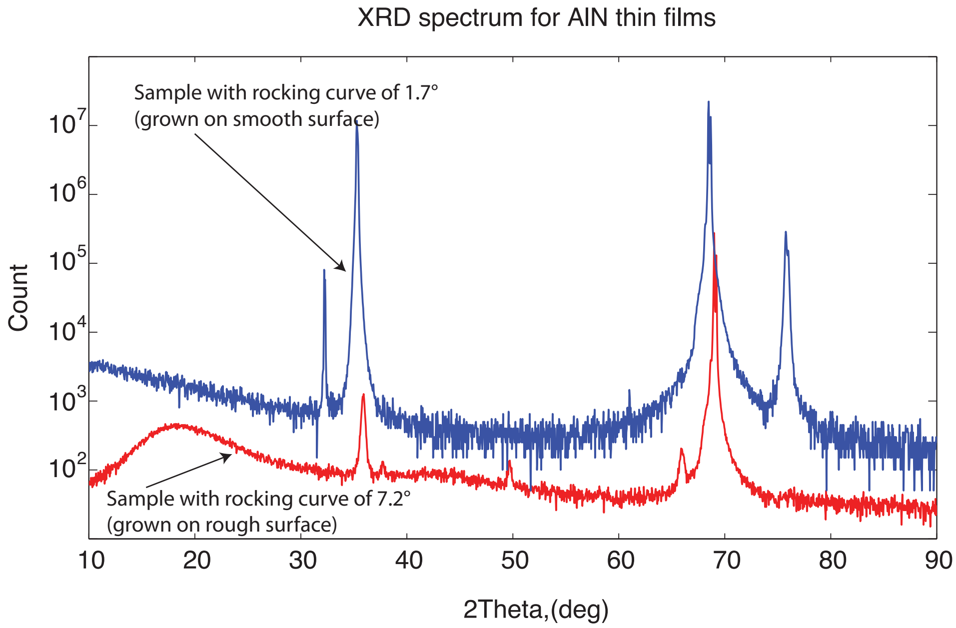

Figure 4.11: XRD scans of AlN films grown on smooth and on rough surfaces of SiO_2

That work was reported on the frequency control symposium and some results were included in the publication entitled "Highly piezoelectric AlN thin films grown on amorphous, insulating substrates" by Artieda et al. (32)

Though thin films of AlN fabricated on the smooth and rough surface achieved with replica method was obtained and characterized, due to the big difference in their properties (stress and orientation), simultaneous growth of such film was not successful. Growth on interface between good and bad AlN was observed to go in unusual way (see fig. 4.12) - along the border that divide rough and smooth region there are animal growth that forms the topographical step of 250 nm and that makes further processing of such a wafer to be impossible.

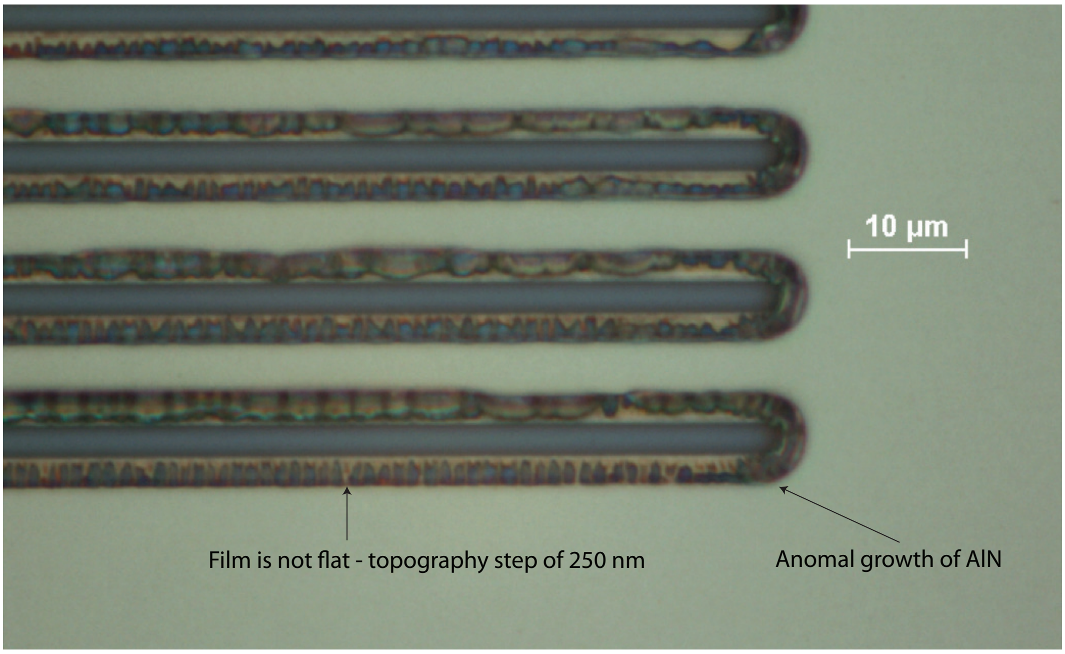

Figure 4.12: Anomaly growth of AlN along the border that divides rough and smooth regions of the SiO_2 substrate

For the further device completion, the rough surface was obtained by using the method of adding the rough layer.

4.4 Device completion

In order to demonstrate of the effect of modulated piezoelectric properties, we introduced the local roughness according to the added layer method as additional fabrication steps to the process flow of the first device 4.2, which was based on a homogeneously smooth surface of the Bragg reflector. The patterns of the added a-Si layer were defined in agreement with the IDT electrode mask. The smooth/rough interface was situated in the center of the electrode.

Bragg reflector and AlN layer thickness were optimized for shear mode operation, targeting the resonance frequency at 2GHz. The electrodes load the resonator non-uniformly. For this reason, we used Al as electrode metal, and kept its thickness as small as possible. This reduces the risk of exciting parasitic waves. In addition, we filled the areas between IDT fingers with SiO_2. A SiO_2 thin film was first sputtered deposited onto the device with completed IDT, and then polished down to the electrodes to flatten the surface. Subsequently, gold layers were evaporated onto the contact pads by a lift-off process.

The device was measured before and after deposition and polishing of SiO_2 (fig. 4.13). The resonance at frequencies around the expected one was observed and it was also observed that the resonance improved after SiO_2 deposition and polishing.

Measurements of the device are shown in fig. 4.13.

In addition to the device fabricated with patterned a-Si, there were also a devices without any rough layer patterns on the same wafer. The purpose was to identify the change introduced by the patterned rough layer, and to verify that the pure shear mode would only exist in the resonators including the rough layer.

Fig. 4.14, shows the measurements of device with patterns of a-Si and without it. The device that doesn't have patterning don't the resonance behavior at chosen frequency.

This work was reported on the ultrasonic symposium, see the paper "PMBAR - shear mode TFBAR based on (001) AlN thin film".

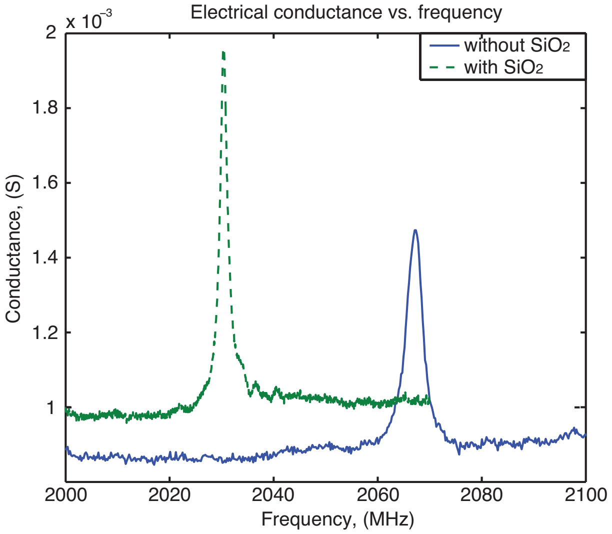

Figure 4.13: Resonances observed for SMR resonators without SiO_2 between electrodes and after it's deposition and polishing

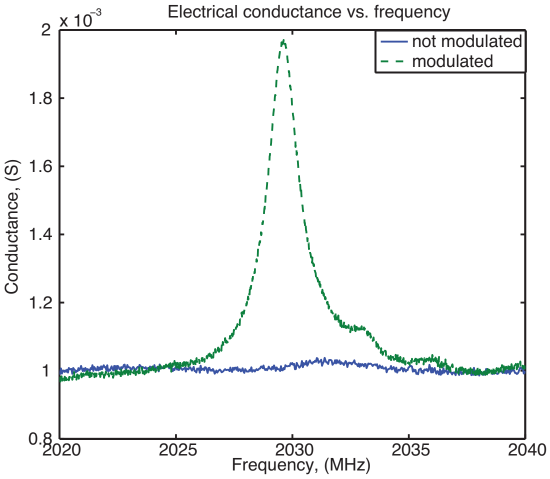

Figure 4.14: Comparative measurements of the device with a-Si patterns and without

PMBAR * - SHEAR MODE TFBAR BASED ON (001)ALN THIN FILM

* Piezo-Modulated Bulk Acoustic wave Resonator

E. Milyutin and P. Muralt

Preprint for Proceedings of International Ultrasonic Symposium, Beijing, 2008

I. INTRODUCTION

The use of quartz crystal microbalances (QCM) as gravimetric sensors in liquids clearly shows the potential of shear acoustic wave resonators for bio-medical applications. As the relative sensitivity increases with working frequency, resonators operated at GHz frequencies are very promising to push down detection limits [1]. Shear mode thin film bulk acoustic wave resonators (TFBARs) with tilted c-axis AlN or ZnO are studied by several groups as an alternative to QCM [2-4]. However, homogeneous deposition of tilted c-axis material is quite difficult, and certainly does not correspond to the AlN needed for the larger telecom market. For this reason, we studied the possibility to achieve shear mode resonators with standard c-axis oriented AlN thin films based on interdigitated electrodes, AlN growth on sputtered SiO_2 films, and acoustic Bragg reflectors for acoustic isolation[5]. Such a structure leads to an excitation of mainly shear mode displacements in the AlN film. However, a more pure mode is expected if only every second electrode section would contain active AlN, thus requiring means to selective disabling the piezoelectricity in AlN. In this article, such Piezo-Modulated BAR structures - abbreviated PMBAR - are studied by the finite element method to evaluate the theoretical performance. In addition, first experimental results are presented.

II. IDEA OF PMBAR

The PMBAR design [6] makes use of a c-axis oriented AlN thin film with modulated piezoelectric properties, i.e. only a part of the film is piezo-active and the rest behaves as a dielectric with mechanical properties of AlN. In fig. 1 one period of such film is shown, half of which is piezoelectric and the rest is not. An interdigitated electrode system is employed to excite the acoustic waves, whereby the piezoelectric activity is modulated in phase with the electrode field, meaning that the piezoelectric sections see all the same direction of the electric field. Non-piezoelectric sections are indifferent to electrical field and they just follow the motion of piezoelectric ones, forming a homogeneous shear deformation of the whole film. Following finite element modeling is confirming this assumption.

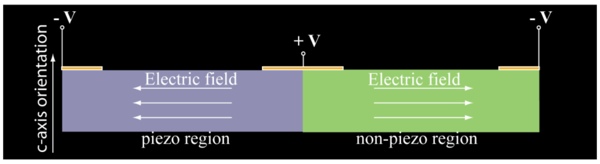

Figure 1. Conceptual design of PMBAR

III. FINITE ELEMENT MODELING

Finite element modeling was performed with the ANSYS program in combination with the module of Microsonics [7], adding a boundary element method (FEM-BEM simulation). This is needed to deal with the boundary between acoustic reflector and silicon wafer by the inclusion of a semi-infinite substrate. First, the concept of PMBAR was verified for a freestanding, piezo-modulated film slab as shown in fig. 1. Piezoelectricity in half of the film was assumed to be zero. The ID electrodes were assumed to be ideally conductive, and absolutely thin. Periodic conditions along the horizontal direction were imposed. Operation in air was modeled by setting boundary conditions of a mechanically free surface. Immersed operation was modeled by applying the BEM to the liquid/resonator interface. The electrodes were set to be isolated electrically from the liquid. The mechanical properties of the liquid were chosen to be the ones for water, except that the viscosity was assumed to be zero. In this ideal case of unloaded resonator, mode trapping occurs at exactly $\lambda/2$. A film thickness of 1.55 microns was used in the calculation, corresponding to a resonance at approximately 2 GHz. The phase of the electrical admittance vs. frequency is shown in fig. 2. A resonance close to 2 GHz is observed. Only a minor change occurs when passing from air into the liquid. This means that acoustic emission into the liquid is practically absent, as expected for an ideal shear mode. The motion in the film, as obtained by the same calculations, shows indeed that the displacements are close to ideal shear mode behavior film. The coupling coefficient k^2 amounts to 0.6 %.

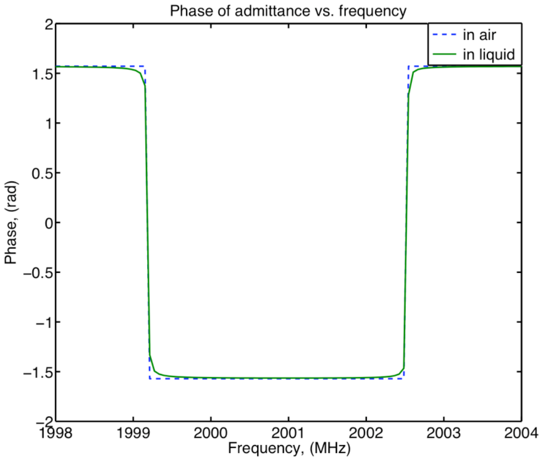

Figure 2. Modeled phase of electrical admittance of free standing membrane PMBAR under operations in air and in liquid

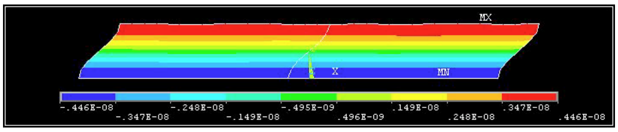

Figure 3. Modeled deformation (contour) and x-displacement (colored) of free standing membrane PMBAR at resonance frequency

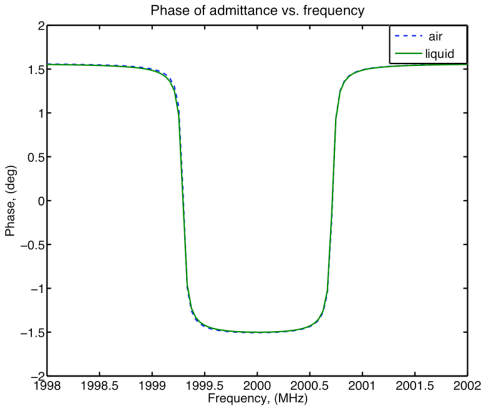

Figure 4. Modeled phase of electrical admittance of solidly mounted PMBAR operated in air and in liquid.

After showing the principle functioning PMBAR's, we added some of the necessary elements for a realistic device, first of all a Bragg reflector for acoustic isolation. The Bragg reflector should be dielectric in order to avoid short-cuts of the electric field through the reflector layers acting like floating electrodes. We chose AlN (high impedance material) and SiO_2 (low impedance material) as reflector materials, as used in earlier works [8-9]. A sufficiently high reflectivity is achieved with 5 layer pairs. These were included in the finite element modeling between silicon substrate and active AlN layer, each layer having a $\lambda/4$ thickness. Fig. 4 shows the simulation result for the admittance phase. There is again no difference between operation in air and liquid. A deterioration of the quality factor is observed, which is due to acoustic losses into the substrate through reflector. However, the remaining value of 25'000 is largely sufficient and won't play anymore a role once the materials quality factors are taken into account. In addition the coupling coefficient k^2 is reduced by about 0.3 %, or half of the previous value. This is most likely due to the parasitic capacity introduced with the Bragg reflector. The calculated displacements and strains are shown in fig. 5. The shear thickness mode resonance and the effect of acoustic isolation by the Bragg grating is clearly observed.

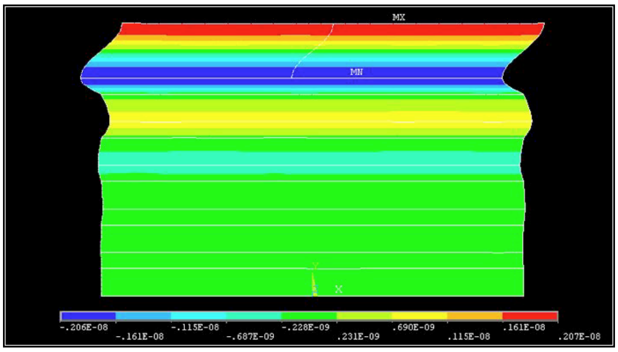

Figure 5. Modeled deformation (contour) and x-displacement (colored) of solidly mounted PMBAR at resonance frequency

IV. EXPERIMENTAL PROTOTYPE

Prototypes of PMBAR, as shown in fig. 5, were fabricated using AlN as piezoelectric material. Thin films of AlN and SiO2 have been deposited by dc-pulsed reactive magnetron sputtering and rf-sputtering respectively, at 300C, similar as in work[10]. The top views of experimental devices are shown in fig. 6. In order to be sure that we observe a resonance with a piezo-modulated AlN, the same device, but without modulation of properties, was fabricated nearby to the PMBAR on the same wafer. The electrical properties of both devices, as measured in air, are displayed in fig. 7. A resonance frequency is found at around 2.0GHz in the modulated device (PMBAR), but not in the non-modulated device for which the resonance would occur at a higher frequency, which eventually is not supported anymore so well by the Bragg reflector. This finding confirms that the selective disabling of piezoelectricity works at least partially, and that the searched mode exists. The width of conductance curve indicates a Q-factor of 1100. The experimental coupling coefficient is considerably lower than theoretically expected, meaning that we still can improve very much the resonator. The experimental method for the modulation of piezoelectric properties is under study, and not yet characterized.

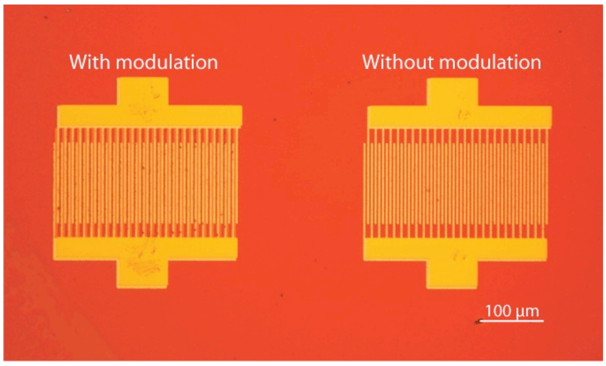

Figure 6. Top view of experimental devices, left on based on modulated film of AlN, right one on non-modulated one.

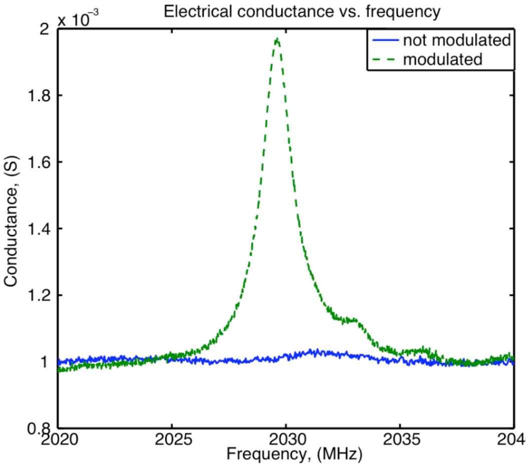

Figure 7. Measured electrical conductance for PMBAR device and for device based on non-modulated AlN.

V. CONCLUSIONS

We have shown a new design of TFBAR based on c-axis oriented AlN thin film that is able to operate in a shear mode. FEM-BEM simulations demonstrated the potential of the device as high-quality resonator for immersed operations.

First devices were fabricated. Their resonance frequency was close to theoretical expectation, i.e. matches with the planned shear mode. The obtained quality factor amounted to 1100, as measured in air. The coupling coefficient was 7 times lower than theoretically possible, meaning that there is a large potential for improving the resonator characteristics by improving mainly materials, and the efficiency of the process disabling piezoelectricity.

VI. ACKNOWLEDGEMENTS

This work was supported by the Swiss National Science Foundation and the European FP 7 project MOBESENS.

REFERENCES

[1] Gabl, R., H.-D. Feucht, H. Zeininger, G. Eckstein, M. Schreiter, R. Primig, D. Pitzer, and W. Wersing, “First results on label free detection of DNA and protein moecules using a novel integrated sensor technology based on gravimetric detection principles”, Biosens. Bioelectron., 2004. 19: p. 615-620.

[2] G. Wingqvist, J. Bjurstrom, A.-C. Hellgren, I. Katardjiev, “Immunosensor utilizing a shear mode thin film bulk acoustic sensor”, Sensors and Actuators B, 127 (2007), p. 248–252

[3] Jan Weber, Willem M. Albers, Jussipekka Tuppurainen, Mathias Link, Reinhard Gabl, Wolfram Wersing, Matthias Schreiter, “Shear mode FBARs as highly sensitive liquid biosensors”, Sensors and Actuators A, 128 (2006), p. 84–88

[4] Takahiko Yanagitani, Masato Kiuchi, Mami Matsukawa, and Yoshiaki Watanabe, “Characteristics of Pure-shear Mode BAW Resonators Consisting of (1120) Textured ZnO Films”, IEE Transactions on Ultrasonics, Ferroelectrics, and Frequency control, vol. 54, no. 8, p. 1680-1686, August 2007

[5] E. Milyutin, S. Gentil, and P. Muralt, “Shear mode bulk acoustic wave resonator based on c-axis oriented AlN thin film", J. Appl.Phys. 104 (2008), in press.

[6] E. Milyutin, Paul Muralt, Patent application, N 61/085,479, 1 August 2008.

[7] Microsonics, contacts: rue des Granges Galand, 37554 Saint Avertin Cedex – France, Tel : +(33) (0)2 47 28 22 34, www.microsonics.fr.

[8] K. M. Lakin, K. T. McCarron, and R. E. Rose, Proceedings of the IEEE Ultrasonics Symposium, Seattle, WA, IEEE, Washington, 1995.

[9] M.-A. Dubois, P. Muralt, H. Matsumoto, and V. Plessky, Proceedings of the IEEE Ultrasonics Symposium, Sendai, Japan, 1998, pp. 909–912.

[10] Lanz, R. and P. Muralt, “Bandpass filters for 8 GHz using solidly mounted bulk acoustic wave resonators”, IEEE Trans. UFFC, 2005. 52: p. 936-946.

5

Advancing AlN growth: Al-polar and N-polar films

5.1 Polarity of sputtered AlN

The work described in the previous chapter dealt with processes to reduce the piezoelectric coefficient in a controlled way on defined areas, and how to build a IDT resonator with such processes. There are, however, disadvantages with polarity reduction. The microstructure of AlN films with a small degree of polar order can be very much different from the one of good films with a high degree of polar order. This difference will result also in a difference of the rigidity, especially if other than (001) orientations are present, and thus acoustic properties will change. This works against having a pure shear mode vibration. Furthermore, as derived in chapter 3, we would achieve in the best case only 1/4 of the maximal possible coupling factor k_t^2, which is realized when we deal with a completely inverted polarity instead of a zeroed polarity:

$$k_t^2 \propto (e_{15}^{(1)} - e_{15}^{(2)})^2 \tag{5.1}$$

We need e_{15} coefficients of different signs. In the ideal case one should use an AlN thin film with periodic patterns having (0002) and (000-2) orientations. In this chapter, approaches to realize such films are studied.

In most applications, the sign of the piezoelectric coefficient does not matter, since the sign is anyhow everywhere the same. No particular orientation, i.e (0002) or (000 -2) is required, as either only the coupling is relevant, or negative and low voltages can be supplied for driving the device. For this reason, the improvement of the e_{33} is much more often the research topic than the sign of the effect.

Regarding AlN films sputtered by our group, $d_{33,f}$ measurements with double side interferometry reveals systematically the same sign when dealing with AlN films deposited by pulsed DC reactive sputtering (32). The obtained polarity is called N-polar. This was also confirmed by etching test allowing to discriminate between the two polarities: Al-polar AlN films are more stable in KOH aqueous solutions than N-polar films. This method is routinely used to determine the polarities of GaN and AlN films, and has the advantage that it does not require electrodes. Films of N-oriented GaN form pyramidal shapes after the etching, and Ga-polar films are not etched at all, or may show conical holes where N-polar regions exist, (33) (see fig. 5.1).

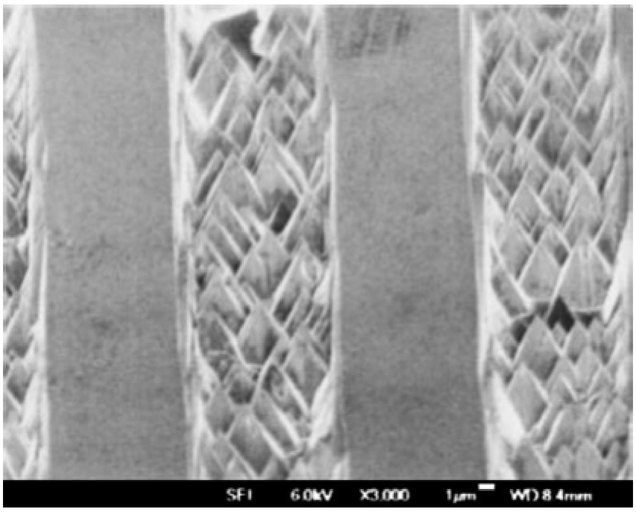

Figure 5.1: SEM image of GaN sample taken after etching in 2M KOH at 908C for 45min. Hexagonal pyramids were formed in the N-polar region while the surface of the Ga-polar region remained smooth and intact, (33)

GaN and AlN are chemically very similar, and exhibit the same crystalline structure. The etching in KOH is thus expected to be very similar. There is, however, a difference: the Al-polar AlN is less resistive to alkaline etchants than Ga-polar GaN because Al is more reactive than Ga. Our N-polar AlN thin films are strongly attacked by aqueous KOH solutions, forming pyramids as shown in fig. 5.2 and fig. 5.3. The worse the film orientation is in terms of rocking curve width and degree of (001)-texture, the less the etching pattern resembles the pattern of isolated pyramids, and the more resistive the film becomes to etching. This is certainly due to the higher density of oppositely polar grains.

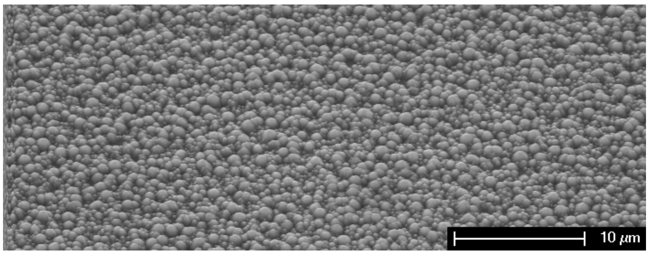

Figure 5.2: N-polar film of AlN after etching in 5M KOH aqueous solution

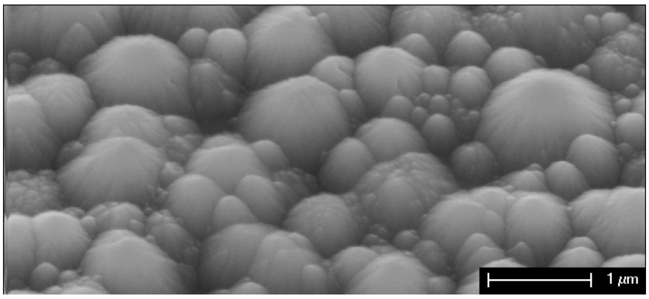

Figure 5.3: Close view on pyramids in N-polar film of AlN after etching in 5M KOH aqueous solution

5.2 Polarity of AlN by other deposition methods

There are others methods of depositing nitrides such as AlN and GaN. For example, MOPVE and MBE method are used to fabricate AlN and GaN for electro-optical applications. For some of the applications, it's important to know the polarity of these nitride films, and even to have different polarities in the same layer (34), so the issues related to polarity of AlN and GaN is more investigated in that field. Few works to switch GaN polarities was reported. One of the methods to switch the polarity is to use the template of the material (AlN or GaN) with desired polarity and then the film that is grown on such template follow the polarity of the template. Such a method is also used to growth the film with Ga-polar/Al-polar and N-polar patterns by patterning the template (35), as in fig. 5.4.

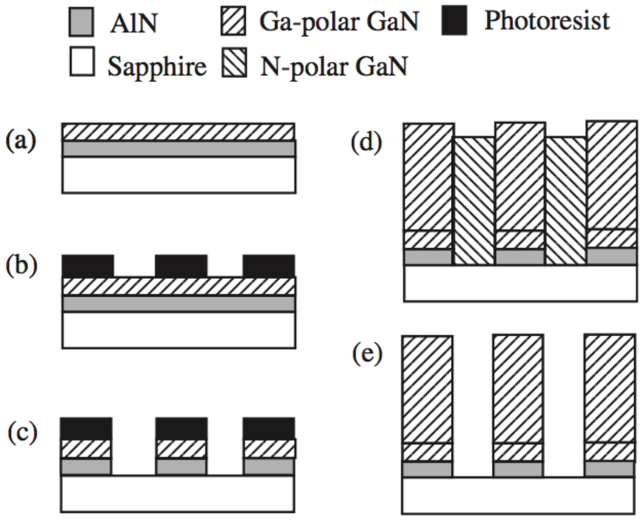

Figure 5.4: Process flow for fabricating GaN microstructures by PSCE: (a) GaN/AlN growth on sapphire by MBE, (b) formation of stripe/hole pattern by optical lithography, (c) plasma etch to expose the sapphire substrate, (d) second growth of GaN by MBE, and (e) PSCE step to remove N-polar GaN, (35)

5.3 Switching the polarity of sputtered AlN

In our work, the goal was to switch the polarity of sputter deposited AlN thin films. Since the DC pulsed sputter process does leads to N-polarity only, we profited from metal organic phase vapor epitaxy (MOPVE) processes delivering the Al-polarity when growth was carried out on crystalline silicon. Both AlN and GaN template layers deposited by MOPVE were used. The polarity is checked by the etching experiment. Fig. 5.5 shows an example of the AlN thin film sputtered onto highly-oriented 500 nm Ga-polar GaN layer, and subsequently etched in the KOH solution. The film was etched much more slowly than N-polar films. Hexagonal holes in AlN are the signs of an Al-polarity film with a certain density of N-polar grains.

Decreasing the GaN film thickness lead to a decreasing quality of the Al polarity in the sputter deposited AlN film. One of the reasons for that is the quality of the seed layer in terms of (001)-texture - for thinner films deposited with MOPVE the quality is worse. In addition to GaN, we tested as well Al-polar AlN grown by MOPVE as a template. The thinnest investigated template had a thickness of 100nm. With this template, the Al-polarity was still copied by the sputter deposited film. In order to

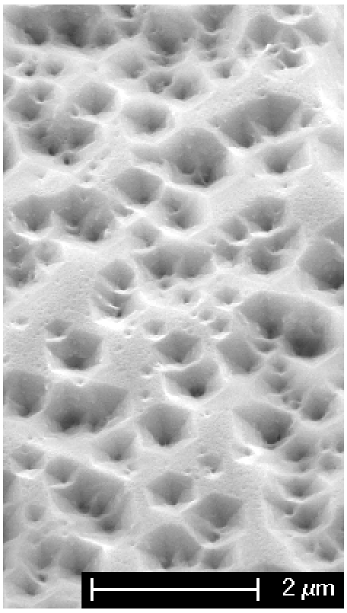

Figure 5.5: Al-polar AlN film after etching test

achieve Al-polar and N-polar regions within a film sputtered at fixed conditions, a thin layer of sputter deposited SiO_2 was patterned on the surface of the template AlN. AlN grown the SiO_2 regions is expected to grow as usual in N-polarity, while the AlN grown on the template is expected to grow with Al-polarity. Fig. 5.6 shows a SEM picture of such a film before and after the etching test.

In addition to the etching test, PFM measurements were carried out to verify the sign of the piezoelectric effect as a proof of local polarity control.

This part of my PhD work is published in "Sputtering of (001)AlN thin films: Control of polarity by a seed layer"

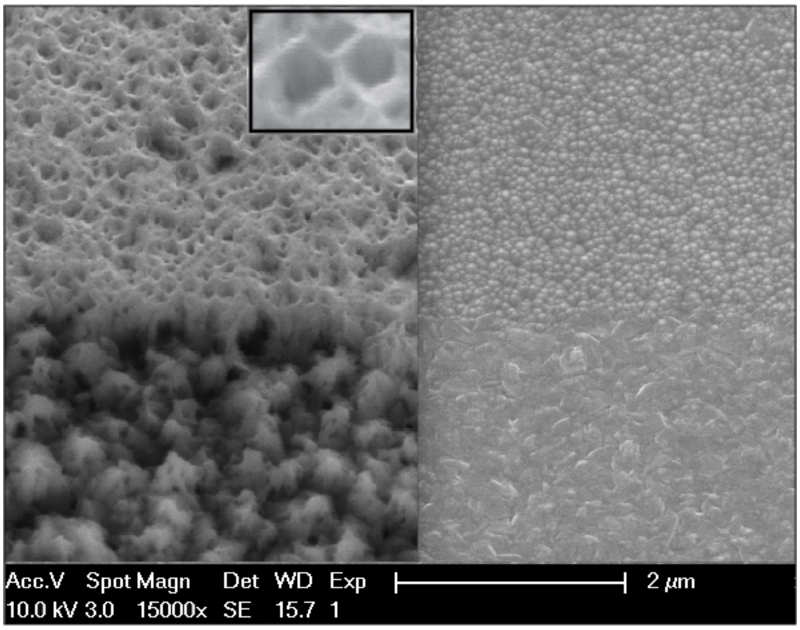

Figure 5.6: Sputtered AlN film with patterned polarities

5.4 Towards a device with locally controlled AlN polarity

Based on the processes as described above, the fabrication of a device was studied. The template layers were only available on 2 inch wafers, which caused considerable complications in processing. For the integration of the template process into the process flow of the device fabrication (see fig 5.7), there are two particular steps to be discussed:

1. In order to avoid any reaction of the AlN template layer with chemicals involved in the photolithography process (especially the alkaline developer of the positive resist is a high risk), we used a shadow mask for patterning the SiO_2 layer on the wafer level. Such a shadow mask was prepared by silicon micro machining using a patterned silicon nitride membrane as mask layer (36).

The SiN membrane of the shadow mask is in contact with a surface of the seed layer on the processing wafer and the SiO_2 deposition is realized through the openings of the shadow mask. The contact of the AlN template layer to photoresist and developer is thus prevented. Nanostencil shadow masks are quite fragile, and for processing several wafers in parallel, that is normally done for the step of evaporation of SiO_2 (step B in the process flow), one would require as much masks as wafers to process. That complicates the fabrication.

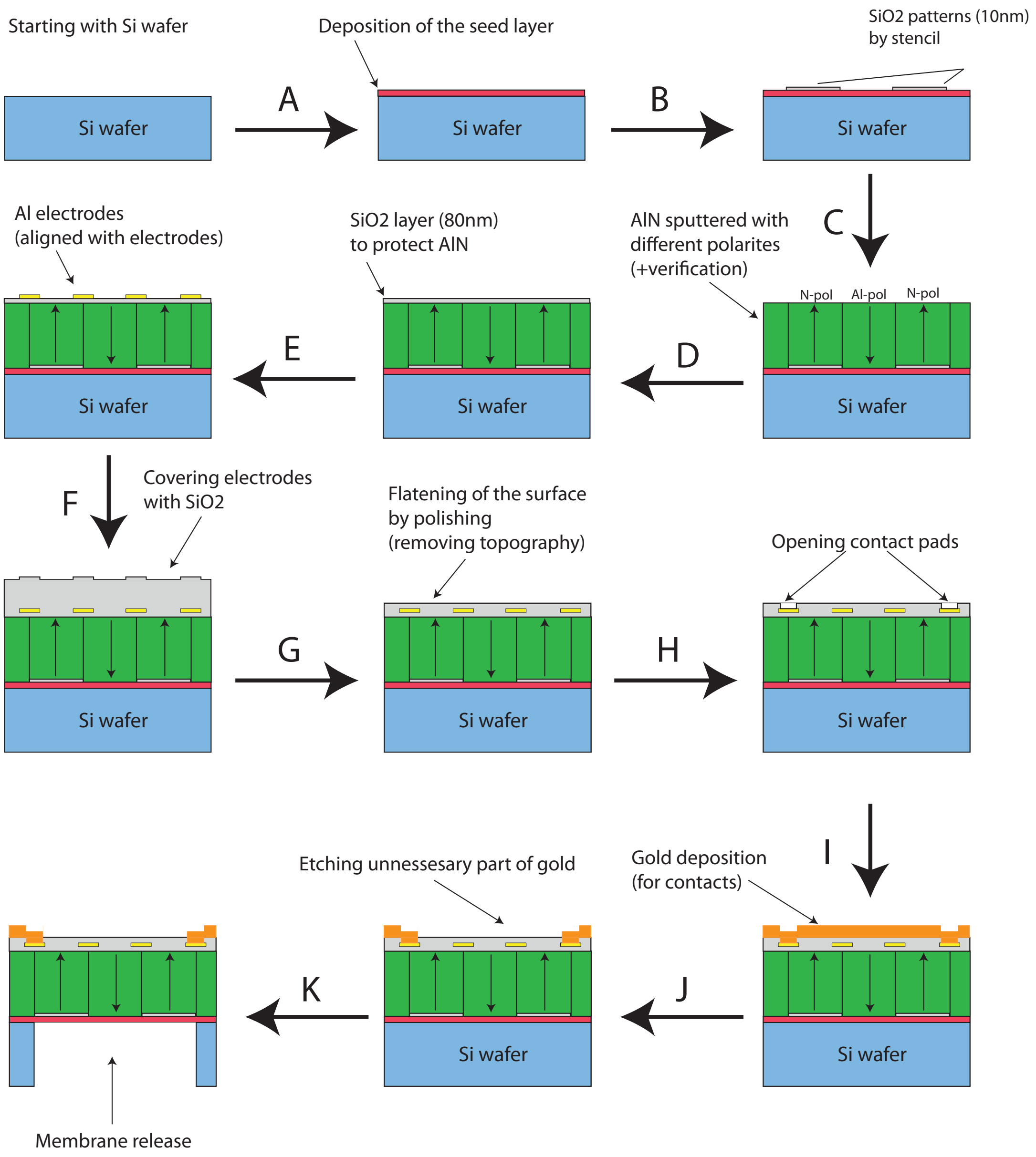

Figure 5.7: Process flow for the fabrication of the device with reversed polarities

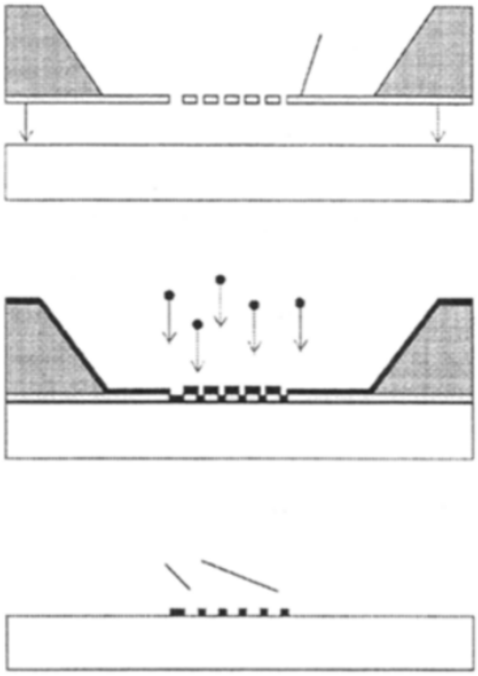

Figure 5.8: Schematic illustration of shadow-evaporation through a nanostencil (36)

After patterning the SiO_2, AlN film with varied polarities was grown in one step, see the fig. 5.9.

2. The patterns of the N-polar and Al-polar in the resulting sputtered AlN film are optically the same and it's difficult to align the electrode pattern (step E of the process flow). To resolve this issue, after the step C and before going with step D, we exposed regions of the wafer with alignment marks to the KOH based solution while protection the devices. Alignment marks are N-polar pattern of AlN in the Al-polar film, so after etching topography appear step appear between Al-polar and N-polar regions. That made the marks well seen under the microscope and thus simplified the alignment of the electrodes on the patterns of AlN (see fig. 5.10).

Result of testing the fabrication processes is shown in fig. 5.11 and confirming its feasibility.

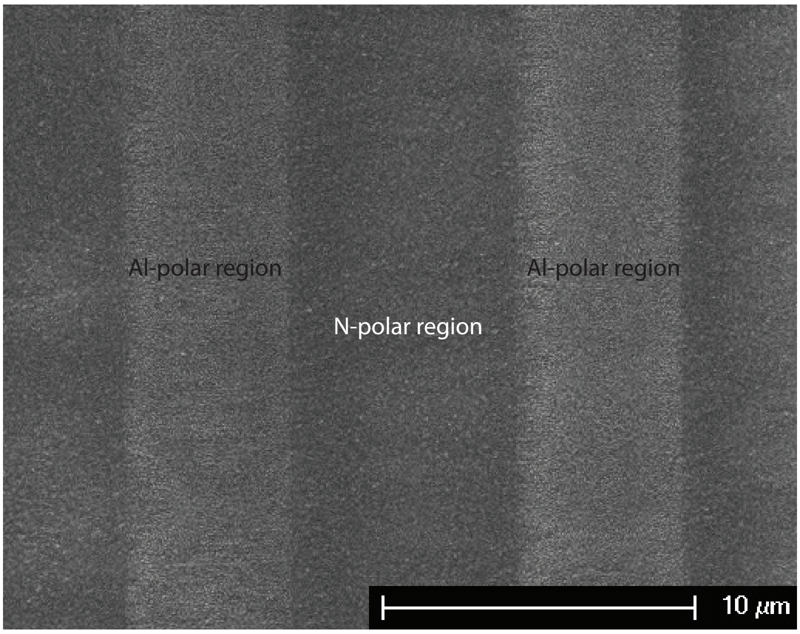

Figure 5.9: SEM picture of the surface of the AlN film with polarity patterns as desired for the device design

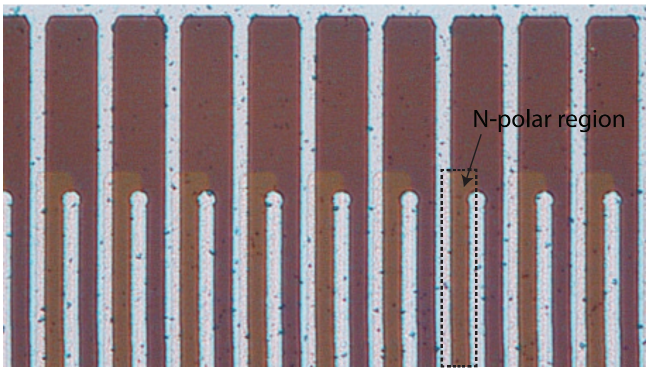

Figure 5.10: Alignment of electrodes respectively to the regions of different polarities

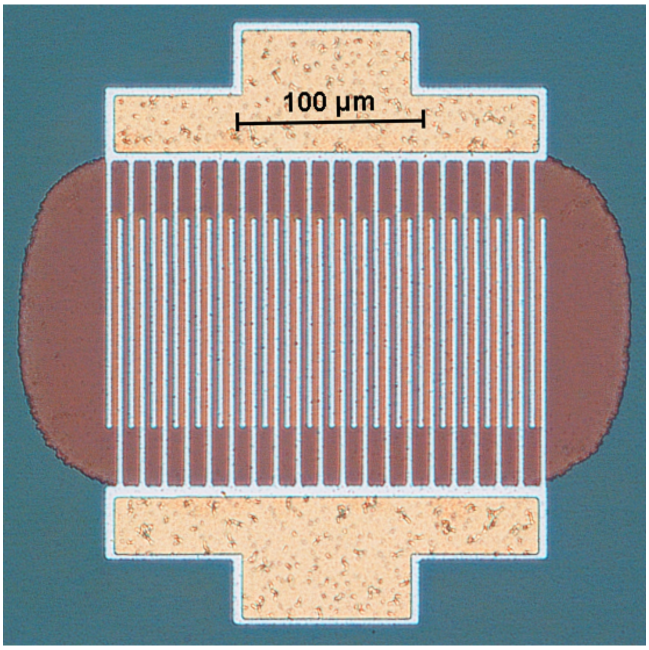

Figure 5.11: Membrane based on AlN with different polarities with IDT electrodes

SPUTTERING OF (001)ALN THIN FILMS: CONTROL OF POLARITY BY A SEED LAYER

E. Milyutin, S. Harada, D. Martin, J. F. Carlin, N. Grandjean, V. Savu, O. Vaszquez-Mena,

J. Brugger and P. Muralt

Preprint for Journal of Vacuum Science and Technology B

I. INTRODUCTION

Polycrystalline, (001)-textured AlN thin films obtained by sputter deposition have important applications in microwave rf filter technology for mobile communication.[1] The deposition is a rf or dc-pulsed[2] reactive sputter process and excels by the high degree of polar ordering at relatively low temperatures of 300 °C or less, which is very attractive for silicon based micro-electro-mechanical systems (MEMS) fabrication. For current ultrasonic applications, it does not matter whether the film grows in Al- or N-polarity (see Fig. 1 for the definition in terms of lattice orientation). It is only required that it is the same everywhere in a single resonator structure, which is a parallel plate capacitor in electrical and geometrical terms. However, the freedom to locally select the polarity opens new possibilities for the design and application of thin film bulk acoustic wave resonators, as well as of Lamb wave devices and surface acoustic wave devices. In this article, the advantage is illustrated for the case of a shear mode thin film bulk acoustic resonator excited by means of an interdigitated electrode on top of a *c*-axis textured film.[3] The coupling to the shear mode is a function of the difference of the piezoelectric coefficients $e_{15}^{(1)}$ and $e_{15}^{(2)}$ in the regions of positive field [upper index (1)] and negative field [upper index (2)], if we give a polarization dependent sign to e_{15}.

$$k_{\text{shear}}^2 = \frac{(e_{15}^{(1)} - e_{15}^{(2)})^2}{4c_{55}\varepsilon_{11}} . \tag{1}$$

Normally, sputter deposited AlN films exhibit N-polarity, irrespective of the substrate. It appears that this polarity is caused by the ion bombardment giving advantage to this polarization during growth, as evidenced by a number of findings such as higher piezoelectric coefficients with larger bias voltage, and higher coefficients with thicker films.[4–6] In a previous study, Akiyama *et al.*[7] reported that the polarity is turned by doping the film with oxygen. This result can possibly explain the effect reported by Ruffner *et al.*,[8] namely, that the oxidation of ruthenium electrodes prior to AlN deposition led to a reversal of polarity, if we assume that RuO_2 is reduced and AlN weakly oxidized during nucleation. The aforementioned results demonstrate the possibility of polarity switching by adding oxygen during the process or when growing AlN on the conductive oxides of noble metals, which are easily reduced. Both results cannot be exploited for local polarity variation and control on insulators within the film deposited at once.

II. EXPERIMENT

The task was thus to find an insulating substrate upon which the AlN grows in Al-polarity. It turns out that this polarity is present in AlN films deposited by molecular beam epitaxy (MBE) or metal organic phase vapour epitaxy (MOPVE) techniques, which are usually carried out in the

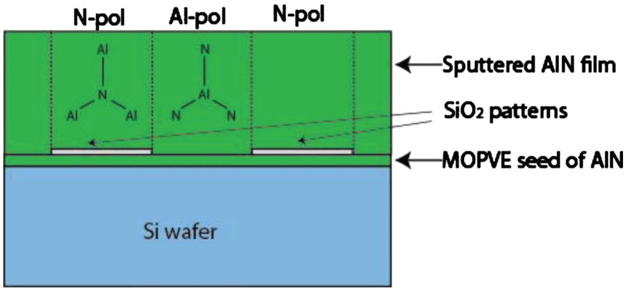

FIG. 1. (Color online) Schematic view of the fabricated structure. The polar ordering of atoms is represented by its basic tetrahedral structure.

temperature range 800–900 °C, with the application targets in the field of photonic devices. We thus tried to use the MOPVE film as a template for the Al-polarity of sputter deposited films and to screen the template locally by an amorphous silicon dioxide film to achieve N-polarity (see Fig. 1). In contrast to sputter deposition, the MBE techniques lead to very high tensile stresses and film cracking. However, as a template, only very thin films are required.

A 200 nm thick seed layer of MOPVE AlN (001) was deposited on a Si(100) substrate according to the description given by Liu *et al.*,[9] i.e., the sample was subject to the Al precursor trimethyl-aluminum prior to AlN deposition—i.e., prior to the addition of the NH_3 precursor—to prevent the formation of an amorphous silicon nitride layer. Subsequently, a 7 nm thick amorphous SiO_2 layer was deposited by evaporation through a shadow mask. Finally, a 1.2 μm thick AlN thin film was deposited by reactive pulsed dc sputtering, explained in more detail in Refs. 4–6, using parameters that allow for unchanged Al-polarity on the AlN seed layer, while at the same time preference is given for N-polarity by the process on the amorphous silica film.

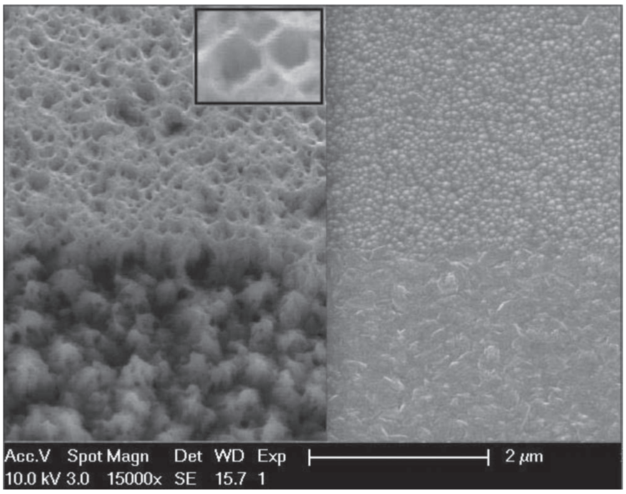

FIG. 2. Scanning electron microscopy images showing the surface of sputtered AlN films deposited on AlN with patterns of SiO_2 substrate after 45 s of etching in 5*M* aqueous solution of KOH (left) and before the etching (right). Closer look on the Al-polar region after etching is also shown, demonstrating hexagonal holes.

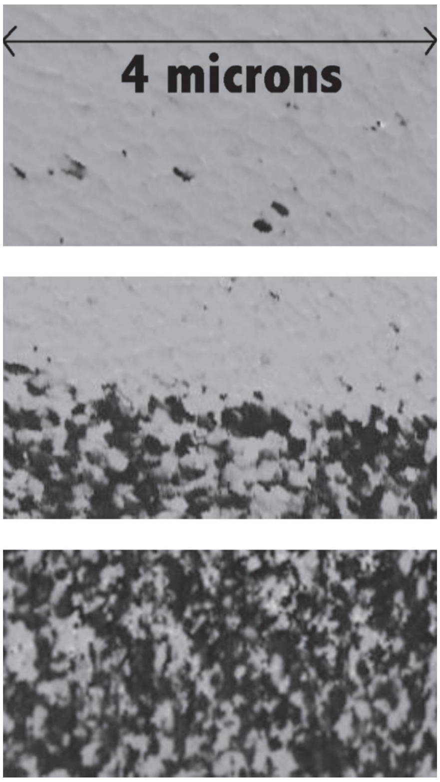

FIG. 3. PFM measurements on the surface of AlN deposited on AlN patterned with SiO_2. Almost uniform polarity for AlN grown directly onto AlN seed (top), transition region (middle), and mixed (ratio=70/30) polarities for AlN grown on SiO_2 patterns (bottom) are observed.

III. RESULTS AND DISCUSSION

The polarities were verified by a wet etching test in KOH.[10] The etching rate depends on the polarity: N-polar films are less resistive to KOH attack. Most of the film is etched away. The remaining part shows typical pyramidal or conical columns. In contrast, Al-polar films resist etching. Conical holes appear where defects and isolated N-polar grains allow an attack. In our experiments, we used a 5*M* aqueous solution of KOH and an etching time of 45 s. The surface of the resultant 1.2 μm thick AlN film, before and after the wet etching test, is shown in Fig. 2.

It can clearly be seen that the AlN film exhibits different polarities depending on the surface it was grown on. The part of the film grown directly on the AlN seed layer shows resistance to the etchant; hexagonal holes are formed on the surface giving evidence of Al-polarity. Therefore, the polarity of the AlN seed layer was replicated in the film. In contrast, the region of the film grown on SiO_2 is not resistant to the etchant, and pyramidlike structures, typical for etched N-polarity films, are visible. Also, one should notice that for the Al-polar region of the film, a good (001) texture with small rocking curve of $\Delta\omega = 1.2° - 1.8°$ is observed due to the fact that the AlN film was sputtered onto the well-oriented epitaxial AlN seed layer. That is not the case for the AlN sputtered onto SiO_2. The surface roughness of the sublayer is duplicated by the SiO_2 layer. Consequently, the rocking curve width is much larger, resulting in a less perfect textured film, even showing same small peaks of other orientations in agreement with Ref. 6. This explains why the pyramid structures are less well faceted in comparison to those seen in Ref. 10. However, the general behavior is still the same: N-polar films are less resistive to etching than Al-polar films.

For confirmation, the films were analyzed using piezoresponse force microscopy (PFM), inspecting the polarity at the nanoscale as shown in Fig. 3. The region of the film that was grown directly on the AlN seed shows almost uniform polarity, with the occasional grain displaying the inverse polarity. On the contrary, AlN grown on SiO_2 shows a mixture of polarities in the ratio of N-polar : Al-polar = 70 : 30. Therefore, the results acquired using PFM correlate well with those of the wet etching tests. The film shows (001) texture, as observed by x-ray diffraction. The N-polarity on amorphous silica is introduced by the sputter process, however, not strongly enough to suppress completely the Al-polarity, which nucleates as well. The process proved to be reproducible many times. For future improvement, we propose to replace amorphous SiO_2 by an oriented, crystalline nonpolar seed layer to achieve a higher quality texture.

IV. CONCLUSIONS

In conclusion, we have demonstrated a method that utilizes substrate polarity as a way of defining the polarity of sputtered AlN films. Patterning of the polarity within the same AlN film, defined by means of lithography, is presented. The procedure relies upon Si wafers and is hence compatible with MEMS fabrication steps such as wafer backside processing, which is not the case for solutions that involve sapphire wafers, for example.

ACKNOWLEDGMENT

The research leading to these results has received funding from the European Community's Seventh Framework Programme (FP7/2007-2013) under grant agreement No. 223975.

[1] R. Ruby, Electron. Lett. **35**, 794 (1999).
[2] M.-A. Dubois and P. Muralt, Appl. Phys. Lett. **74**, 3032 (1999).
[3] E. Milyutin and P. Muralt, Proceedings of IEEE Ultrasonyc Symposium, Beijing, China, 2008 (unpublished), p. 1215–1217.
[4] M.-A. Dubois and P. Muralt, J. Appl. Phys. **89**, 6389 (2001).
[5] F. Martin, P. Muralt, M.-A. Dubois, and A. Pezous, J. Vac. Sci. Technol. A **22**, 361 (2004).
[6] A. Artieda, C. Sandu, and P. Muralt, J. Vac. Sci. Technol. A **28**, 390 (2010).
[7] M. Akiyama, T. Kamohara, K. Kano, A. Teshigahara, and N. Kawahara, Appl. Phys. Lett. **93**, 021903 (2008).
[8] J. A. Ruffner, P. G. Clem, B. A. Tuttle, D. Dimos, and D. M. Gonzales, Thin Solid Films **354**, 256 (1999).
[9] R. Liu, F. A. Ponce, A. Dadgar, and A. Krost, Appl. Phys. Lett. **83**, 860862 (2003).
[10] D. Zhuang and J. H. Edgar, Mater. Sci. Eng. R. **48**, 1 (2005).

6

Conclusions and Outlook

6.1 Conclusions

In this thesis work, we studied a new type of bulk acoustic wave resonator operating on a fundamental thickness shear mode. The motivation was to investigate thin film shear mode BAW's for bio-medical and environmental sensor applications. In this work we restricted the study on (0001)-oriented AlN thin films. The following results and understanding were achieved:

1. In the paper "Shear mode bulk acoustic wave resonator based on c-axis oriented AlN thin film" the excitation of shear mode vibrations in c-axis oriented films of AlN through e_{15} coefficient was suggested and explained in details. The electric field is applied to a interdigitated electrode on top of a homogeneous AlN thin film. A device based on the SMR concept, fabricated and characterized. The mode excited in this way, cannot be a homogeneous shear mode, due to the periodic alteration of the sing of the in-plane electric field. Some local piston movement cannot be avoided, which leads to emission of parasitic waves into the liquid.

2. In the paper "Electro-Mechanical Coupling in Shear-Mode FBAR With Piezoelectric Modulated Thin Film" it was suggested to use the (0001)AlN film with periodically alternated piezoelectric properties in order to excite pure shear mode vibration in the film. It was shown that utilization of AlN with bad piezoelectric properties in combination with AlN with good piezoelectric properties is one

possibility to excite the desired shear mode. The more the properties of two AlN regions differ, the stronger is the excitation of the pure shear mode. The strongest coupling is achieved when the two regions have maximal piezoelectric coefficients of opposite sign, i.e. when using selectively Al-polar and N-polar AlN regions. This part of the work was purely theoretical, and gave the confidence that the sought phenomenon is existing and giving the correct behavior.

3. In the paper "PMBAR - shear mode TFBAR based on (001)AlN thin film" solidly mounted resonator based on AlN with two different properties was fabricated and characterized. In this work, the piezoelectric coefficient was reduced in one type of regions. A resonance behavior at expected frequencies was observed only for the device with non-uniform AlN film and not for the device with uniform AlN, confirming the importance of modulation of piezoelectric properties for exciting shear modes.

4. In the paper "Sputtering of (001)AlN thin films: Control of polarity by a seed layer", a process for simultaneous growth of Al-polar and N-polar regions during the same AlN thin films process was studied and established. The applied method was based on template layers of the Al-polarity grown by another deposition technique than our sputter method yielding N-polarity. In addition we showed that such a method can be integrated to the process flow of shear mode BAW device fabrication. Time was too short to achieve functional devices due to the unavailability Al-polar AlN thin films on 4 inch wafers. We had to used two inch wafers, which complicates too much lithography, and processing in 100 mm tools with automatic wafer handling, thus increased considerably fabrication time and risks of failures. This is not a major obstacle, because the same MOPVE process is in principle available on 4 inch wafers.

6.2 Outlook

Shear mode BAW devices definitely have a high potential in sensor applications. However, development of fully functional sensors is a challenge that requires the contributions from different fields of research and engineering, from material science to biology and chemistry. With regard to the shear mode BAW device investigated in this thesis, there are many aspects to work on before a fully functional and reliable sensor is established. One of the key issues is the attachment of the immobilization layer to the resonator. We could show in collaboration with a chemist group that functional layers of type "brushes" could be attached by plasma treatment onto SiO2 layers. This gives the opportunity to attach functional layers either on top of the device, i.e. on the polished capping layer covering the IDT, or onto the backside of the membrane. In the latter case, one would need to deposit first an oxide layer onto the AlN seed layer. The temperature drift should be addressed as well. It can be assumed that at a certain thickness ratio of SiO2 to AlN, a TCF close to 0 ppm/K can be achieved. Furthermore, the sensor might be subject to certain pressure differences across the membrane. This may also result in a cross sensitivity to pressure. Finally the resonator must be integrated into a fluidic package with micro valves and micro pumps.

Bibliography

[1] G. Sauerbrey, The use of quartz oscillators for weighing thin layers and for microweighing. Z. Phys. 155 (1959), pp. 206–222 2

[2] T. Nomura and M. Iijima, Electrolytic determination of nanomolar concentrations of silver in solution with a piezoelectric quartz crystal. Analytica Chimica Acta, v. 131 (1981), pp. 97-102 3, 9

[3] S. Rey-Mermet, R. Lanz and P.Muralt. AlN thin film resonators operating at 8 GHz used as sensors for organic films, IEEE Ultrasonics Symposium, 2005 4, 5, 7, 8, 11, 14

[4] David M. Gryte, Michael D. Ward and Wei-Shou Hu. Real-time measurement of anchorage-dependent cell adhesion using a quartz crystal microbalance, Biotechnol. Prog. 9, 105-108 (1993) 5, 6

[5] M. Benetti, D. Cannatà, F. Di Pietrantonio, V. Foglietti and E. Verona. Microbalance chemical sensor based on thin-film bulk acoustic wave resonators, Applied Physics Letters 87, 173504 (2005) 5, 6

[6] R. Gabl, H.-D. Feucht, H. Zeininger, G. Eckstein, M. Schreiter, R. Primig, D. Pitzer and W. Wersing. First results on label-free detection of DNA and protein molecules using a novel integrated sensor technology based on gravimetric detection principles, Biosensors and Bioelectronics 19 (2004) 615–620 6, 7, 10, 11, 14

[7] G. Wingqvist, J. Bjurstrom, A.-C. Hellgren, I. Katardjiev. Immunosensor utilizing a shear mode thin film bulk acoustic sensor, Sensors and Actuators B 127 (2007) 248–252 7, 8, 9

[8] Jan Weber, Willem M. Albers, Jussipekka Tuppurainen, Mathias Link, Reinhard Gabl, Wolfram Wersing, Matthias Schreiter. Shear mode FBARs as highly sensitive liquid biosensors, Sensors and Actuators A 128 (2006) 84–88 9, 10, 14

[9] Henry Wohltjen and Raymond Dessy, Surface Acoustic Wave Probe for Chemical Analysis. I. Introduction and Instrument Description. Anal. Chem. 51, v 51, N. 9 (1979), pp. 1458-1464 9

[10] R.L. Baer, C.A. Flory, M. Tom-Moy and D.S.-Solomon, STW chemical sensors, Proc. IEEE Ultrasonics Symp.. Tucson. AZ (1992), pp. 293. 9

[11] Gizeli E, Goddard N. J., Lowe C. R., Stevenson A. C., A love plate biosensor utilizing a polymer layer. Sens Actuators B, 6:131 (1992) 9

[12] Kovacs G, Venema A, Theoretical cpmparison of sensitivities of acoustic shear wave modes for bio-chemical sensing in liquids. Appl. Phys. Lett., 61:639 (1992) 9

[13] White R. M., Wicher P. J., Wenzel S. W., Zellers E. T., Plate-mode ultrasonic oscillator sensors, IEEE Trans UFFC 34:162 (1987) 9

[14] Wingqvist G., Bjurstrom J., Liljeholm L., Yantchev V., Katardjiev I., Shear mode AlN thin film electro-acoustic resonant sensor operation in viscous media. Sens Actuators B, 123 (2007), pp. 466–473 10, 14

[15] Kosslinger C., Drost S., Aberl F., Wolf H., Koch S., Woias P., A quartz crystal biosensor for measurements in liquids. Biosens. Bioelectron, 7 (1992), pp. 397–404 11

[16] Ballantine D. S., White R. M., Martin S. J., Ricco A. J., Zellers E. T., Frye G. C., Wohltjen H., Acoustic wave sensors. Academic, San Diego (1997) 11

[17] Harding G. L., Du J., Design and properties of quartz-based Love wave acoustic sensors incorporating silicon dioxide and PMMA guiding layers. Smart Mater. Struct., 6 (1997), pp. 716–720 11

[18] Junshu Wu and Dongfeng Xue, Progress of Science and Technology of ZnO as Advanced Material, Science of Advanced Materials, Vol. 3, pp. 127–149, (2011) 11

[19] Marc-Alexandre Dubois and Paul Muralt. Stress and piezoelectric properties of aluminum nitride thin films deposited onto metal electrodes by pulsed direct current reactive sputtering, Journal of Applied Physics, (2001), pp. 6389-6395 11, 53, 54

[20] Martin, F., Muralt, P., Dubois, M.-A., Pezous, A., Thickness dependence of properties of highly c-axis textured AlN thin films. J. Vac. Sci. Technol. A., 22 (2004), pp. 361–365. 12

[21] Bjurstrom J., Rosen D., Katardjiev I., Yanchev V. M., Petrov I., Dependence of the electromechanical coupling on the degree of orientation of c-texture thin AlN films. IEEE Trans UFFC 51 (2004), pp. 1347–1353 15, 16

[22] Nicolas Schuewer and Harm-Anton Klok, Tuning the pH Sensitivity of Poly(methacrylic acid) Brushes. Langmuir 2011, 27, 4789–4796 16

[23] S.J. Martin, G.C. Frye, K.O. Wessendorf, Sensing liquid properties with thickness-shear mode resonators, Sensors and Actuators A, 44, (1994), 209-218 17

[24] Rudolf Thalhammer, Stefan Braun, Branka Devcic-Kuhar, Martin Groeschl, Felix Trampler, Ewald Benes, Helmut Nowotny, and Milan Kostal, Viscosity Sensor Utilizing a Piezoelectric Thickness Shear Sandwich Resonator, IEEE transactions on ultrasonics, ferroelectrics, and frequency control, vol. 45, no. 5, 1998, pp. 1331-1340. 17

[25] Lakin, K.M., K.T. McCarron, and R.E. Rose. Solidly mounted resonators and filters. in IEEE Ultrasonics Symposium. 1995. Seattle (Washington, USA): IEEE. 21

[26] Lanz, R. and P. Muralt, Bandpass filters for 8 GHz using solidly mounted bulk acoustic wave resonators. IEEE Trans. UFFC, 2005. 52: p. 936-946. 21

[27] E. Iborra, J. Olivares, M. Clement, L. Vergara, A. Sanz-Hervas, J. Sangrador. Piezoelectric properties and residual stress of sputtered AlN thin films for MEMS applications, Sensors and Actuators A, 115 (2004), pp. 501-507 54, 55

[28] K. Tonisch, V. Cimalla , Ch. Foerster , D. Dontsov , and O. Ambacher. Piezoelectric properties of thin AlN layers for MEMS application determined by piezoresponse force microscopy, Phys. Stat. Sol. (c) 3, No. 6, 2274-2277 (2006) 54, 55

[29] Rajan S. Naik, Joseph J. Lutsky, Rafael Reif, Charles G. Sodini, Andy Becker, Linus Fetter, Harold Huggins, Ronald Miller, John Pastalan, Gee Rittenhouse, and Yiu-Huen Wong, Measurements of the Bulk, C-Axis Electromechanical Coupling Constant as a Function of A1N Film Quality, IEEE Trans. UFFC, v. 47, N. 1, 2000, pp. 292-296 55

[30] S. Mishin, D. R. Marx, B. Sylvia , V. Lughi, K. L. Turner and D. R. Clarke. Sputtered AlN thin films on Si and Electrodes for MEMS resonators: relationship between surface quality microstructure and film properties, IEEE Ultrasonic symposium, pp. 2028 - 2032 (2003) 54, 56

[31] Alvaro Artieda, Michela Barbieri, Cosmin Silviu Sandu, and Paul Muralt, Effect of substrate roughness on c-oriented AlN thin films, Journal of Applied Physics, 105, 024504 (2009) 54, 56, 59

[32] Alvaro Artieda, Cosmin Sandu, and Paul Muralt, Highly piezoelectric AlN thin films grown on amorphous, insulating substrates, Journal of Vacuum Science and Technology A: Vacuum, Surfaces, and Films, v. 28, issue 3, pp. 390-393 (2010) 61, 70

[33] D. Zhuang and J.H. Edgar, Wet etching of GaN, AlN, and SiC: a review, Materials Science and Engineering, R 48, pp. 1-46 (2005) 70

[34] T. Myers, Polarization Electronics – A Path to Multifunctional Nanoscale Materials, IEEE MELECON 2006, May 16-19, Benalmádena (Málaga), Spain 71

[35] Hock M. Ng, Wolfgang Parz, Nils G. Weimann and Aref Chowdhury, Patterning GaN Microstructures by Polarity-Selective Chemical Etching, Jpn. J. Appl. Phys. Vol. 42 (2003) pp. L 1405–L 1407 71, 72

[36] J. Brugger, J.W. Berenschot, S. Kuiper, W. Nijdam, B. Otter and M. Elwenspoek. Resistless patterning of sub-micron structures by evaporation through nanostencils, Microelectronic Engineering 53 (2000), 403-405 74, 76

7

Appendix A

List of publications

Letters

E. Milyutin and P. Muralt, Electro-Mechanical Coupling in Shear-Mode FBAR With Piezoelectric Modulated Thin Film, IEEE TRANSACTIONS ON ULTRASONICS, FERROELECTRICS, AND FREQUENCY CONTROL, Vol. 58, N. 4, APRIL 2011

E. Milyutim, S. Harada, D. Martin, J. F. Carlin, N. Grandjean, V. Savu, O. Vaszquez-Mena, J. Brugger and P. Muralt, Sputtering of (001)-AlN thin films: Control of polarity by a seed layer, J. Vac. Sci. Technol. B 28(6), Nov/Dec 2010

Regular papers

Evgeny Milyutin, Sandrine Gentil and Paul Muralt, Shear mode bulk acoustic wave resonator based on c-axis oriented AlN thin film, JOURNAL OF APPLIED PHYSICS 104, 084508 (2008)

7. APPENDIX A

Proceedings papers

Evgeny Milyutin and Paul Muralt, PMBAR - shear mode TFBAR based on (001)AlN, IEEE Ultrasonics Symposium, Beijing (China), Nov. 2-5, 2008

Patents

Evgeny Milyutin and Paul Muralt, Piezoelectric resonator operating in thickness shear mode, PCT application, WO 2010/013197 A2

Publications in books

Evgeny Milyutin and Paul Muralt, Thin Film Bulk Acoustic Wave Resonators for Gravimetric Sensing, in Nanosystems Design and Technology, Springer Science + Business Media LLC (2009), pp. 103-116

8

Acknowledgements

I would like to thank my thesis director, Professor Paul Muralt, for providing me with the possibility to work with his group. His deep knowledge in a wide range of research fields such as materials, micro-fabrication and physics and also his ability to constantly listen and teach me are among of the principal reasons for the completion of my thesis.

I am grateful to Professor Alexander Tagantsev for the discussions related to the theory on acoustics and acoustic devices, that was extremely helpful especially in the beginning of my thesis, when discussions in Russian were still easier than in English.

I would like to acknowledge Professor Nicolas Grandjean, Professor Juergen Brugger and their teams for their contribution to the research on material growth.

I acknowledge Professor Nava Setter, the head of Laboratory of Ceramics, for her initiative to organize seminars and competitions in the laboratory and in the department.

I thank the team of the Center of Micro and Nanotechhnology (CMI), in particular Jean-Baptiste Bureau, Boris Lunardi, Cyrille Hibert, Nareg Simonian, Guy Clerc and Dr. Philippe Langlet, for their guidance in processing.

I would like to thank everyone in the LC team, in particularly my office mates - Scott, Monika, Kaushik, Andy, Florian and Brahim.

Special thanks to my my Russian and Slavic friends - Max ”the Ded”, Serguei Okhonin, Marko from Sinj, Professor Yury, Sasha for their support and in particularly to Valya and Jenya for making the most complicated year of my thesis sufficiently comfortable and much less disturbing as it could have been.

И конечно, я хотел бы поблагодарить моих родителей и мою сестру, Юлю, за их теплоту, понимание и заботу, которая чувствуется даже на расстояние в 5769 км. Эта диссертация во многом ваше достижение!

Name: Evgeny Milyutin

Date of birth: 07.08.1985

Contacts: +41-76-217-9112, evgeny.milyutin@epfl.ch

Professional interests: Mathematics, Physics, Engineering, Computer Science, Teaching, Start-ups.

Education:

Sept. 2006 – present time
Swiss Federal Institute of Technology (EPFL), PhD student
June 2009
Swissnex Boston, Workshop on start-ups and entrepreneurship
Jan. 2005 - June 2008
Russian Research Center, Diploma work on Micro-technology
Sept. 2002 – June 2008
Moscow Institute of Physics and Technology (State University), Department of General and Applied Physics
Sept. 2000 – June 2002.
Last two years of senior school – studying at The Specialized Scientific Center (Physics and Mathematics School) of Novosibirsk State University
Sept. 1998 – June 2002.
Correspondence school of physics and mathematics at Moscow Institute Of Physics and Technology (State University)

Achievements:

April 2009
Selected to be part of Swiss National Start-up Team
June 2008
Master degree
June 2006
Bachelor degree (mean score 4.71 of 5)
2001/2002 - Senior pupil at school. II degree diploma at the regional physics contest (Siberia region), II degree diploma at All-Russian Physics Contest.
1999/2000 9th grade. III degree diploma at regional physics contest (Siberia & Far East), participant of the final stage of All-Russian Physics Contest.

PC skill:

Available to use PC as a tool. Also I have skills of programming on C, Pascal, Mathematica and Matlab.

Hobby:

Physics, mathematics. Sports: swimming, mount skiing. 1st adult category of judo